POLITECNICO DI TORINO
Repository ISTITUZIONALE

A critical review of laser wire directed energy deposition: Toward large-scale metal additive manufacturing

Original
A critical review of laser wire directed energy deposition: Toward large-scale metal additive manufacturing / Melentiev, R., Long, Y.e., Wagih, A., Chen, G., Zhang, C., Catalano, A.R., Priarone, P.C., Fangda, X.u., Piano, S., Spitas, C., Nan, Y.u.. - In: MATERIALS SCIENCE & ENGINEERING R-REPORTS. - ISSN 0927-796X. - 171:(2026). [10.1016/j.mser.2026.101273]

Availability:
This version is available at: 11583/3015672 since: 2026-09-17T12:12:02Z

Publisher:
Elsevier Ltd

Published
DOI:10.1016/j.mser.2026.101273

Terms of use:

This article is made available under terms and conditions as specified in the corresponding bibliographic description in the repository

Publisher copyright

(Article begins on next page)

16 October 2026

Materials Science & Engineering R 171 (2026) 101273

Contents lists available at ScienceDirect

Materials Science & Engineering R

journal homepage: www.elsevier.com/locate/mser

A critical review of laser wire directed energy deposition: Toward large-scale metal additive manufacturing

Ruslan Melentiev [a,b,*], Long Ye [c], Ahmed Wagih [d,e], Guoda Chen [f,g], Chengzhe Zhang [f,g], Angioletta Rita Catalano [h], Paolo C. Priarone [h], Fangda Xu [i], Samanta Piano [b], Christos Spitas [j], Nan Yu [c,k,**]

[a] Research and Innovation Institute, Faculty of Science and Engineering, University of Nottingham Ningbo China, Ningbo 315100, China
[b] Manufacturing Metrology Team, Faculty of Engineering, University of Nottingham, Nottingham, UK
[c] Institute for Materials and Processes, The University of Edinburgh, Edinburgh EH9 3FB, UK
[d] Mechanics of Composites for Energy and Mobility Lab, Physical Science and Engineering Division, King Abdullah University of Science and Technology (KAUST), Kingdom of Saudi Arabia
[e] Department of Mechanical Design and Production Engineering, Faculty of Engineering, Zagazig University, Zagazig, Sharkia 44519, Egypt
[f] College of Mechanical Engineering, Zhejiang University of Technology, Hangzhou 310023, China
[g] Zhejiang Key Laboratory of High-Precision and Efficiency Hybrid Processing Technology and Equipment, Zhejiang University of Technology, Hangzhou 310023, China
[h] Politecnico di Torino, Department of Management and Production Engineering, Corso Duca degli Abruzzi 24, Torino 10129, Italy
[i] Rongsu Technology ltd, Fuda Road, Taicang, Suzhou, Jiangsu CN 215412, China
[j] Department of Mechanical, Materials and Manufacturing Engineering, Faculty of Science and Engineering, University of Nottingham, Ningbo, China
[k] National Key Laboratory of Laser Spatial Information, Harbin Institute of Technology, Xili University Town, HIT campus, Shenzhen, Guangdong 518055, China

ARTICLE INFO

Keywords:
Directed energy deposition
Additive manufacturing
3D printing
Laser
Metal
Microstructure
Mechanical properties
Modelling
Manufacturing defects
Process monitoring
Sustainability

ABSTRACT

The future of additive manufacturing (AM) is evolving beyond small-scale prototyping toward the production of large-scale, high-performance, and high-value metal components. Laser wire directed energy deposition (LW-DED) has emerged as a promising AM technology in this scenario, offering meter-scale builds, kilogram-per-hour productivity, near-zero material waste, and laser-based precision, with research activity having grown tenfold in the past few years. This comprehensive state-of-the-art review integrates the fragmented knowledge landscape of LW-DED, covering its historical evolution, process fundamentals, machine architectures, material–process–structure–property relationships, multi-physics modelling, sustainability and techno-economic considerations, and AI-driven in-situ monitoring, supporting the transition toward fully autonomous digital manufacturing. We critically assess demonstrated applications, ranging from titanium structures to tungsten components for fusion reactors, distinguishing between optimistic expectations and genuine industrial value. This work provides a framework for positioning LW-DED within the broader landscape of large-scale metal additive manufacturing, and identifies key unresolved challenges to outline a research roadmap for industrial deployment.

1. Introduction

In the chronicles of technological evolution, few innovations have promised to reshape the fabric of industry as profoundly as additive manufacturing (AM) [1–4]. Yet, although AM has been commercially viable for over 30 years and heralded as a catalyst of the 4th industrial revolution and, more recently, Industry 5.0 paradigms [5–7], it represents only 0.15% of the worldwide manufacturing market ($21.9 B [8] out of $14.8 T [9] in 2025). Following the ironic, yet not less iconic, vision of Love et al. [10] "*There's plenty of room at the top*", this is probably because AM has been competing in a "suboptimal" application domain. Most AM technologies [11–16] can be characterised as making small parts [17–23] (typically below one metre in characteristic size) at slow build rates (typically $<100\ cm^3/h$) [24–27] with expensive feedstocks (greater than $50/kg) [28–31], often attempting to compete with conventional manufacturing. However, it is large, rather than small

* Corresponding author at: Research and Innovation Institute, Faculty of Science and Engineering, University of Nottingham Ningbo China, Ningbo 315100, China.
** Corresponding author at: Institute for Materials and Processes, The University of Edinburgh, Edinburgh EH9 3FB, UK.
E-mail addresses: ruslan.melentiev@nottingham.edu.cn (R. Melentiev), nan.yu@ed.ac.uk (N. Yu).

https://doi.org/10.1016/j.mser.2026.101273
Received 9 December 2025; Received in revised form 17 June 2026; Accepted 13 July 2026
Available online 22 July 2026
0927-796X/© 2026 The Author(s). Published by Elsevier B.V. This is an open access article under the CC BY license (http://creativecommons.org/licenses/by/4.0/).

parts, where the foundry industry is in need of a breakthrough [32], which can be provided by AM [33]. For now, AM has made minimal inroads into the arena of large part manufacturing [34,35] – arguably the most transformative frontier of AM [36–39]. However, scaling AM technologies to produce meter-sized parts has faced technological and financial challenges [40–42]. If production rates in AM can take a Moore's law approach, growing from one to ten and potentially to hundreds of kilograms per hour, the foundry of the future may be tool-less, directly printing parts with a low-cost infrastructure that can be distributed locally.

Among all the metal AM technologies [43,44], directed energy deposition (DED) technologies are likely the most easily scalable [45]. In DED, feedstock material, supplied in the form of powder or wire, is melted by a focused energy source such as an electric arc, plasma, ion beam or laser beam and deposited on a substrate or previously deposited material layer by layer [46]. The laser beam wire-based DED process (LW-DED, or DED-LB/w according to ASTM terminology [47]) is among the most recent and promising DED variants. Compared to powder processes, where nearly half of metal particles rebound from the substrate [48], increasing contamination of the working environment and potential operator exposure risks [49], wire feeding is simpler, cheaper, more productive, safer, and results in nearly zero material waste [50]. Furthermore, unlike widely used electric arc or plasma sources, laser beam is more stable, controllable and accurate, especially when using recently developed coaxial laser systems [50,51], which may come at a cost today, but offer capabilities beyond other energy sources, including precise heat input, smaller heat affected zone, finer microstructure, less base metal dilution, lower residual stresses and shape distortions, less surface finishing and thermal postprocessing [52,53].

The LW-DED development has spanned over a century, only recently entering a phase of rapid growth in research and commercialisation, attracting leading players in high-value manufacturing sectors. The first DED applications were documented in California during the oil and gas boom in the 1930s for repair of drilling equipment [54], and later for repair of agricultural and heavy machinery in the USSR [55] and elsewhere. However, those approaches used either electric arc, gas or plasma torch as the heat source rather than laser, which was introduced for DED only in 1997 by Sandia National Laboratories [56]. Nevertheless, the technology remained relatively niche for over two decades. In the past five years, the convergence of increased materials and energy costs, sustainability and re-manufacturing trends, as well as technological progress in optics and machine tools, substantiated an abrupt rise of LW-DED research and commercialisation activities. The number of LW-DED equipment manufacturers and service providers has quadrupled, and the volume of research increased tenfold in the 2020–2025 period. In fact, our literature survey indicates that more LW-DED research has been published in 2024–2025 than in the preceding two decades. The financial impulse was sparked by major industrial parties, such as NASA [57] and GKN Aerospace [58], centralised national funding, such as the U.S. Department of Defense [59] and Department of Energy [60], and considerable venture capital investment in technology around the globe [61]. Drawing a parallel to the core 3D printing technologies, SLA and FDM were developed in the 1980s and took nearly 30 years to take off in the 2010s. Approaching the same age, LW-DED is expected to enter a similar phase of rapid growth.

A substantial body of knowledge on the LW-DED process has been generated. Yet, a comprehensive vision of this technology has not been assembled, owing to its multi-disciplinary nature, fragmented fundamental understanding, and until recently, the limited number of systematic experiments. First, the laser deposition studies originate from optics, heat transfer, metallurgy, and manufacturing fields, which often do not integrate each other's aspects and advances. Further, due to this multi-disciplinarity, LW-DED research lacks standards and even unified terminology. Researchers and start-ups have coined a variety of names for LW-DED, e.g. laser 3D welding, laser cladding, welding-based deposition, welding-based rapid prototyping, direct light fabrication, near-net shape manufacturing, and other titles as collected in [62], complicating the search and knowledge exchange. In addition, as with many other 3D printing technologies, LW-DED is increasingly surrounded by marketing hype that often inhibits understanding of the real value the technology has to offer. In the past few years, LW-DED has been demonstrated to be capable of printing everything from wheel disks to pedestrian bridges [45], yet it remains unclear which items in that range may come with added value and be commercially viable. Several DED reviews have been published in the past 5 years [46,50–53,62–66], in which LW-DED content was either absent, narrowly focused, scarce, or backed up by arc- or powder-DED studies. Over a hundred LW-DED studies have been published in 2024 and 2025 alone (and about ten times fewer before that), finally maturing the topic for an independent comprehensive review.

The time is ripe to consolidate the fragmented understanding of LW-DED into a coherent scientific framework. The scope of this review is reflected in the graphic abstract and structured into ten sections: following this introduction (1), we discuss the historical evolution of LW-DED (2), machine tools and process fundamentals (3), feedstock materials and their processing peculiarities (4), processing-structure-property relationships (5), modelling and simulation (6), online monitoring and automation (7), economic and sustainability indicators (8), competitive application domains (9), and a critical outlook for future work (10). If the past three decades of AM were about printing the small and intricate parts, the AM wave in this decade focuses on printing large and heavy components.

2. Evolution of LW-DED

Shaping and repairing parts by overlay-welding has been well documented in the 20th century across the globe. The research on welding-based additive manufacturing processes has been fragmented geographically and terminologically, and only recently formally grouped under the DED category within the rapidly expanding AM technological umbrella [47,67]. Ding et al. [62] listed over a dozen other, less widely adopted terms for wire-based DED technologies, among which are 3D welding, laser cladding, welding-based deposition, direct light fabrication, welding-based rapid prototyping, wire-arc additive manufacturing, near-net shape manufacturing and many others (see Table 4 in [62]). For this reason, it is relevant to review the LW-DED evolution and key developments so far in an attempt to better comprehend its future trajectory. Three conceptual stages of LW-DED evolution can be identified: (*i*) technological foundation, (*ii*) tools and process consolidation, and (*iii*) materials expansion with process digitalisation (Fig. 1).

2.1. Technological predecessors in the 20th century

Wire-DED technologies have their roots in welding. One of the earliest patents related to what is now referred to as wire-DED was registered in 1887 as "*Process of and apparatus for working metals by direct application of the electric current*" by Benardos and Olszewski in St. Petersburg, Russia [68], and three years later by Coffin et al. in Detroit, US [69], followed by several patents on various related variations of the same concept at the beginning of the 20th century. Industrial application emerged later, to the best of the authors' knowledge, in California. In 1921, the brothers Winston F. and Shelley M. Stoody opened the Stoody Welding Co, a workshop for tractor repair [54]. The following year oil was discovered nearby, and the brothers reoriented their business to deposit abrasion-resistant chromium alloys onto drill bits used in oil rigs [54]. The following decade saw the application of DED to Co-Cr-W alloys, called "*hardfacing*" at that time, to internal combustion engine valves. In the second half of the 20th century, hardfacing was widely applied to farming equipment and heavy machinery in the USSR [55]. However, those DED approaches used either an electric arc, gas or a plasma torch as the heat source instead of a laser.

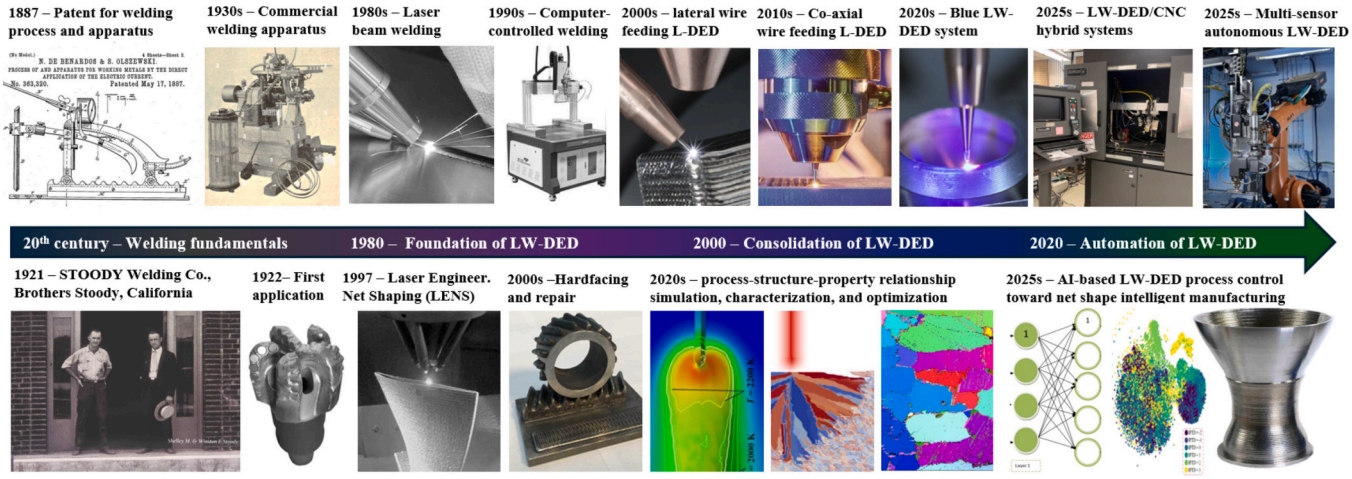


Fig. 1. Historical evolution and key technological milestones, including early welding-based predecessors, leading to the development of laser wire directed energy deposition (LW-DED), highlighting the transition toward modern automated systems.

2.2. Foundation in 1980–2000

The groundwork for LW-DED was set in the 1980s with the development of laser beam welding [50]. The 1990s saw the advent of computer-controlled laser systems, which improved precision and enabled early research into coaxial wire feeding techniques [50]. During this period, laser-based metal deposition techniques were first explored for rapid prototyping and part repair applications. A major milestone was the development of Laser Engineered Net Shaping (LENS) at Sandia National Laboratories in 1997, which introduced a method for fabricating near-net-shape metallic components using a high-power laser to melt metal powder layer by layer [56], later leading to wire DED variants. By the early 2000s, industrial adoption of DED technologies was gaining momentum, with Optomec's LENS technology and Sciaky's Electron Beam Additive Manufacturing (EBAM). Wire-based DED systems gained traction due to their superior material utilisation (nearly 100% material utilisation [70]) and high deposition rates compared to powder-based ones [71].

2.3. Process consolidation in 2000–2020

During the early 2010s, the transition to wire-based feedstock was driven by several factors, including improvements in wire feeding mechanisms, laser control systems, and process monitoring technologies. A significant technological improvement in the 2010s was the refinement of wire feeding strategies, which played a crucial role in stabilizing the LW-DED process. Early implementations faced challenges such as wire misalignment, inconsistent melting rates, and irregular deposition profiles. The issues were mitigated in the early 2020 s with some of the first comprehensive studies on wire feed angles, scanning strategies, and shielding gas application to enhance deposition stability and mechanical properties [72]. The introduction of hybrid manufacturing, which combines DED with CNC machining, demonstrated a significant reduction in material waste and production time [70], thereby enabling net-shape components with as-designed dimensional accuracy and surface finish [73]. Another advancement in hybrid manufacturing involves the combination of wire and powder feedstocks, allowing for more versatile material properties, e.g., Ti−6Al-4V with TiC reinforcement [71]. However, the material utilisation efficiency and process cleanliness remain challenging for wire-powder hybrid systems. Oscillating laser techniques were integrated into LW-DED in the mid-2020s to address heat accumulation and residual stresses, thereby improving tensile strength and ductility of the deposited parts [70,74]. Oscillations also improved layer uniformity, making the process more viable for complex part geometries [70]. Advances in preheating strategies emerged to mitigate solidification cracking in superalloys such as Inconel [75,76] and alloys such as Ti−6Al-4V [77–79], expanding their potential applications in aerospace. Preheating strategies also improved deposition efficiency up to 3.1 kg/h without sacrificing mechanical properties [80]. One of the persistent challenges of LW-DED was wire positioning and melting consistency, leading to irregular deposition layers and incomplete fusion. A breakthrough came with the introduction of coaxial wire feeding in 2018, which eliminated constraints associated with lateral wire feeding [81], enabling uniform and direction-independent deposition with improved accuracy, reduced surface roughness, and thus reduced post-processing costs [51,53]. While DED has come a long way, the availability of new hardware provided a certain boost to the technology in the past decade.

2.4. Automation and materials expansion in 2020–2025

Since 2020, researchers have prioritised materials expansion and process automation with CNC, digital twins and AI. Among the most active research areas in LW-DED are process-microstructure-property relationships, particularly for superalloys [82], the development of microstructure modelling for predicting part properties [83], and the implementation of AI-driven process monitoring models for online process control [84]. Certain efforts were directed towards the processing of composite alloys (e.g., Mg–Li) to yield the best combination of part accuracy and structural integrity [85]. High-entropy alloys (HEAs) and metal matrix composites (MMCs) are being explored for their superior strength and wear resistance [74]. Dual-wire approaches have emerged to improve deposition flexibility and enable bimetallic processing [86]. Hybrid feed systems now allow for in-situ alloy composition adjustments, enabling the fabrication of functionally graded materials (FGMs) with variable properties [70]. AI-driven monitoring and adaptive feedback systems have further enhanced hybrid LW-DED applications, optimising deposition efficiency in real-time [87]. These systems enable automated adjustments to laser power, wire feed rate, and scanning speed, reducing defect formation [88–90]. Machine learning models are now being used to predict optimal deposition parameters based on real-time sensor data, leading to improved repeatability and reduced material wastage [91,92]. Overall, the expansion towards difficult-to-machine alloys, multi-material deposition, hybrid manufacturing, AI-driven monitoring, and real-time defect mitigation represents some of the key topics today.

2.5. Research trajectories in 2024–2025

The lifetime of focal points in LW-DED research is short: topics

researched a decade ago barely remain in focus today. In addition, the momentum of LW-DED research has increased rapidly, necessitating an analysis of the primary research drivers. A manual expert search on Web of Science identified fewer than one hundred LW-DED papers published before 2024 and nearly one hundred additional papers published in 2024–2025 alone. Following the bibliometric principles in [93,94], a keyword analysis was conducted on the LW-DED studies published in 2024–2025 to identify the latest research hotspots. The analysis shows four research trajectories (Fig. 2) as key approaches to optimising and improving the LW-DED process and outputs: (*i*) materials expansion, (*ii*) process automation, (*iii*) process simulation, and (*iv*) process modification. The material expansion trajectory is primarily motivated by aerospace applications, as evidenced by the keywords related to high-entropy alloys. The automation trajectory targets improving process stability and turning LW-DED into an autonomous technology using data-driven AI tools. The simulation trajectory similarly targets this objective, however, it does so by using fundamental principles of heat and mass transfer. The modification trajectory pushes the LW-DED boundaries using new hardware, such as oscillatory and blue lasers, wire preheating, and hybrid machining, among others. Each trajectory serves to either understand, control, or improve the process-structure-property relationships (as illustrated by the green keyword cluster connected to all other clusters). Interestingly, none of the trajectories have yet been effectively integrated with each other (as evidenced by the disconnected clusters, excluding the green cluster), indicating their early stage and potential for future symbiosis.

3. Fundamentals

3.1. Technical realisation

The technical realisation of the LW-DED process is among the simpler configurations of metal AM systems. The basic configuration is illustrated in Fig. 3a [95]. The laser source and optical components that alter the laser energy distribution or focus the laser beam are central to this process. A wire-feeding mechanism ensures the continuous supply of metal wire. A shielding gas nozzle is typically required to prevent oxidation of most metals if the process is not enclosed. Finally, the system typically includes numerically controlled machine tools or robotic arms capable of multi-axis movement. Apart from these key components, auxiliary systems can include equipment for wire preheating, ultrasonic oscillations, melt pool shock modulation, process monitoring using IR cameras, laser scanners, X-ray tomographs, and others for specialised applications, e.g., low-gravity or underwater deposition [50]. In simplified terms, the LW-DED process can be as simple as the laser welding head mounted on a CNC machine instead of a cutting tool, or as the integration of a set of complex and precise electromechanical systems to achieve improved manufacturing performance.

Two main deposition types exist: lateral and coaxial wire feeding. The first one is essentially a wire-laser welding process, where the wire is supplied under the laser spot at a 15–60° angle (typically 30°–40°) [81] to be melted and solidified on the substrate (Fig. 3b). Such a setup can cost approximately $5k–10k and is best suited for unidirectional cladding or welding purposes; however, when applied to 3D deposition, it often results in asymmetric geometry and properties within the layer. Much of the current understanding of LW-DED has been generated on such systems. The second type is with the wire fed coaxially at the centre of the laser beam, which is first split into multiple beams annularly around the wire and then converged on the wire near the substrate (Fig. 3c). As of 2025, the simplest LW-DED systems with coaxial laser heads start from approximately $50k–100k (depending on the country of the manufacturer), and the selection is quite limited. Our analysis shows that, since 2024, nearly a third of LW-DED articles in Web of Science have operated with coaxial systems. Other systems exist with different laser arrangements and combined wire and powder feeding systems [96], but are not mainstream.

The fundamentals of LW-DED can be understood based on laser welding with wire feed. When the laser beam is focused on the metallic substrate, the local temperature rapidly rises above the melting point of the metal, forming a dynamic melt pool [46]. Meanwhile, the metal wire is fed into the front of the melt pool at an appropriate rate by the wire-feeding mechanism. The end of the wire melts under the combined action of laser irradiation and the conductive heat from the melt pool, and mixes with the molten metal, driven outward from the pool centre due to the Marangoni flow [97] (Fig. 3d). As the deposition spot continuously moves relative to the substrate, the melt pool is continuously replenished with freshly fed wire, while the melt track behind cools down and solidifies, forming a dense deposition layer. Layer-by-layer deposition results in a part with a typically wavy

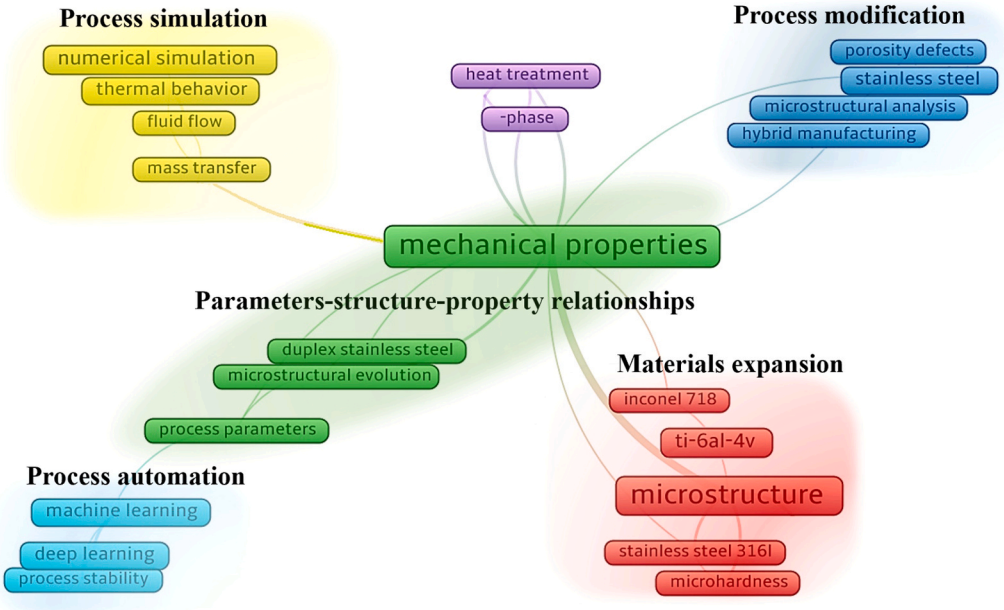


Fig. 2. Keyword analysis of LW-DED research published in 2024–2025, highlighting the main research trajectories identified in this work.

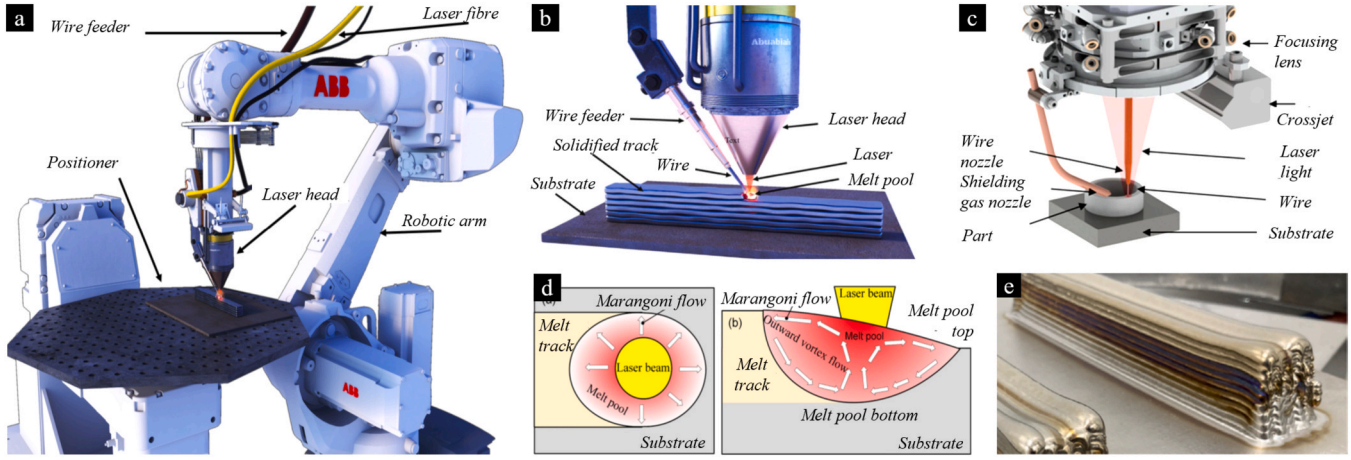


Fig. 3. Technical realisation of the LW-DED process: (a) representative configuration of a robotic system [100]; (b) deposition with lateral wire feeding [101]; (c) deposition with a coaxial wire-laser head [102]; (d) schematic representation of melt pool dynamics [97]; and (e) typical layered morphology of wire-fed laser deposited metal [98].

appearance as shown in Fig. 3e [98]. All these processes take place in an inert gas environment or using flux-cored wires [99] to prevent excessive oxidation of the metal [63].

3.2. Process control

Laser power, wire feed rate, and travel speed are the three key parameters of the LW-DED process. These parameters govern the process behaviour and do not act independently, but instead exhibit strong coupling relationships [76,100,103,104]. Laser power directly determines the thermal input, and thus influences the temperature and size of the melt pool, affecting the cooling rate, solidification dynamics, microstructure, mechanical properties, and morphology of the deposited track [105–107]. Faster wire feeding accompanied by a proportional increase in laser power enlarges the size and temperature of the melt pool and overall volume of deposited material [105,108–110]. The travel speed of the deposition head, also referred to as laser scan speed, determines how the energy (laser power) and mass input (wire feed rate) are distributed over the surface of the substrate, and thus also affects the melt pool temperature and size, cooling rate, solidification microstructure, and geometrical accuracy of the deposition [105,109–111]. The coupling of laser power, wire feed rate and travel speed is commonly described by the concept of energy density, which can be expressed through four related metrics of the deposition process: volume energy density, E_v (Eq. 1), linear energy density, E_L (Eq. 2), global energy density, E_g (Eq. 3), and normalised energy density, E_n (Eq. 4):

$$E_v = \frac{P}{v \cdot h \cdot t} \tag{1}$$

$$E_L = \frac{P}{v} \tag{2}$$

$$E_g = \frac{P}{v \cdot d} \tag{3}$$

$$E_n = \frac{P}{v \cdot t} \tag{4}$$

where P, v, h, t, and d represent laser power, travel speed, deposition path spacing, layer height and spot size, respectively [104]. These physical parameters can be correlated with deposition quality, including porosity and material density [112], geometric accuracy [113], and microstructure [105]. In brief, an excessive energy input leads to an overly large melt pool, melt pool instability and spattering, melt-through defects, droplet formation and metal dripping [95], while insufficient energy input leads to incomplete melting and lack of fusion, leading to lack-of-fusion defects, voids and increased susceptibility to cracking [95], as well as protrusion of semi-solid wire and stub formation (when pieces of wire stick out from the deposited bead) [84]. Other process parameters, including laser beam characteristics, wire feeding position and angle, as well as path strategies, can also be adjusted, yet these are typically kept constant during a given deposition process.

Laser beam characteristics include energy distribution, defocusing distance, wavelength, and waveform (Fig. 4). Lasers typically have a Gaussian energy distribution, but can be shaped into inverse-Gaussian and super-Gaussian (flat-top) distributions, affecting melt pool formation [114,115]. The laser spot can also be generated by the coupling and superposition of several individual laser beams [116]. This configuration is commonly implemented in DED heads with coaxial wire feeding, which have become increasingly common in recent years (nearly a third of the studies published in 2024–2025 used coaxial heads). The laser defocusing distance refers to the distance between the focal point of the laser beam and the actual interaction point on the substrate, thus affecting the laser spot size, shape, and energy distribution [117–119]. The laser wavelength determines how much of the laser energy is absorbed by the wire material [111,120]. Shorter wavelengths are generally more readily absorbed by most metals [121], but since light absorptance is a material property, it will be discussed in the corresponding section. Regarding the waveform, lasers can operate in continuous wave, pulsed wave, oscillating continuous wave, and oscillating pulsed wave modes, with the latter, for instance, showing advantages in suppressing porosity and refining the microstructure [122].

Wire feeding positions can be classified into lateral wire feeding and more recently coaxial wire feeding. In the first scenario, the wire is fed into the melt pool at a certain angle to the laser beam and substrate, as in laser welding. The wire feeding angle also affects the processing [106,110], but normally is fixed at around 45 ° between the laser axis and the substrate plate. Such a feeding system is cheap and common for laser welding apparatus, but it is not convenient for AM, due to asymmetry of the deposition [123]. In coaxial wire feeding, the wire is fed along the main axis perpendicular to the substrate, while the laser beam is split into multiple beams annularly around the wire and then coupled into one spot at the tip of the wire, or near [116,124,125]. The scanning path influences the thermal history of each deposited region within the entire part, due to its multiple re-melting and re-heating, thereby influencing part microstructure and residual stresses [126]. Optimizing the scanning path can reduce the need for support structures or machining allowances in special structures, enhancing forming efficiency and saving costs [127–130].

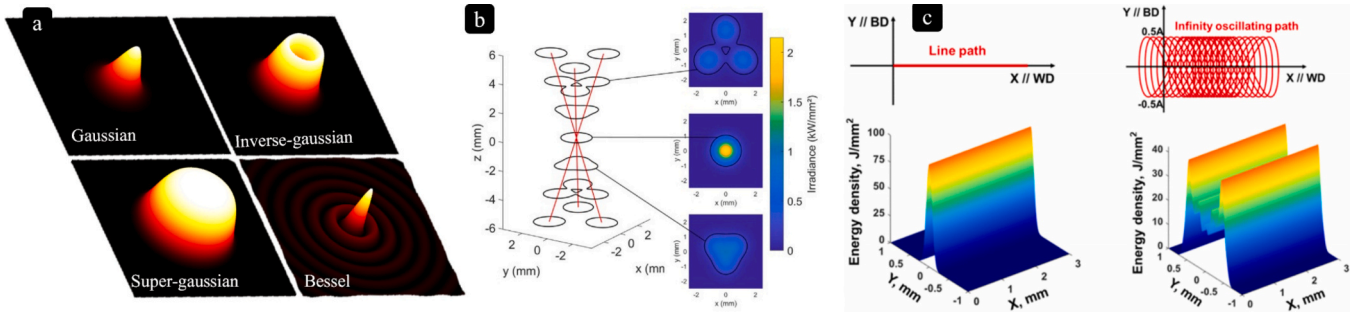


Fig. 4. Laser beam characteristics in LW-DED: (a) representative laser energy distributions, (b) effect of beam shaping and defocusing on irradiance distribution [125], and (c) scanning strategies and resulting energy density distributions [122].

3.3. Machine tools

The laser head is the primary component in any LW-DED system. Aside from the lateral wire feeding, two coaxial wire-feeding configurations of laser heads have been recently developed: with multiple lasers or a fibre-split beam configuration. To illustrate the difference, representative commercial coaxial laser heads are shown in Fig. 5, and their characteristics are listed in Table 1. In brief, the first type of coaxial laser head consists of multiple lasers, typically 6 (e.g., those produced by Meltio 3D or Rongsu Tech, among others), which are arranged circularly around the wire nozzle and focused at a central point below the wire nozzle, typically at the wire tip. The application of multiple lasers enables highly adjustable laser spot size, shape, and energy distribution [131]. Some producers specifically developed a control system for tuning each laser individually (e.g., the VEAM system by Rongsu Tech) allowing substrate preheating, controlled wire deposition, and reduction of the cooling rate of the melt pool by dynamically deflecting the laser beams. The focusing distance is an important factor here, as a deviation of several millimetres from the focal plane affects the laser energy distribution, as shown in Fig. 4b. The second type of laser head uses a set of optics and a curved optical path to split a fibre beam into a ring-shaped beam, introduce the wire at the centre of the ring, guide the ring-shaped laser beam along the centrally located wire, and then merge the ring-shaped beam back to a central focal point at the wire tip. Such heads are larger, heavier, geometrically complex (e.g., Precitec and Additec), are more costly and are typically equipped with peripheral tools such as optical and thermal cameras, laser height sensors and other devices for real-time measurement of deposition quality. These two types of laser heads entered the market nearly 5 years ago and were employed in approximately half of the research articles published in 2024 and 2025, while the rest used lateral wire feeding. The deposition with lateral wire feeding can be realised using a regular laser welding machine, which is up to ten times cheaper than those with coaxial laser heads. However, as the competition among DED machine producers grows, coaxial laser heads are more affordable today than they were five years ago, and are expected to be more affordable in the coming years.

Motion control of the laser head is realised through two main approaches: by integrating the head into a CNC machine or mounting it on a robotic arm. The multi-axis CNC machining centres have been the main equipment for implementing DED, but this is increasingly shifting toward robotic arm-based systems. The CNC-DED integration differs from conventional expectations. Compared with the traditional machining centres, such as those used for milling or laser cutting, where the tool head is usually moved around the fixed or rotating workpiece, the DED machining centre often adopts a configuration in which the laser head is fixed, while the workpiece is moved across 3–5 axes. This choice is related to the complex structure of the laser head and the fact that the optical path is prone to misalignment during movement, as well as the gravitational effects on the melt pool and deposited material. In addition, CNC machining centres create a series of issues for DED, such as limited manufacturing space, the need for support structures in specific geometries, and insufficient equipment expandability. Therefore, researchers and producers are shifting to a second approach using multi-axis robotic arms or a combination of several arms. Robotic arms overcome the limitations in manufacturing space and support structures, especially when accompanied by a tilting rotary stage for the workpiece. In addition, robotic arms offer high adaptability and spatial flexibility, allowing the integration and simultaneous operation of multiple tools (e.g., IR camera) for in-situ monitoring of the deposition process [132–134]. The early prototypes of such a 3D printing approach used two robotic arms with a combined $3+3$ degrees of freedom for support-free extrusion-based AM of thin-walled parts [135]. Later, a

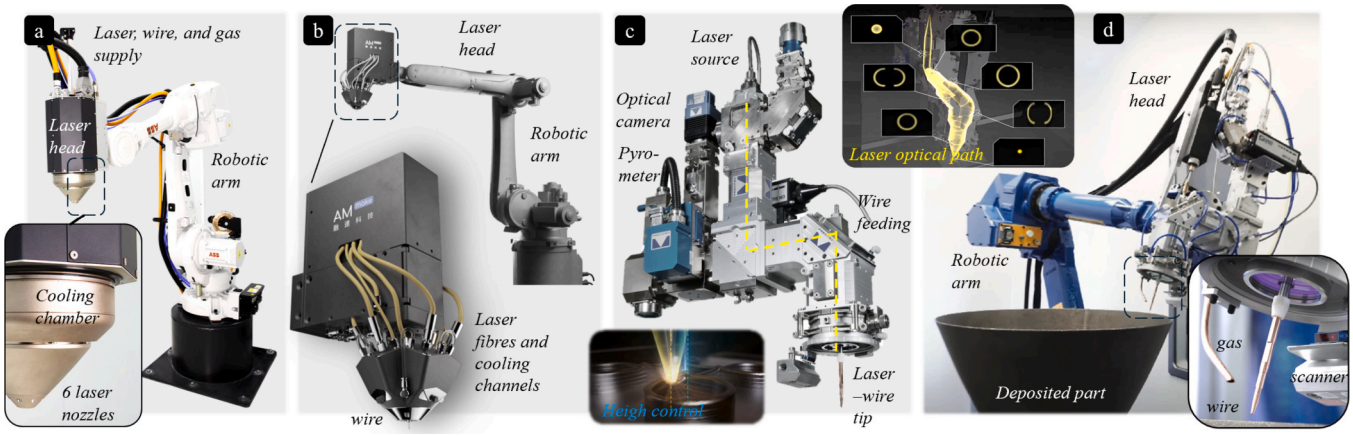


Fig. 5. Coaxial laser-wire systems for directed energy deposition: (a) Meltio Engine Blue head (Meltio3D); (b) RoboL1 Lite head with six lasers (Rongsu Tech); (c) CoaxPrinter head with deposition control system (Precitec); (d) AMDROiD head with power modulation system (Additec).

Table 1
Commercial LW-DED head systems and their characteristics.

Producer	Model	Laser configuration and type	Structure / Function	Advantages
Meltio	Meltio 450	Coaxial IR (1.2 kW)	6 lasers × 0.2 kW each, inert atmosphere chamber	Closed-loop, laser power and wire feed modulation, among the first systems on the market, well-documented performance in the literature
Rongsu	RoboL1	Coaxial Blue (1.5 kW)	6 lasers × 0.25 kW each, blue-light melt pool camera	Individual laser control for custom beam spot distribution, real-time melt pool monitoring, precision deposition
Precitec	CoaxPrinter	Coaxial IR (6 kW)	Beam shaping tools, deposition track scanning system	Real-time measurement of deposition depth and height, versatile settings for flexible deposition
Additec	AMDROiD X	Fibre IR (12 kW)	Multi-axis robotic integration system, thermal monitoring	Large-scale, high productivity, closed-loop laser power modulation using pyrometer

6-DOF Stewart platform manipulator was demonstrated for multi-directional printing of support-free structures capable of replacing the building platform of the printer [136]. In 2024–2025, several publications have shown LW-DED integrated with robotic arms, yet mostly for printing straight walls, cubes, or cylinders, which can be attributed to path programming complexity. The research on path planning in robotic-assisted AM to avoid collisions between the processing head and printed elements of complex non-planar components is still emerging [132–134,137]. In these studies, the print accuracy and forming quality are addressed via software development. For example, a multi-robot coordinate calibration method based on a cross-source 3D point cloud model for collaborative deposition [138], and an innovative arbitrary polygon division method and a hybrid path planning strategy based on tiny primitives [126] have been proposed. However, these approaches have yet to be integrated with the metallurgical aspects of LW-DED.

Auxiliary tools were integrated to improve specific aspects of the LW-DED process, such as increasing productivity, reducing microstructural defects, and monitoring the deposition process. Among the most studied auxiliary processes are inductive wire preheating [76,80,139–144], substrate preheating [145], laser beam oscillations [74,77,86,146–149], substrate vibration [150], and different sensors for geometrical [89,90,151], thermal [70,72,91,143,152–154], and microstructural [155–157] in-situ monitoring. Wire preheating decreases the amount of heat input needed from the laser, thereby enhancing the deposition rate of low-power laser heads [51,76], and can modify the melt pool behaviour and the quality of the deposited components by affecting the thermal history [105]. When the substrate is cold, the quality of the first deposited layer can be compromised by rapid cooling, triggering a heat sink effect that leads to defects such as cracks or voids in the cladding layer [158]. Substrate preheating can mitigate the first layer defects by slowing down the cooling rate during its deposition [158] and influence grain growth by lowering the thermal gradient within the deposited material [145]. Laser beam oscillations have been demonstrated to be an effective way to promote melt pool flow and improve the distribution of alloying elements [146] among other effects [74,77,86,146–149]. Ultrasonic vibrations applied to a build plate have shown a positive effect on grain refinement, yield and tensile strength [159], as well as texture

Table 2
Materials aspects summary for LW-DED processing.

Material	Applications	Issues in LW-DED processing	Process strategies
Stainless steel	High corrosion resistance, good mechanical properties, weldability	High thermal expansion, distortion and cracking [52]	Wire preheating refines microstructure [144], alloying with Mo reduces oxidation [217], alloying with Nb enhances hardness [219]
Ti-based alloys	High strength-to-weight ratio, corrosion resistance, biocompatibility	High residual stress, columnar grain growth, porosity [50]	Ultrasonic vibration improves microstructure [77], dual-wire oscillation reduces residual stress [86], melt pool size control reduces porosity [218]
Ni-based alloys	High-temperature strength, superior mechanical properties and wear resistance at high temperature	Complex phase transformations [157], solidification cracking [53]	Wire preheating reduces cracking [80], pre-melted wire suppresses columnar grains [157], oscillating laser refines grains [148]
Al-based alloys	High strength-to-weight ratio, high thermal and electrical conductivity, corrosion resistance	Low laser absorptivity [121], welding-induced oxidation, porosity and bonding issues [50]	Multiphase flow control can reduce porosity [70], oscillating laser improves strength and ductility [74], alloying with Cu and Mn improves weldability [146]
Tungsten	Extremely high melting temperature, high hardness, corrosion resistance, and strength at elevated temperatures	Low deposition rate [221], surface waviness and balling [221], difficult remelting and reprocessing [154]	Wire preheating could improve productivity [80], substrate heating could reduce cracks and porosity [154], surface waviness can be reduced by remelting [221]
Functionally graded materials	Tailored mechanical and thermal properties, reduced stress concentration	Interfacial defects [82], thermal expansion mismatch cracking [211], reduced deposition rate [86]	Laser shock modulation reduces porosity [82], multi-alloy transition improves bonding [211], dual-wire deposition enables composition control [86]
Metal matrix composites	Enhanced strength and stiffness, improved wear resistance and thermal stability	Particle agglomeration, interfacial instability, porosity [163], [164]	Premixing powder into wire improves efficiency, material distribution, and reduces porosity [210], oscillating laser reduces defects in powder-wire DED [74]

optimisation of the deposited steel [150]. Light-based CMOS sensors and laser scanners allow on-machine geometrical and surface waviness control of the built geometry [89,90,151]. Infrared cameras were used for in-situ observation of melt pool temperature, enabling closed-loop control systems [70,72,91,143,152–154], and have already been integrated into some commercial LW-DED printers (e.g., RoboL1 model by Rongsu Technology in Table 1). Operando synchrotron X-ray imaging and diffraction techniques have been used to penetrate relatively thick metal deposits to acquire information regarding the interior of the melt pool and microstructure [155–157]. Acknowledging the above progress, it might be worth noting that, while many of these tools are valuable for understanding LW-DED fundamentals, they may not always present a strong case for commercialisation due to added costs and complexity. For instance, wire and substrate preheating require additional heating structures and temperature monitoring units, while substrate vibration demands extra vibration generators and supporting control systems; laser beam oscillations typically rely on laser galvanometer scanning systems, which are relatively costly. The incorporation of these auxiliary devices, particularly the high-cost laser galvanometer systems, can significantly increase the overall equipment cost; however, these auxiliary processes typically improve material performance by approximately 5–20% [74,76,77,144–150]. Given the lack of systematic research on the comprehensive cost of such equipment, their commercial viability requires further investigation.

3.4. Hybrid systems

All manufacturing methods have limitations and LW-DED is no exception. LW-DED does not match conventional manufacturing in terms of forming accuracy and process stability, yet it has advantages that cannot be readily achieved by machining, particularly in handling complex internal structures and material utilisation, where LW-DED performs well. Thus, it has been recognised that combining LW-DED with conventional machining and other forming processes can significantly improve the overall manufacturing performance for a given component. Several types of hybrids exist: DED/CNC [160–162], wire/powder-laser DED [71,86,153,163–165], and wire-laser/arc DED [95], as shown in Fig. 6. Other hybrids exist, e.g., DED/LPBF [166], but these are not currently mainstream approaches.

Hybrid additive–subtractive manufacturing DED/CNC systems have attracted significant attention in the past decade, and the approach is now expanding from laser cladding of cylindrical components towards the deposition of complex structures. Whether used to improve part precision by first adding and then subtracting, or to enhance geometric complexity by first subtracting and then adding, the hybrid systems generally reduce material waste, tool wear, and associated costs [103, 167–169]. The hybrid approach was reported to reduce the manufacturing time for a steel impeller from 3536 min to 792 min (corresponding to a 77.6% reduction) and material waste from 74% to 9% compared with traditional machining [170]. Yet, machining of deposited material differs from machining conventional billets [160], and the deposition on a machined surface differs from deposition over previous beads [161]. The milled surfaces exhibit higher specular reflectivity compared to deposited surfaces, leading to a smaller melt pool and, if not compensated for, to inhomogeneous and anisotropic microstructures [161]. This could potentially be addressed by integrating a powder-blasting nozzle near the wire feeder to intentionally roughen the CNC-milled reflective surface prior to deposition; however, this approach remains largely unexplored [171,172]. Liu et al. [162] emphasised that hybrid process planning is still underdeveloped to meet the needs of interleaved additive and subtractive operation scheduling for arbitrarily shaped parts. The existing methods are effective only for 2.5D structures and structures with columnar features [162], highlighting a key challenge in robotics and computer-integrated manufacturing. Beyond physical integration, a digital thread for hybrid DED/CNC requires effective data fusion across additive and subtractive stages [170]. Process planning for DED/CNC remains fragmented: deposition parameters, monitoring data, and machining toolpaths are managed in separate software environments without interoperability [162]. A smart manufacturing framework could unify these layers through data schemas (e.g., MTConnect, OPC UA), enabling feedback loops where metrology data from CNC probing adjusts deposition strategies. Digital twins of hybrid cells could simulate the material state after each operation, guiding whether to add or remove material next. Such integration remains largely unexplored but is essential for autonomous, reconfigurable hybrid manufacturing.

Wire-powder DED hybrid systems aim to combine the high productivity of wire-fed processes with the higher accuracy of powder-fed systems. Powder-based DED offers higher accuracy compared to wire-based DED [173,174], yet it comes at the expense of lower productivity and material utilisation [51]. Several research teams have attempted to combine the advantages of both via synchronous or asynchronous feed of wire and powder in a single laser DED system with certain degrees of success [71,86,153,163–165]. Powder and wire can be used in two scenarios: to deposit separate regions of the component, or by feeding powder directly into the wire-formed melt pool. The first scenario creates interfacial issues. Although a defect-free interface between powder- and wire-deposited zones can be obtained [175], microstructure formation proceeds differently [175]. The remelting of grains in wire-deposited zones can act as nucleation sites for epitaxial growth in powder-deposited zones, which also exhibit higher Laves phase concentration and finer grain and dendritic sizes compared to

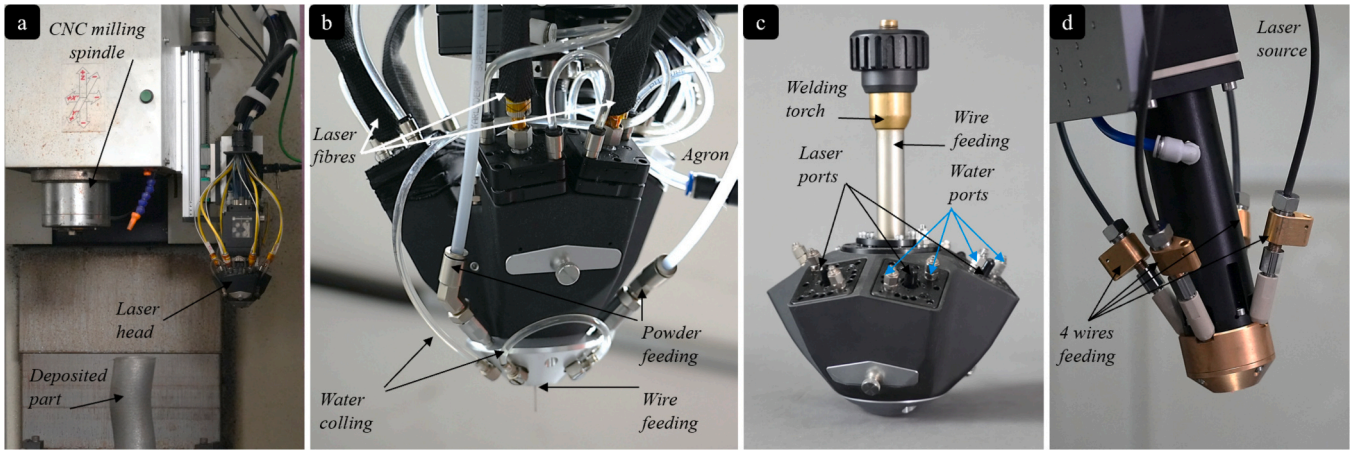


Fig. 6. Hybrid deposition systems: (a) LW-DED with CNC machining; (b) concurrent wire and powder feed laser-DED; (c) laser wire DED assisted by an electric arc torch; and (d) multi-wire laser DED. Photos courtesy of Rongsu Tech.

wire-deposited zones [175]. Parts with as-printed interfaces were reported to be 99.8% dense but exhibited poor dimensional accuracy [163]. Surface roughness is affected by powder feeding and impacts the absorption of the laser beam and, therefore, melt pool dimensions [163]. In cases where the powder metal has a considerably different melting point from that of the wire, the higher-melting-point material may require a surface treatment [176,177] similar to those applied before joining dissimilar materials [178–181] if metallic bonding is jeopardised. In the second scenario, called synchronous [182] or concurrent [183] deposition, the powder penetrates the wire-formed melt pool, yet not uniformly across its thickness. The kinetic energy of the high-velocity metal particle is converted into heat upon impact [184], facilitating its melting within the superficial layer of the melt pool. Five distinct trajectories of powder particles were observed before entering the melt pool, including direct entry into the melt pool, entry after impacting the wire, spattering onto the solidified region, deposition at the melt pool boundary, and rebound from particle agglomerates and solidified skins [153]. At a high powder feed rate, more bubbles occurred along the melt pool boundary or near the wire-melt pool interface [153]. The wire-powder deposited Ti–6Al–4 V samples demonstrated comparable strength to the forged Ti–6Al–4 V substrate (969.7–1015.5 MPa) and slightly lower elongation (9.1%–10.2%) [109]. However, to obtain those properties, the powder feed rate was set to just 0.08 kg/h [109], which is nearly an order of magnitude lower than the typical wire feed rate in most recent studies, thus evidencing a rather low (1/10) degree of powder-wire hybridisation. Bimetallic compositions, e.g., TC4–Cu functionally graded alloys with varying Cu compositions, were reported with up to 10% mixing ratio as well [182]. Combined wire- and powder-based DED processes have also been successfully demonstrated for joining dissimilar materials, e.g., NiTi and SS316L alloys [185]. Among disadvantages, the wire/powder combination reintroduces the issues related to workspace contamination and occupational health risks.

Wire-laser-arc DED hybrids may exhibit synergistic effects on productivity and energy efficiency. While LW-DED offers high precision, it has relatively low efficiency and high energy consumption, whereas arc-based wire DED has high productivity but poor precision and increased defect formation. The combination of laser and arc energy sources in a single wire-based DED system has been shown to improve productivity and energy efficiency of the process [95]. The interaction between plasma and laser is as follows: the plasma generated by the laser reduces the resistance of the arc channel, thereby increasing the utilisation rate of the arc energy. Simultaneously, the plasma modifies the arc characteristics by acting on the surface of the melt pool, thereby enhancing laser absorption. Consequently, the laser-arc hybrid AM offers high forming efficiency and good part quality [95]. Considering the forming accuracy, spatter level, and porosity, the process achieved parts with 0.7% porosity, 1% spatter, and 85% forming accuracy under optimal process parameters (1.2 mm AA2024 wire fed at 4.3 m/min under 2 kW laser power) with a deposition rate of nearly 0.8 kg/h [95]. Comparing these parameters to those of other studies, it can be tentatively suggested that, although not more productive, this hybrid process may be approximately 20% more energy efficient than LW-DED for similar alloys [186,187]. Another potential advantage is the dual thermal control capability for bimetallic deposition [188], as the energy input and spatial distribution [189] of laser and arc can be managed separately to tailor material properties [190].

Multi-wire deposition with typically two wires [191] or occasionally four wires [192] can offer higher deposition efficiency and a wider variety of materials [52] or even control bead width and height [192]. This flexibility means that the composition of the fabricated parts is no longer restricted to commercial wire materials. The metal composition of the parts can be tailored by controlling the relative feed rates of the two wires, enabling the formation of new materials with physical and chemical properties different from those of the base materials [86]. The deposition of dissimilar materials can proceed either sequentially (one-by-one) or simultaneously. Li et al. [191] used a dual-wire technique to merge TiNb and Al wires into a Ti_2AlNb alloyed component with a dual-droplet transfer control. The sensing, control, and influence mechanisms of droplet transfer distance in dual-wire deposition have been investigated, and a corresponding closed-loop control system has been developed. Other progress in joining dissimilar materials is discussed in the materials section. Aside from the interfacial and metallurgical issues of dual-wire deposition, the process can face a tool manipulation challenge, where one wire feeding head or several individual heads can collide with the previously deposited geometry. Thus, toolpath planning strategies must account for the increased geometrical complexity of the deposition system or the sequential manipulation requirements of multiple laser heads, further emphasising the importance of robotics in LW-DED research.

4. Material selection and processing characteristics

Before examining materials processability, the structure of this section is defined by the breadth of materials already processed via LW-DED. To date, LW-DED has been applied to more than 40 distinct metals and alloys, ranging from common engineering grades to specialised and niche materials. These include: 316 L, 316LSi, DSS 2209, DSS 2101, ER70S−6, ER110S-G, ER70S-X, 304, 201, 410, 52100, Q690D HSS, A36 mild steel, mild steel, Mn steel, X45CrSi9–3, 10CrNi3MoV steel, Ti−6Al-4V, TC11, TC4-Cu, AA7075, 2319 Al, 2320 Al, 5052 Al, 5356 Al, 5087 Al, 6082 Al, 5A06 Al, Al alloys, AlSi5, AlSi12, AlSi10Mg, AlMg5, Al-Mg-Sc, Inconel 625, Inconel 626 + Cu, Inconel 718, GH3039 Ni alloy, Ni + WC, NiTi (Nitinol), Ni–Al bronze, C103 Nb alloy, and tungsten. A detailed, mechanism-level analysis of precipitation behaviour, solidification pathways, and phase transformations for each individual material falls outside the scope of a single review section and would require a dedicated materials-focused study. Instead, the available literature is systematically organised by base metal class (e.g., Fe-based, Ti-based, Ni-based, Al-based), with emphasis on identifying common processing peculiarities. The discussion therefore focuses on how each class responds to laser absorption, melt pool dynamics, defect formation, and the recurring strategies used to mitigate these effects. The objective is to extract transferable, cross-study trends that inform parameter selection and process design across material classes. For alloy-specific and phase-resolved analyses, direct references to the original studies are provided.

Light absorption of metals determines the fraction of laser energy that is converted into heat within the metal. To demonstrate this fundamental dependency, we refer to the solar absorptance data collected by NASA in 1969 for 12 different metals by direct and indirect measurements over the temperature range 250–550 K [121]. Since the solar absorptance was largely independent of temperature within this range [121], the corresponding room-temperature absorptance values are presented in Fig. 7. It should be noted that these data represent broadband solar absorptance and are used here for qualitative comparison, rather than direct prediction of laser-material interaction. Metals such as gold and silver, which have high reflectance in the visible and near-infrared regions, show low absorptance. In contrast, metals such as titanium and vanadium display higher absorptance due to lower reflectance and increased intrinsic absorption. Lasers with various wavelengths can be used, such as red (630–670 nm), green (520–532 nm), and blue (450–500 nm), to compensate for the low laser absorptance by certain metals. Blue lasers are particularly efficient for depositing copper and gold, requiring approximately 4–8 times less energy in reported studies compared to red laser systems, consistent with the trends shown in Fig. 7. Although several commercial LW-DED systems have been introduced using alternative laser wavelengths, their adoption in the scientific literature remains limited. Among 90 LW-DED studies published in 2024–2025, only 51 explicitly reported the laser wavelength used, and none employed blue, green, or red lasers; instead, all relied on infrared sources in the range of 900–1100 nm. Infrared

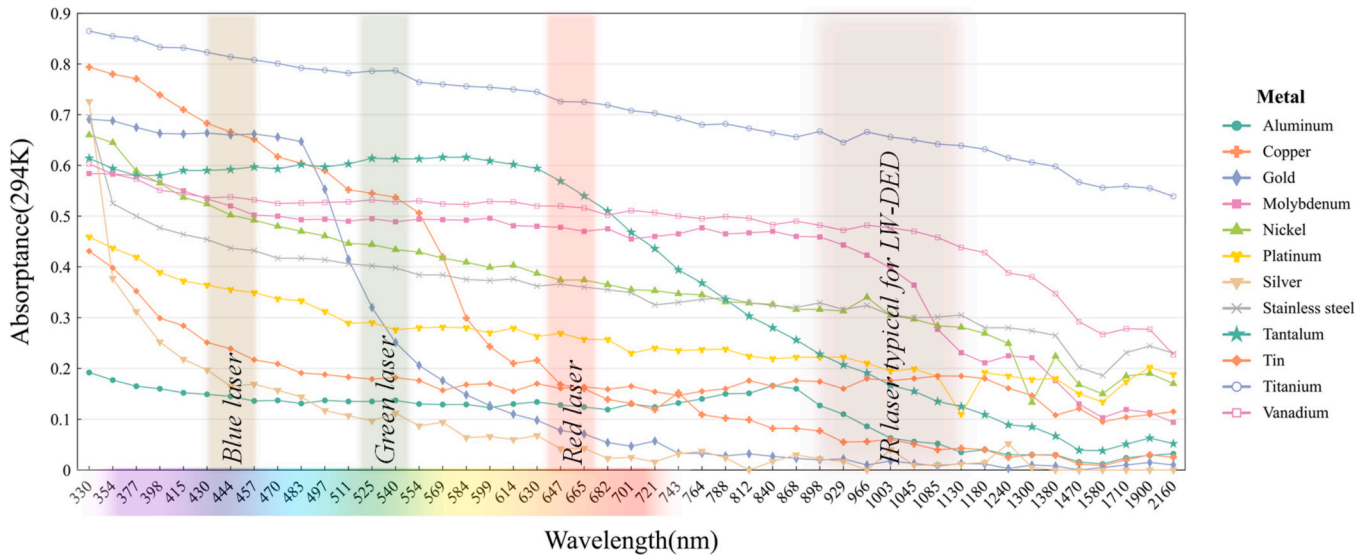


Fig. 7. Spectral absorptance of selected metals as a function of wavelength, based on NASA solar absorptance data [121], with indicative wavelength ranges of common industrial lasers.

lasers are typically less efficient for melting many engineering metals, requiring approximately 2–10 times more energy depending on the material (see Fig. 7). This observation suggests that the role of laser wavelength is often underreported or insufficiently discussed in current LW-DED research, as nearly half of the studies do not specify this parameter in the Materials and Methods section. One possible explanation lies in industrial practice, where the higher cost of alternative laser sources (e.g., blue lasers) may not always be offset by the potential gains in energy efficiency. In addition to higher costs, blue lasers dissipate more energy along the optical path than infrared lasers, limiting their maximum operational power. Despite recent progress by DED system manufacturers in reducing energy losses in optical fibres (from approximately 10% to around 3%), this still results in about 30 W of heat dissipation within the laser head per 1 kW of laser power, contributing to thermal loading of the system. Consequently, commercial LW-DED systems employing blue lasers are typically limited to power levels of 1–2 kW. Higher-power blue laser systems require alternative optical designs, which are likely to increase head dimensions or reduce process flexibility. Furthermore, blue lasers exhibit significantly higher absorptance than infrared lasers at room temperature; however, this difference decreases at elevated temperatures approaching the melting point. Since a substantial portion of the deposition process occurs after the melt pool has been established, the practical advantage of blue lasers in terms of absorptance may be reduced. Therefore, blue lasers do not necessarily represent a definitive next step in LW-DED process physics, and their overall value in industrial manufacturing contexts remains to be fully validated.

Different metals require different amounts of energy to deposit a unit mass of material. Fundamentally, thermophysical and optical properties of metals, such as heat capacity, melting temperature, latent heat of fusion, thermal conductivity, density, and laser absorptivity, influence the amount of laser energy needed to create and maintain the melt pool [186]. Thus, high-entropy alloys generally require higher energy input per unit mass of deposited material compared to low-melting-point alloys. Based on this reasoning, one might expect higher deposition rates for Fe-, Ni-, and Ti-based alloys compared to Al- and Cu-based alloys under similar power conditions. However, this is not consistently observed in the reported literature. Deposition rate is primarily governed by process parameters (e.g., wire feed rate and power settings), rather than intrinsic material thermodynamics alone. We collected experimental data from 88 studies published in 2024–2025 [52,63,70–80,82–86,88–91,98,139–149,151,152,154–157,163–165,170,186,187,193–234] and calculated (where not directly reported) the deposition rate (kg/h) and specific deposition energy (kJ/g) for five alloy groups, as shown in Fig. 8. The data highlight a highly scattered trend resembling a logarithmic decay of specific deposition energy (kJ/g) with increasing deposition rate (kg/h), indicating improved energy efficiency at higher deposition rates. In addition, a slight vertical separation between the alloy groups suggests that, in the current state-of-the-art, deposition of aluminium and titanium alloys often requires – on average – nearly twice as much energy (≈15 kJ/g) compared to stainless steels and Inconel (≈8 kJ/g). In some studies, significantly higher energy demand (up to 50 kJ/g) was reported when depositing W-, Ti- and Al-based alloys at lower deposition rates (<0.4 kg/h); however, those studies were not focused on productivity. In a further attempt to explain the data scatter, deposition rate was plotted against individual process parameters and their combinations. A weak correlation was observed with respect to laser power; however, higher laser power did not consistently result in increased productivity (see upper right corner of Fig. 8). This suggests that wire feed rates are often not optimally matched to the applied laser power. Overall, robust parameter selection guidelines are still lacking. Finally, each group of alloys exhibits specific processing peculiarities, as briefly detailed below.

4.1. Stainless steel

Stainless steel, particularly 316 L, is the most studied material for LW-DED, e.g. [72,75,143,145,163,197,198,200,204,235,236], accounting for nearly 40% of all studies published in the past few years, due to its excellent corrosion resistance and mechanical strength. The unique advantage of LW-DED for forming stainless steel parts consists in a moderate solidification regime, between casting and L-PBF, where cooling is fast enough to avoid cast-scale segregation but slow enough to preserve controllable δ-ferrite/austenite (F/A) competition rather than forcing the almost fully austenitic, high-undercooling state common in L-PBF [200]. DeNonno et al. [200] showed that laser-wire DED can switch 316 L solidification between F-A and A-F, producing skeletal, lathy, or interdendritic δ-ferrite depending on solidification velocity, composition and shielding, while the ferrite/austenite orientation relationship controls the final build-direction texture. Bernauer et al. [145] further showed that LW-DED thermal history is not a passive consequence but a tunable variable: melt-pool temperature rises with build height, cooling rate falls, the primary dendrite arm spacing coarsens, improving plasticity. This layerwise reheating is largely absent in

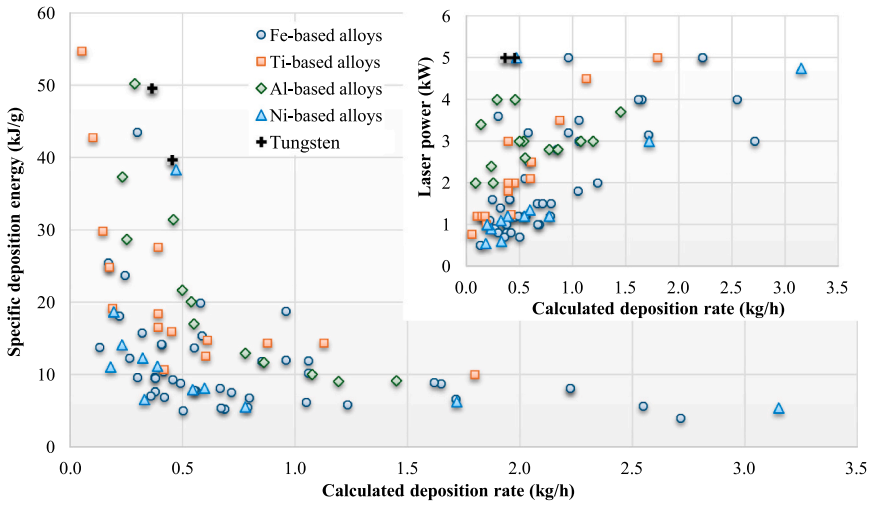


Fig. 8. Specific deposition energy as a function of deposition rate in laser wire DED, with data points calculated from process parameters reported in [52,63,70–80,82–86,88–91,98,139–149,151,152,154–157,163–165,170,186,187,193–234]. The inset shows the relationship between laser power and deposition rate.

casting, where heat extraction is bulk-scale and mold-controlled, and it differs from L-PBF, where extremely small melt pools and high scan speeds suppress much of the ferrite-retention window [200]. The defect formation physics in LW-DED steel can also be different: Ai et al. [204] showed that wire-fed deposition can be realized via droplet transfer, Marangoni flow, free-surface oscillation and corrugated bead formation, meaning defects arise from melt transfer rather than powder spreading or powder denudation. Aditya et al. [72] showed that conduction mode is the preferred stability window; balling appears at insufficient energy, while excessive energy drives keyhole penetration and vapor-pore risk. Xiao et al. [197] made this distinction sharper by deliberately moving the keyhole into the wire rather than the substrate, increasing absorption and deposition efficiency while avoiding substrate keyhole porosity. Compared with powder DED and L-PBF, wire also changes contamination physics: Kushwaha and Basak [198] found wire-fed 316 L had smoother surfaces and fewer oxide inclusions than powder-fed deposits. LW-DED is therefore uniquely suited to stainless steel when the target is not just density, but controlled ferrite retention and large-section epitaxy. However, the thermal properties and susceptibility to oxidation of stainless-steel present challenges in achieving uniform deposition and defect-free microstructures. Among the attempts to handle process stability, Aditya et al. [72] highlighted the need to optimise wire feeding direction (in a non-coaxial process) to achieve an optimal penetration-to-width ratio of 3/2, enhancing the tensile strength and interlayer bonding. Adjustments in laser power and scanning speed affected the cooling rate and consequently the microhardness of the clad layer [209]. Although most process parameters can affect microstructure, their effect on mechanical properties can be overestimated [237]. Another approach to influence deposition of steels is microalloying, where the introduction of trace elements such as Mo has been shown to refine grain structures and enhance corrosion resistance [217]. For corrosion resistance, deposited steel can undergo laser nitriding during post-processing. Li et al. [219] found that Nb-containing stainless steels deposited via LW-DED exhibit higher hardness and pitting resistance. Deposition of steels can also be improved by promoting controlled cooling rates using induction assistance, specifically, synchronous induction-assisted LW-DED was found to increase heat outflow velocity by a third, which refines grain structures and reduces microcracks [144].

4.2. Titanium alloys

Titanium alloys, particularly Ti−6Al-4V, are the second most researched material class for LW-DED [71,77–79,83,141,155,195,213,218], driven by their high strength-to-weight ratio and superior biocompatibility, which are critical for aerospace and biomedical implant applications, respectively. The advantage of LW-DED for titanium alloys lies in a thermokinetic window that neither LPBF nor casting can reproduce: a large, directionally solidifying melt pool combined with near-β-transus reheating, delivering not just deposited Ti−6Al-4V but thermally re-transformed during deposition [141,195]. Chainiau et al. [195] showed thermal bands matching deposited beads with columnar prior-β grains and basketweave α/β with location-dependent α-lath size, proving that earlier layers are repeatedly rewritten by later thermal cycles rather than frozen once as in casting. Halder et al. [141] showed that this repeated thermal cycling controls α-variant selection: slower cooling and shorter interlayer delay strengthen type−2 α/α boundaries and create white bands with fewer α variants than surrounding bulk, directly linking LW-DED thermal history to texture-mediated anisotropy. This is fundamentally different from LPBF, where extreme cooling commonly drives α′ (alpha-prime) – martensite in Ti−6Al-4V, which forms when β-phase cools extremely fast. Lee et al. [83] showed that laser-wire deposited Ti−6Al-4V can avoid LPBF-like α′ when interpass temperature is controlled. Fu et al. [155] made the mechanism explicit: increasing heat input shifted the transformation from acicular α′ toward lamellar α + β and finally basketweave α + β, meaning LW-DED can suppress or decompose martensite in situ rather than relying only on post-build heat treatment. Wire laser deposition of titanium alloys also has specific defect physics. Abranovic et al. [98] showed that Ti−6Al-4V defects can originate from wire dripping, arcing, melt-pool oscillation and stubbing. Arcing can trigger keyhole flaws and oscillation changes bead width creating inter-bead void risk. This is unlike LPBF, where defects are dominated by powder spreading, denudation, lack of fusion between powder layers and keyhole collapse. Titanium also makes shielding integral to the physics, not an auxiliary condition: Barroi et al. [79] and Orue et al. [78] showed that oxygen protection is essential for preventing α stabilization and brittle α-case. Finally, wire diameter and laser-power scheduling allows to tune heat accumulation, cooling rate, α-lath coarsening, prior-β grain size, porosity and strength, proving that LW-DED gives titanium a controllable route between cast-scale coarseness and LPBF martensitic brittleness [139,218]. However, when depositing these alloys via LW-DED, there is a tendency for columnar grain growth, porosity, as well as high residual stresses. As a partial solution, different vibration sources have been shown to be effective in grain refinement, porosity reduction, and mechanical property enhancement. Dual ultrasonic vibration treatment reduced grain size fourfold (from 1 to 2 mm to <500 μm), while increasing yield and ultimate tensile strength by nearly 25% [77].

Oscillating laser beams have been found to reduce peak temperature by nearly 20%, leading to a 15% improvement in layer uniformity and a 10% reduction in residual stress [86]. Zhang et al. [139] pointed out that low laser power settings may increase porosity due to inadequate melting, while excessive laser power introduces thermal stress and melt pool instability. Compared to samples fabricated with constant laser power, a more uniform and consistent microstructure was observed in the samples fabricated using layer-varying laser power. Later, Zhang et al. [218] reported that larger Ti−6Al-4V wire diameters led to increased microstructural defects and reduced tensile properties, primarily due to inconsistent melt pool sizes, greater heat accumulation, and lower cooling rates.

4.3. Nickel-based superalloys

Nickel-based alloys, such as Inconel 625 and 718, as well as NiTi and Ni–Al alloys, are the next most researched class of materials for LW-DED [75,76,80,82,148,156,157,193,212,227], which are favoured for high-temperature applications but are prone to solidification cracking due to complex phase transformations. Wire laser deposition is uniquely advantageous for nickel-based alloys because its melt pool gives direct control over the exact variables that make Ni alloys difficult: Nb/Mo segregation, Laves formation, dilution, cracking, and heat-affected precipitation. In Inconel 625, Su et al. [76] showed that hot-wire laser deposition separates the energy roles: resistance heating softens/melts the wire, while the laser mainly sustains the melt pool, enabling 1.7 kg/h defect-free deposition without the excessive laser heat input that would otherwise enlarge the pool, slow solidification, and intensify interdendritic segregation. This is fundamentally different from LPBF, where powder melting occurs in very small, rapidly solidified pools and defects are dominated by powder spreading, keyhole collapse, lack-of-fusion between tracks, and spatter. In Inconel 718, Gao et al. [157] showed that under energy-deficit, the wire can reach the melt-pool bottom incompletely melted and release sub-micron carbide particles near the mushy zone, suppressing columnar grain growth and refining microstructure. This means that, in LW-DED, the feedstock is also a physical actor inside solidification, its melting state can introduce heterogeneous nucleation sites, a mechanism absent in casting and LPBF. Preis et al. [82] showed that travel speed can move Inconel 625 from a mainly columnar structure to a refined columnar-equiaxed mixture by changing solidification rate and thermal gradient. The high-speed condition increased solidification rate and reduced thermal gradient, improving build-direction yield strength through microstructural refinement and dislocation strengthening. Casting cannot offer this local, layerwise control: it usually produces coarser dendrites [76], larger segregation length scales, shrinkage/gas porosity, and long-cycle post-processing needs [193]. Thus, LW-DED is uniquely powerful for nickel alloys because it converts their main weakness (segregation-sensitive solidification) into a tunable processing variable. Preheating strategies and optimised laser parameters have been shown to mitigate defects and improve ductility of Ni-based alloys. Inductive heating of the wire has often been used to increase the deposition rate of Ni-based alloys [80,143,229]. Preheating the wire increased deposition efficiency to 3.1 kg/h (a record-high deposition rate for LW-DED) and improved hardness to 253.5 HV while preventing additional crack formation [80]. In an operando synchrotron study by Gao et al. [157] regarding the effects of melting and solidification in Inconel 718, it was shown that microstructure can be controlled using wire feeding. The X-ray diffraction provided direct evidence that, when the insufficiently melted wire reaches the melt pool bottom, it releases solid particles, primarily carbides, suppressing the growth of large columnar grains and causing the formation of unique microstructural heterogeneity [157]. However, with appropriate laser scanning strategies [190], the mechanical properties of Inconel alloys can surpass AMS5662 forging standards. For Inconel, Zhou et al. [159] reported that the UV assistance resulted in refined grain structure (from mm to <100 μm), equiaxed crystallization, homogenized element distribution, decreased proportion of the Laves phase, and increased strength (from 750 MPa to 830 MPa). For Ni-Al bronze, oscillating laser processing can be used to reduce grain size, e.g., from 120 μm to 75 μm [148]. Subsequent heat treatment at 675°C for 6 h resulted in a 12% increase in ultimate tensile strength (from 557 MPa to 626 MPa) and a 13% improvement in hardness (from 162 HV to 183 HV), albeit at the cost of a 6.7% decline in corrosion resistance due to increased κ-phase precipitation [148]. Generally, maintaining stable deposition of Ni-Al bronze is challenging, reducing the achievable deposition rate to around 0.5 kg/h [227].

4.4. Aluminium alloys

Laser deposition has been investigated for a range of aluminium alloys, including 7075 [210,234,238], 2320 [146,147], 5356 [216], 5A06 [86,186,232], AlSi- and AlMn-series [70,74,151,187,196,224]. LW-DED is advantageous for aluminium alloys because it allows better control over problems that make aluminium difficult in laser processing: high reflectivity, high thermal conductivity, low viscosity, hydrogen porosity, hot cracking, solute evaporation, and unstable wetting. Unlike LPBF, where aluminium is processed through 25–50-micron layers dominated by powder packing, oxide films and denudation, in LW-DED, the 0.5–1.5 mm thick wire adds a beneficial thermal and mechanical boundary condition versus oxidation, defects and weak texture. This is why LW-DED is not simply a larger laser processing for aluminium, but a different solidification platform. Mao et al. [147] showed that 8-shaped beam oscillation in Al-Cu deposition redistributed laser energy, reduced the thermal gradient, intensified melt convection and promoted columnar-to-equiaxed transition; the result was lower porosity, lower crack density, weaker texture, reduced grain-boundary Cu segregation and much higher tensile strength than non-oscillating. In the Sc-modified Al-Cu system, the same oscillating wire process became a true in-situ microalloying route: Al_3Sc particles supplied heterogeneous nuclei, refined the grain size down below 20 μm (very fine as for DED), while suppressing θ/θ'-Al_2Cu segregation at grain boundaries [146]. Casting cannot reproduce this because the alloy solidifies once under mold-controlled heat extraction. LW-DED repeatedly remelts and reheats each layer, so nucleation, epitaxy, solute partitioning and precipitate distribution can be rewritten locally [146,147]. For crack-sensitive AA7075, Wang et al. [234] showed that cracking is governed by melt-pool lifetime and maximum melt-pool temperature: insufficient backfilling of solidification shrinkage initiates solidification cracking, while later reheating drives downward liquation cracking and upward solidification cracking. This makes LW-DED useful because cracking can be mitigated through pool lifetime and heat accumulation control, not only through post-processing. Defect physics is also aluminium-specific: high-speed deposition hump defects arise from backward molten-metal accumulation, recoil pressure, surface tension and flow instability, not from LPBF-style powder-bed melting [186,232]. Multi-layer simulations further showed that heat accumulation increases with layer number, but layerwise laser-power attenuation stabilizes flow and improves bead geometry [86]. However, like in welding, aluminium alloys pose significant challenges in LW-DED due to their low laser absorptivity, formation of a high-melting-temperature oxide film and porosity [121]. Aluminium rapidly oxidises when not properly shielded, forming a thin oxide layer with a far higher melting temperature (2072 °C) than aluminium (660 °C). By the time the oxide film is melted, the aluminium melt pool may become too large and unstable, jeopardising geometrical accuracy of the bead and its interlayer bonding. Thus, proper gas shield is necessary [238]. The dynamics of hydrogen bubbles within the melt pool of aluminium alloys lead to significant porosity in the solidified part [70]. The hydrogen pores mainly form at the interface between columnar and equiaxed grains, because the lower solidification rate in columnar regions limits the ability to trap hydrogen bubbles. The bubbles are prone to escape due to strong flow (Marangoni effect) in the top region of the melt pool [70].

This makes aluminium alloys highly sensitive to laser power and scanning speed. Huang et al. [186] reported that, under a laser power of 3 kW, hump defects occur when the travel speed exceeds 3 m/min. Adjusting process parameters such as wire feeding angle and laser incidence angle was not sufficient to suppress these defects. The multiphase flow simulations in [70] revealed that hydrogen pores larger than 50 μm were trapped at the columnar-equiaxed transition, reducing ductility by 23%. Liu et al. [70] pointed out the need to adjust the wire feed angle and scanning speed to reduce porosity and improve strength. Laser oscillation was reported to have a strong effect on the deposition quality of aluminium alloys [86]. Oscillating LW-DED of SiCp/Al composites resulted in a 35% increase in tensile strength and a 14.5% improvement in ductility [74]. Based on [151,187], Al-Cu-Mg alloys appear to exhibit superior weldability and mechanical stability under high-temperature conditions, and demonstrate lower residual stress and higher thermal conductivity compared to AA7075 [146]. Liu et al. [196] extended LW-DED processing to cable-stranded wires of Al50Si6Ti8-Fe12Cu12Ni12 and Al50Si6Ti8Cr12Cu12Ni12 – two novel lightweight aluminium-based high-entropy alloys with good high-temperature fluidity, enabling uniform cladding layers. Further studies on process-microstructure-property relationships in LW-DED of aluminium alloys can be found in [196,216,220,232,234]. Overall, aluminium is a particularly challenging material to process.

4.5. Tungsten

The possibility of depositing tungsten components is of particular interest, as tungsten is extremely difficult to manufacture using conventional methods and most other AM routes. Its exceptionally high melting temperature (3422 °C) and intrinsic brittleness severely limit processability. Unlike stainless steels, titanium alloys and nickel superalloys, tungsten offers virtually no solid-state phase transformation to alleviate residual stresses or accommodate thermal strains during processing. Consequently, defect formation is governed predominantly by thermal gradients, wetting behaviour and crack propagation. In this regard, LW-DED fundamentally differs from LPBF, where defects are typically associated with powder spreading, denudation, incomplete melting and keyhole collapse. Instead, LW-DED tungsten is governed by wire–melt pool interactions, gas entrapment, balling and thermal-stress-induced cracking [221]. Notably, several challenges typically associated with AM of tungsten can be mitigated in LW-DED. For example, low-porosity layers and stable stacking without delamination have been demonstrated. Tweer et al. [221] showed that the deposition of tungsten onto tungsten substrates using the LW-DED process is feasible. They optimised first a single melt path, and then a multilayer build. Importantly, stable deposition was only achieved when the wire was positioned at the leading edge of the melt pool, demonstrating that wire-pool coupling becomes a primary governing mechanism in tungsten processing. This behaviour is fundamentally different from powder-bed processes, where feedstock delivery and melt-pool formation are largely decoupled. Surface waviness increases with increasing number of stacked layers; however, it can be reduced below 100 μm by remelting [221]. Beyond improving surface quality, remelting also modifies the underlying thermal history, locally recrystallising previously deposited material and altering the heat-affected zone. However, excessive remelting energy may increase pore formation, highlighting the narrow process window imposed by tungsten's extreme thermophysical properties [221,239]. The microstructure of the solidified tungsten consisted of large epitaxially grown grains elongated in the Z-direction but with relatively random crystallographic orientations, which is potentially favourable for more isotropic mechanical properties. This epitaxial grain growth is particularly significant because it represents a fundamentally different solidification from both casting and LPBF. Casting typically produces large equiaxed or dendritic grains controlled by mould-scale heat extraction, while LPBF generates numerous micron-scale melt pools characterised by extremely rapid solidification. In contrast, LW-DED produces directional solidification over larger melt pools, enabling continuous epitaxial growth directly from the substrate and previously deposited layers [221]. Notably, one of the most powerful laser heads on the market (5 kW) was required to deposit 1-mm diameter tungsten wire at 0.4 m/min feed rate [221], which is 2–3 times less productive than depositing stainless steels [198,219,220], nickel-based alloys [76,82], and titanium alloys [78,228], due to the extremely high melting temperature of tungsten. Nevertheless, productivity is not the principal value proposition of LW-DED tungsten. Rather, its unique capability lies in enabling localised material addition, remelting and microstructural reconstruction in regions where conventional manufacturing or replacement would be impractical. In a subsequent study, Tweer et al. [154] demonstrated that LW-DED can also be used for crack healing in thermally-damaged tungsten components, such as plasma-facing components, by laser remelting the cracked and roughened zones and depositing additional tungsten onto the treated region. Following repeated thermal shocks, crack networks extending hundreds of micrometres into the substrate were successfully removed through deposition of approximately 500 μm of new tungsten, producing metallurgically bonded repairs with area densities exceeding 99% [154]. The deposited layer not only restored lost material but also re-engineered the near-surface microstructure through local remelting and recrystallisation, something that neither casting nor most other AM routes can achieve in situ. In general, AM of tungsten remains highly challenging for LPBF and nearly infeasible for sinter-based AM processes. The above discussed studies of Tweer et al. [154,221,239] collectively evidence that LW-DED is uniquely suited to tungsten because it combines directional epitaxial rebuilding, crack healing, local remelting, near-complete feedstock utilisation and repair of high-value components within a single process chain, thereby overcoming limitations that continue to restrict alternative manufacturing routes.

4.6. Functionally graded materials

The possibility of producing functionally graded materials (FGMs) has been well explored with wire-arc DED [52], yet only a few reports exist on processing FGMs via LW-DED. Laser wire deposition is advantageous for FGMs and bimetallic structures because it treats the interface as a controllable transient thermochemical zone rather than as an abrupt joint or uncontrolled bulk-mixing region. In LPBF the material switching is constrained by powder exchange and mixed-powder contamination, while in casting the interface formation is governed by bulk melt mixing and slow, mold-scale solidification. It is more readily controlled in LW-DED, especially for metallurgically compatible alloys. Feng et al. [240] successfully deposited 308 L and 304 graded steel components. In SS316L–Inconel 625, Tyagi et al. [75] showed the defect-free only 50 μm thick interface with epitaxial columnar grain growth from SS316L into Inconel 625, low-angle grain boundaries leaning toward the Inconel side and a strong $< 001 >$ build-direction texture. The interface hardness fell between the parent alloys, showing a real graded transition rather than a brittle fusion boundary. The same study contrasts this with reported LPBF SS316L–IN718 interfaces, where transition zones were thicker and interface cracking occurred because residual and thermal stresses were less effectively relieved [75]. The unique physics is not only compositional but thermo-fluidic: Huang et al. [86] showed that oscillating dual-wire laser deposition can reshape the melt pool by redistributing heat and stabilizing flow. Circular oscillation produced more uniform heat distribution and stable molten-pool circulation, while frequency and amplitude controlled melt-pool depth, peak temperature, width and wire-melting stability. This matters for FGMs because dilution, intermetallic formation and cracking depend on how long dissimilar elements remain in the liquid and how strongly Marangoni flow mixes them before solidification. Biester et al. [199] demonstrated another distinct advantage: LW-DED can create a hard/ductile material architecture before forming, depositing X45CrSi9–3 and X2CrNiMo19–12 layers onto a C22.8 steel core. Subsequent die forging redistributed the layers,

refined the weld microstructure and retained martensitic hard regions up to 700 HV for wear resistance [199]. This is not achievable by casting or LPBF in the same process chain because the graded layer is deliberately placed before thermomechanical redistribution. However, Yao et al. [211] show the limits of this approach: direct TC11–304SS deposition produced delamination or cracks because Fe and Ti interdiffusion formed FeTi/Fe_2Ti-type intermetallics and hardness peaks up to 550 HV, while TC11–pure Ti bonded much better. Lawson et al. [212] co-deposited Inconel 625 and GRCop−42 (70 and 30 wt%, respectively) within each weld bead. The first one is a nickel superalloy offering high strength at elevated temperatures, whereas the second one is a dispersion-strengthened copper alloy that provides high thermal conductivity. Applications for pairing these materials include nozzle liners in rocket engine combustion chambers or heat exchangers. He et al. [220] employed in situ laser shock modulation of the melt pool to reduce porosity defects at the interface between a 7075 aluminium alloy substrate and a 304 stainless steel deposit. At present, no large-scale demonstrator components are available in the literature to illustrate LW-DED of FGMs, highlighting the early stage of development of this field. In general, LW-DED is advantageous for FGMs and bimetals because it makes dilution, epitaxy, heat flow, layer chemistry and interface hardness designable, yet just as other AM, it cannot completely override intrinsically brittle phases.

4.7. Metal matrix composites

Metal-matrix composites (MMC) can be deposited via LW-DED in two ways: by using composite or powder-filled wires, or by spraying the ceramic powder over the metallic melt pool. The first scenario requires custom wire composition and is thus not readily available, while the second scenario is more easily implemented by adding a powder feeding nozzle into the LW-DED system similar to those used in metal spray [241] or abrasive jet systems [242]. The incorporation of reinforcement during deposition rather than relying on pre-mixed powder or bulk melt stirring is the exact advantage of LW-DED for metal matrix composites over other routes. Zhou et al. [164] fabricated SiC-reinforced stainless-steel parts using a coaxial wire-powder-fed DED hybrid process. In their study, ceramic particles were fed above the laser spot focused on the steel wire, embedding them into the melt pool, resulting in a relatively high concentration of particles at the layer interfaces. SiC particles increased porosity in the samples and promoted the δ-ferrite phase; they also reduced average grain size, thereby enhancing tensile strength and reducing the ductility of the composite [164]. At the same time, higher SiC content reduced melt-pool temperature and length, weakened convection, increased particle floating time, promoted particle islands and changed porosity distribution [164]. Therefore, MMC defects in LW-DED are not only powder defects, but flow-solidification defects. Xu et al. [74] showed this more deeply for SiCp/Al: ordinary LDED produced discontinuous Al_4C_3 at the SiC/Al interface, while oscillating LDED increased peak-temperature duration, broadened compositional undercooling and promoted finer, denser Al_4C_3/Al_4SiC_4 carbides with diverse crystallographic orientations. This created an interlocking high-entropy interface with coherent boundaries, improving matrix strengthening by 50 MPa, load-transfer strengthening by over 20 MPa, tensile strength by 1/3, and ductility by 1/6 [74]. This is different from LPBF, where reinforcement is trapped in rapidly solidified powder-bed pools with limited control of particle residence time, and from casting, where long liquid residence promotes flotation, sedimentation and coarse reaction layers. Waqar et al. [210] deposited titanium carbide reinforced aluminium matrix composites using an AA7075 wire containing TiC particles (1% volume fraction). The microstructure was found to contain mainly θ-Al Cu particles with clusters of TiC nanoparticles. Despite a fine grain size of 19.02 μm, there were limitations to the grain refinement and extent of equiaxed grains achieved, as agglomerations of TiC particles observed around intermetallic phases indicated a non-optimal level of TiC particles [210]. Gao et al. [188] introduced up to 6% of TiC microparticles into martensitic high strength steel; exceeding this ratio resulted in TiC particle agglomeration and reduction in material plasticity. While not an MMC, it is noteworthy that Lv et al. [243] successfully deposited quartz glass. They conducted a large number of experiments (3 ×64 ×4 trials) and identified relatively low process parameters. In particular, the laser power was 0.13 kW, which is approximately an order of magnitude lower than that used for metal deposition. Nevertheless, glass deposition via LW-DED remains a unique capability and has potential for both MMC and FGM applications, especially given that the fabricated parts were fully transparent [243]. The value of LW-DED for MMCs is not perfect dispersion, but it is the ability to tune whether particles survive as inoculants, react into beneficial carbides, float, cluster, or become trapped as defects.

5. Parameters-structure-property relationships

5.1. Geometrical and surface quality

The geometrical quality of LW-DED parts is generally less competitive compared to many AM methods because it is strongly affected by process instabilities. Even small deviations in layer height or bead width can accumulate and destabilise the build. Unlike powder-based DED where the melt pool self-regulates by partially rejecting unmelted particles when the temperature drops, the wire-fed process continuously supplies 100% of the feedstock into the melt pool; therefore, any mismatch between the intended and actual deposit height immediately impacts process stability, leading to further geometrical deviations. Typical unstable regimes include incomplete melting (insufficient energy input leading to discontinuous deposition), stubbing (wire not fully melting and protruding into the bead), and dripping (excessive melt causing droplets to be deposited in both intended and unintended locations) [84] (Fig. 9a). Due to inherent stochastic fluctuations during deposition, the boundaries between these regimes are often indistinct in practice; however, understanding these regimes allows intuitive correction of energy input. High scan speeds can also induce periodic bead irregularities known as hump defects, as the rapid motion and insufficient time for melt redistribution cause the molten metal to develop into ripple-like instabilities [226] (Fig. 9b). There is a critical scan velocity beyond which the combination of a narrow melt pool and high surface tension leads to backward-flowing liquid and eventually leads to jet-like ejections of melt that form humps [204]. All these phenomena adversely affect the dimensional fidelity, surface roughness, and overall morphology of the deposited part. It is often argued that most LW-DED parts need CNC post-processing anyway to achieve a net shape. While this is true, larger geometrical errors and waviness significantly increase post-processing time and cost (see the technoeconomic analysis section below). A thicker deposited allowance for CNC milling requires more passes of the cutting tool, and this also applies to other post-processing steps. Biester et al. [199] demonstrated this in a forming scenario: they deposited a steel wire onto a gear preform and then hot-forged it into a bevel gear. When a thin cladding (1.5 mm) was used, approaching the accuracy of LP-DED [173,174], the extreme deformation during forging caused the clad layer to thin unevenly and led to a risk of cracking; doubling the initial deposited layer thickness to 3 mm helped reduce this thinning and prevented cracking. Despite process optimisation, it was observed that the clad layer thickness after forming was still non-uniform at different tooth locations. This highlights that even post-deposition processes rely on consistent additive geometry. Therefore, a uniform additive layer ensures more predictable outcomes in subsequent operations.

Depositing defect-free geometry, or at minimum closely matching the CAD model, requires consistent maintenance of layer height and bead cross-section. Several works have developed closed-loop control strategies for this purpose. Bernauer et al. [88,90] implemented a segmentation-based feedback control approach using a laser line scanner to map each layer's top profile and dividing the weld bead into small

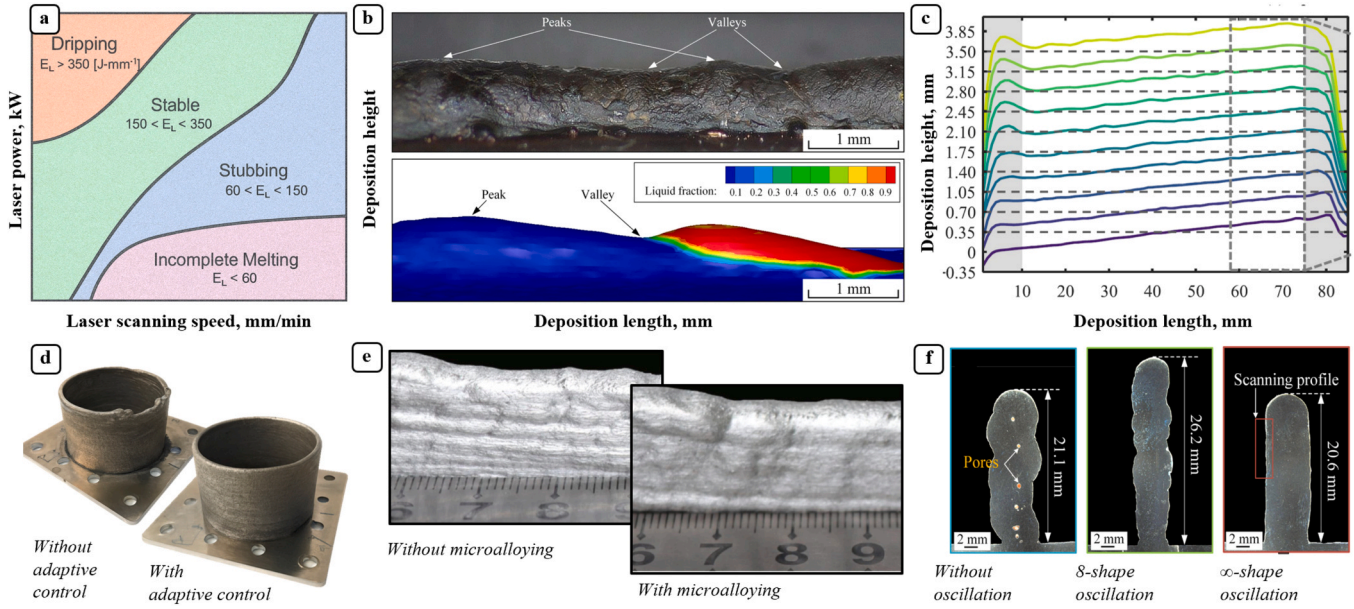


Fig. 9. Geometric aspects of the laser wire deposition: (a) dependence of deposition regimes on process parameters [84]; (b) shape of a single deposited track obtained from experiment and simulation in a stable regime [226]; (c) layer height evolution during multi-layer deposition in a stable regime [90]; (d) deposited part geometry with closed-loop control [151]; (e) deposited surface morphology with microalloying [146]; (f) deposited wall profile with laser oscillation [149].

segments for localised correction. By adjusting the wire feed rate in each segment of the subsequent layer, height deviations can be compensated within a few layers, effectively maintaining the desired layer height even under process disturbances. This approach reduced the cumulative buildup of error by nearly an order of magnitude compared to uncontrolled deposition (Fig. 9c). Onuseit et al. [151] likewise demonstrated that adaptive control of deposition height can stabilise thin-walled structures. In their setup, an optical coherence tomography sensor measured the track height coaxially, and a camera monitored the melt pool brightness (as a proxy for temperature); an adaptive controller then adjusted wire feed speed and laser power in real time. By dynamically tuning these parameters, they also reduced layer height deviations by a factor of 10 and achieved defect-free walls (Fig. 9d). Besides height deviation, the adaptive control also helps to maintain the desired tilt of the deposited wall. Gibson et al. [244] reported a 5-axis deposition process with a tilting build plate for producing large overhangs, enabling the printing of complex shapes with unsupported overhangs up to 45°. Without tilt, an overhang of 40° led to over 10 mm of sagging and deviation, whereas with adaptive control and tilt the deviation was approximately half of that value. The height control system automatically compensated for areas where overlapping beads would normally cause extra buildup. In-process 3D scanning of the as-built parts confirmed that the closed-loop approach maintained much closer adherence to the intended CAD geometry. In addition to parameter control and monitoring, there is also the effect of gravity on melt pool behaviour. Ai et al. [204] found that when building "uphill" on an inclined surface, the backward component of gravity causes the molten metal in the pool to oscillate towards the trailing end of the pool. This back-and-forth oscillation leads to a characteristic wavy morphology. Essentially, the melt pool is driven backward between solidification and gravitational forces, creating ripple-like height variations. This can affect surface roughness in non-horizontal builds. Ai et al. [204] suggested that adjustments such as modified process parameters or oscillation damping might be needed when depositing on inclines to counteract the gravity-driven flow, thereby improving the layer smoothness in complex geometries.

Another approach to influence the built geometry is by controlling the laser-material supply and interaction. Xiao et al. [197] developed a high-efficiency "keyhole mode" process that intentionally creates a laser keyhole at the tip of the wire, rather than in the substrate. This keyhole-mode melting of the wire dramatically increases energy absorption (up to ~80%) and triples the deposition rate compared to conventional conduction heating of the wire by the melt pool. Crucially, Xiao et al. [197] mapped out a process window to maintain deposit quality while using this high energy input. If parameters were mismatched – for instance, too high a wire feed speed or too low a laser energy input per unit length – the result was insufficient melting and a very rough, irregular bead. Conversely, too high an energy input at slow travel could induce an unstable keyhole in the substrate, causing spatter and porosity. Between these extremes lies the optimal regime: when power, travel speed, and wire feed were balanced, the melt pool remained stable and produced smooth, fully fused tracks [197].

Surface topography of the deposited parts can be improved by laser beam oscillation and microalloying. Cai et al. [149] introduced beam oscillation to modify the melt pool shape and control bead dimensions and quality (Fig. 9 f). This periodic laser motion influences the melt pool distribution, allowing the deposited layer's width and height to be tuned. By selecting the oscillation pattern (e.g., "8-shape" or "∞-shape"), frequency, and amplitude, this enables variation of the deposited layer's width-to-height ratio from approximately 2–5 [149]. Oscillation also improved the as-built surface finish and density without sacrificing deposition rate. Mao et al. [146] coupled beam oscillation with in-situ microalloying to control surface morphology. Compared with conventional Al–Cu deposition, the Al–Cu–Sc component exhibited consistent layer height and reduced waviness (Fig. 9e), with surface roughness decreasing by nearly a factor of two (from 24 μm to 13 μm, R_a). This smoothing came from the oscillatory energy distribution, which homogenised the temperature field and suppressed heat accumulation, while Sc addition promoted heterogeneous grain nucleation, transforming coarse columnar grains into fine equiaxed ones. The resulting equiaxed microstructure minimised anisotropic shrinkage and interlayer distortion, yielding a macroscopically flatter sidewall. In essence, Mao et al. [146] demonstrated that alloying chemistry can co-stabilise melt pool geometry and achieve smoother surfaces. For comparison, this level of surface roughness (R_a = 10–30 μm) is comparable to that obtained with LP-DED [245] and thus represents a competitive alternative for specific applications (e.g., hydrodynamic performance in closed channels) [245].

In summary, across all these studies the consensus is that the overall geometric accuracy and surface roughness are strongly dependent on controlling melt pool and bead dimensions. Without effective control, small errors can accumulate into major defects [88,90]. Techniques such as oscillating the laser beam or employing high-speed imaging feedback can be used to control the melt pool behaviour so that the deposited track remains within desired dimensions. Closed-loop control strategies have proven effective in mitigating geometrical deviations in real time, yielding parts that closely match the intended CAD dimensions and with far fewer surface irregularities.

5.2. Microstructure evolution

The grain structure in a deposited layer depends on the solidification rate: slower cooling results in coarse columnar grains, while faster cooling leads to finer and equiaxed grains [70] (Fig. 10a). Since the melt pool in LW-DED is considerably larger than in LPBF, the solidification rate is correspondingly slower, resulting in a coarser microstructure. In general, LW-DED produces a characteristic microstructure of columnar dendritic grains that grow epitaxially along the build direction [73,75,77,80,82,146,148,157,195,205,213,246,247]. In cases of faster cooling (e.g., smaller melt pool, or geometrically enhanced conduction, or external convection) the top of the deposited layer can exhibit finer equiaxed grains [216] (Fig. 10b). This crystallographic texture is

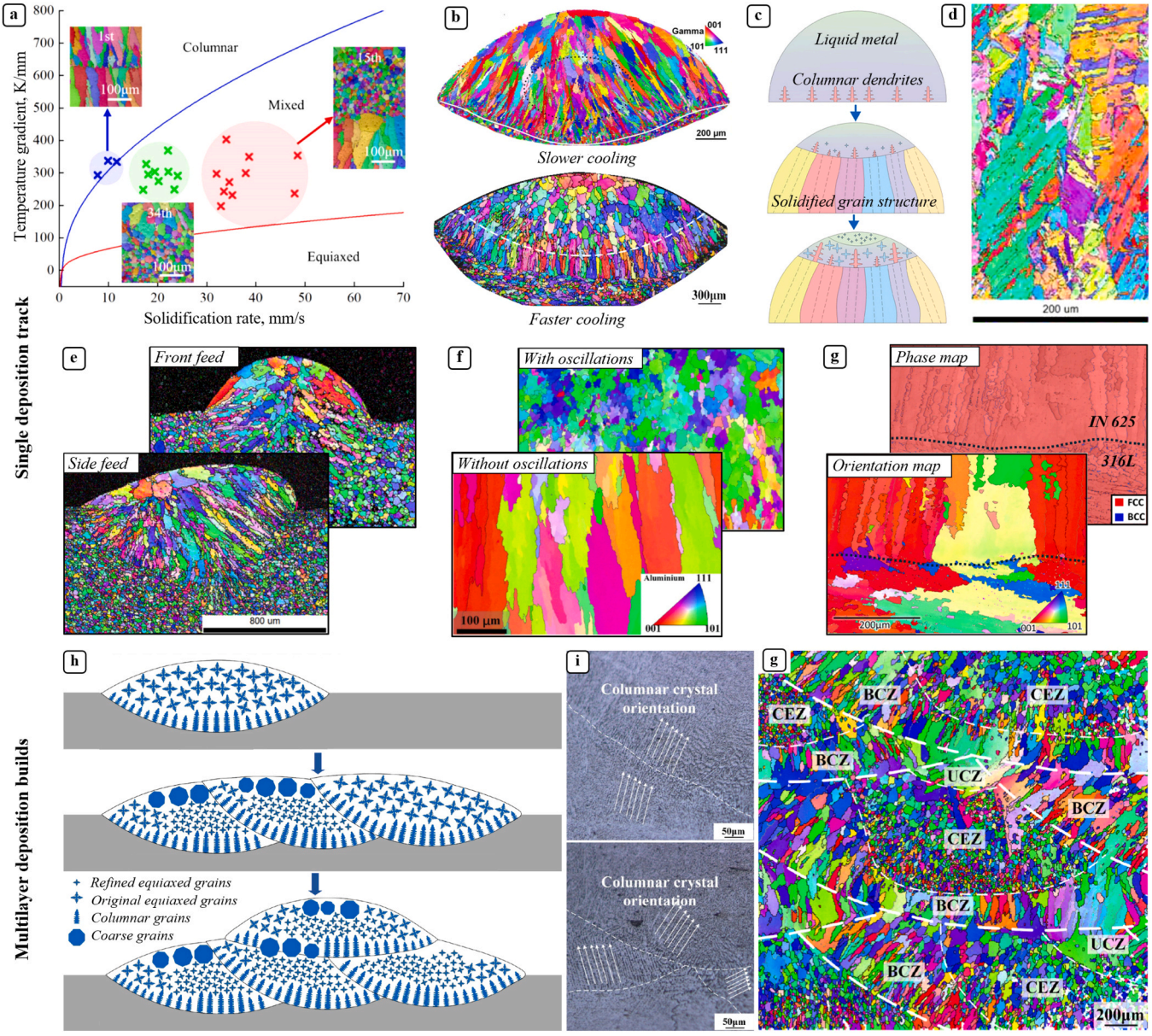


Fig. 10. Microstructure evolution in laser wire directed energy deposition: (a) solidification map showing that faster cooling rate suppresses coarse columnar grains and results in finer equiaxed grains [70]; (b) cross-sectional microstructure pattern in a single deposited layer showing a typical distribution of columnar grains at slow cooling rate [157] and columnar/equiaxed grains at faster cooling rates [216]; (c) solidification dynamics schematic explaining how columnar and equiaxed dendrites form the typical microstructure [205]; (d) columnar dendrites showing preferred growth orientation along the thermal gradient [73]; (e) cross-sectional microstructure obtained under different wire feeding angles [72]; (f) microstructure obtained with and without laser oscillations [146]; (g) bimetallic interface showing metallurgical bonding [75]; (h) illustration of grain evolution in multitrack builds where grains are locally refined and coarsened with each successive track [216]; (i) interfaces between two and three adjacent deposition layers showing columnar crystal alignment and misalignment [216]; (j) overall microstructural pattern in larger multilayered builds with multiple Bottom Columnar Zones (BCZ), Central Equiaxed Zones (CEZ), and Upper Columnar Zones (UCZ) [216].

commonly observed across many metals and alloys owing to the solidification dynamics in a deposited layer [75]. Solidification begins at the bottom of the melt pool where the substrate acts as a heat sink. Initially, planar grains form along the fusion boundary due to high thermal gradients and then evolve into columnar dendrites growing upward along the temperature gradient (Fig. 10c). As solidification proceeds and the temperature gradient decreases, constitutional supercooling ($\Delta Ts = T_{equilibrium} - T_{actual}$) increases until it reaches a critical value (ΔTn), allowing equiaxed grains to nucleate and grow in the upper region of the pool. This transition produces three characteristic zones: the columnar region at the bottom, a columnar-to-equiaxed transition region in the middle, and an equiaxed region at the top, where isotropic grains solidify due to nearly uniform thermal conditions. The columnar region is typically the largest and consists of coarse elongated dendritic grains [73] (Fig. 10d). The inherent anisotropy of properties arising from such microstructure is a generally undesired phenomenon. The primary approach to mitigate the prevalent columnar grains is through thermal management of the process [73]. The thermal history governed by input energy, interaction time, and cooling conditions influences grain size, phase formation, and defect occurrence. Yao et al. [91] observed via infrared thermography that the cooling rate of the clad correlates closely with the microhardness distribution along the deposited track. Faster cooling tends to produce finer and harder microstructures [91] with more equiaxed grains [70], while slower cooling leads to coarser [91] and columnar grains [70].

Process parameters like laser power and travel speed were shown to significantly affect the cooling rate: increasing laser power or decreasing speed raises the heat input and generally slows cooling, which can promote more annealed microstructures, while lower power or faster scanning produces the opposite effect [73,82,85,102,145,152]. Another approach to thermal control in LW-DED is the use of hot-wire feeding, where the wire is resistively preheated before entering the melt pool to maintain a more stable melt pool temperature [80,199,248] and more uniform microstructures [76,143,249,250] with fewer defects [227]. The laser scan path can be used to control solidification dynamics and produce microstructures with varying degrees of uniformity and properties [72]. Laser shock can be used to deflect, break, and disperse growing dendrites within the cooling melt pool, creating new nucleation sites for finer microstructures [205]. In non-coaxial systems, the wire feeding angle has a significant effect, particularly in the case of side-feed, which leads to shallower and asymmetric melt pool penetration depth, resulting in anisotropic microstructures [72] (Fig. 10e). Mao et al. [146] demonstrated that laser oscillation during deposition breaks up the columnar grains via enhanced melt pool convection, facilitating a finer and more equiaxed grain structure [146]. However, this was demonstrated on an Al alloy, which conducts heat approximately an order of magnitude faster than steel and titanium alloys; thus, the effect may not be generally transferable. Grain structure can be relatively continuous even in multi-material builds. Tyagi et al. [75] examined a 316 L stainless steel to Inconel 625 bimetallic build and found epitaxial growth of grains across the dissimilar interface – the columnar grains originating in 316 L continued into the 625 deposit with a consistent crystallographic direction. Despite the change in composition, a uniform grain structure was maintained across a 50 μm mixed transition zone, indicating a good level of metallurgical bonding [75]. Overall, for a single track, the deposited metal tends to have highly oriented grain structures, and the current fundamental understanding allows control of the microstructure to a high degree. However, this simplicity diminishes when depositing successive tracks to form a larger build.

Multitrack deposition involves repeated remelting and overlapping that alters local heat flow by lowering and redirecting the thermal gradient, such that columnar grains lose their alignment and sequentially interact with clusters of equiaxed grains, which are also refined and coarsened depending on their proximity to the melt pool of subsequent tracks (Fig. 10 h). The residual clusters of columnar crystals can appear aligned or completely misaligned with columnar grains in a subsequent deposit depending on track overlap (Fig. 10i). The resulting microstructure becomes spatially heterogeneous, featuring complex arrangements of unidirectional grain packets and frequent columnar-to-equiaxed transitions (Fig. 10j). Local thermal and compositional variations lead to diverse ferrite morphologies (skeletal, lathy, or interdendritic), further complicating the texture. Unlike single-track deposits, larger builds can contain a wide range of microstructures and phases in different locations of the part (e.g. Fig. 6 in [91]). Indeed, inspection of such cross-sections shows that one could selectively identify microstructural features to support specific local phenomena, yet that might have a negligible effect on the overall performance of a part. A broader microstructure-property perspective is needed. Overall, while a single layer exhibits a simple, directionally solidified structure, multilayered DED builds develop complex, orientation-dependent microstructures that influence material properties. Instead of further focusing on a single layer microstructure, the emphasis should shift to microstructures of multilayer builds that are representative of the final parts.

5.3. Mechanical performance and anisotropy

The mechanical properties of LW-DED parts can be comparable to, inferior to, or even superior to wrought alloys depending on how well the process is controlled. Kyvelou et al. [231] noted that their 316 L deposits showed yield and tensile strengths in the range (UTS: 550–700 MPa) consistent with or even above annealed wrought 316 L. Pal et al. [235] similarly found UTS values around 600 MPa for 316LSi in both build orientations, with some specimens reaching up to ~680 MPa, indicating that the additive material can achieve higher strength levels than cast steel (~600 MPa). The as-printed materials often benefit from fine cellular sub-structures and residual stress-induced hardening, which can raise strength. However, the ductility and toughness may be slightly reduced relative to wrought material due to the aforementioned anisotropy and microstructural inhomogeneity. For aluminium alloys, which are more prone to solidification cracking and coarse grains, process improvements have yielded significant gains in performance. An oscillation strategy [146] produced Al–Cu alloy samples with ultimate tensile strengths of ~334 MPa (horizontal) and 327 MPa (vertical), representing a 40–65% increase compared to non-oscillated deposits of the same alloy. The elongation at break increased by 14–20%. The deposited Ti–6Al–4 V can achieve a fully martensitic α' microstructure that yields strength in the as-built state comparable to wrought Ti–6Al–4 V [219]. However, this as-printed martensitic structure can be quite brittle and, thus, can benefit from a post-build stress relief via annealing to improve ductility [219]. The hardness and strength of deposited Inconel alloy were reported to surpass those of the AMS5662 forging standard, although this required a more complex energy input strategy [190]. Multi-material builds have also shown promising mechanical integrity: Tyagi et al. [75] found that their 316 L/In625 bimetal part had a robust tensile performance with the failure occurring in the 316 L section (the lower-strength material) rather than at the interface. The bimetal's yield and tensile strengths were essentially comparable to those of the 316 L alone, while the Inconel region was stronger, indicating that the joint did not compromise overall strength [75]. Hardness profiles across such bimetal interfaces showed a smooth gradient between the two materials, which is desirable for minimising stress concentrations [75]. The UTS of deposited Ti6Al4V reached 947 MPa with an elongation of 18.4%, which is comparable to the annealed standard (950 MPa at 15% elongation) [131]. Jeong et al. [251] deposited a C103 Nb refractory alloy, where the yield strength exceeded the ASTM B654 standard by more than 10%. Overall, the properties of deposited parts are often comparable to their wrought counterparts (with the exception of fatigue [236]); however, concluding the discussion at this point would be incomplete, as the deposited parts experience a notable degree of anisotropy as explained further below.

The anisotropy of the mechanical properties in LW-DED parts arises

from the layered nature of additive builds, which results in anisotropic microstructures. The degree of anisotropy depends on the material and build strategy, but a common trend is that properties along the build direction differ from those within the deposition plane. Pal et al. [235] tested SS316LSi walls produced by LW-DED and found that they are less ductile along the layers than across the layers. The elongation to failure along the layers was about 15–20% less than across the layers, even though ultimate strengths were comparable [235]. This has been attributed to the columnar grain structure: loading along the deposited layers distributes the load perpendicular to the long columnar grains, where cracks can localise and propagate more easily [235]. Kyvelou et al. [231] likewise observed significant mechanical anisotropy in steel and captured it clearly on thin samples (Fig. 11a). Their tensile tests showed that while yield strength and UTS did not change drastically with orientation, the elongation at fracture was found to be higher for specimens pulled along the build direction [231]. They also linked this effect to crystallographic texture, where loading along axes of columnar grains allowed higher ductility. However, this explanation appears to be inconsistent with the findings of Shakibi et al. [237], who deliberately tuned hatch spacing to obtain a range of grain sizes (from 130 to 250 μm), which nonetheless resulted in similar strength values. Further, in thicker (8 mm) specimens, an accumulated, nearly randomised grain structure yielded nearly isotropic properties [231]. Low mechanical anisotropy was also reported in deposited Ti–6Al–4 V [131]. The laser scan path appears to be an important factor influencing anisotropy. Pixner et al. [252] reported a 30% variation in hardness across the sample depending on the laser scan path (Fig. 11b), reflecting thermal-cycle-driven microstructural changes. Samples that experienced slower deposition and more uniform reheating showed consistent hardness throughout the sample. In contrast, the samples that cooled faster and accumulated more heat near the top exhibited a graded hardness distribution. Anisotropy is not limited to steels; other alloys exhibit similar behaviour. Microstructural texture contributes to different responses in nickel-based alloys [148,156,252]. Additionally, anisotropy is not limited to mechanical properties; other properties dependent on grain structure and phase distribution, such as pitting resistance [217], may also exhibit anisotropy to a certain extent. Several approaches can be considered to mitigate anisotropy. One of them is post-deposition heat treatment to homogenise the microstructure [253]. Pal et al. [235] applied annealing to the steel walls and found that the overall ductility of both vertical and horizontal specimens decreased by ~15%, presumably due to grain coarsening and relief of residual stresses, while the gap between orientations narrowed slightly [235]. Other approaches to mitigate anisotropy involve refining the grain

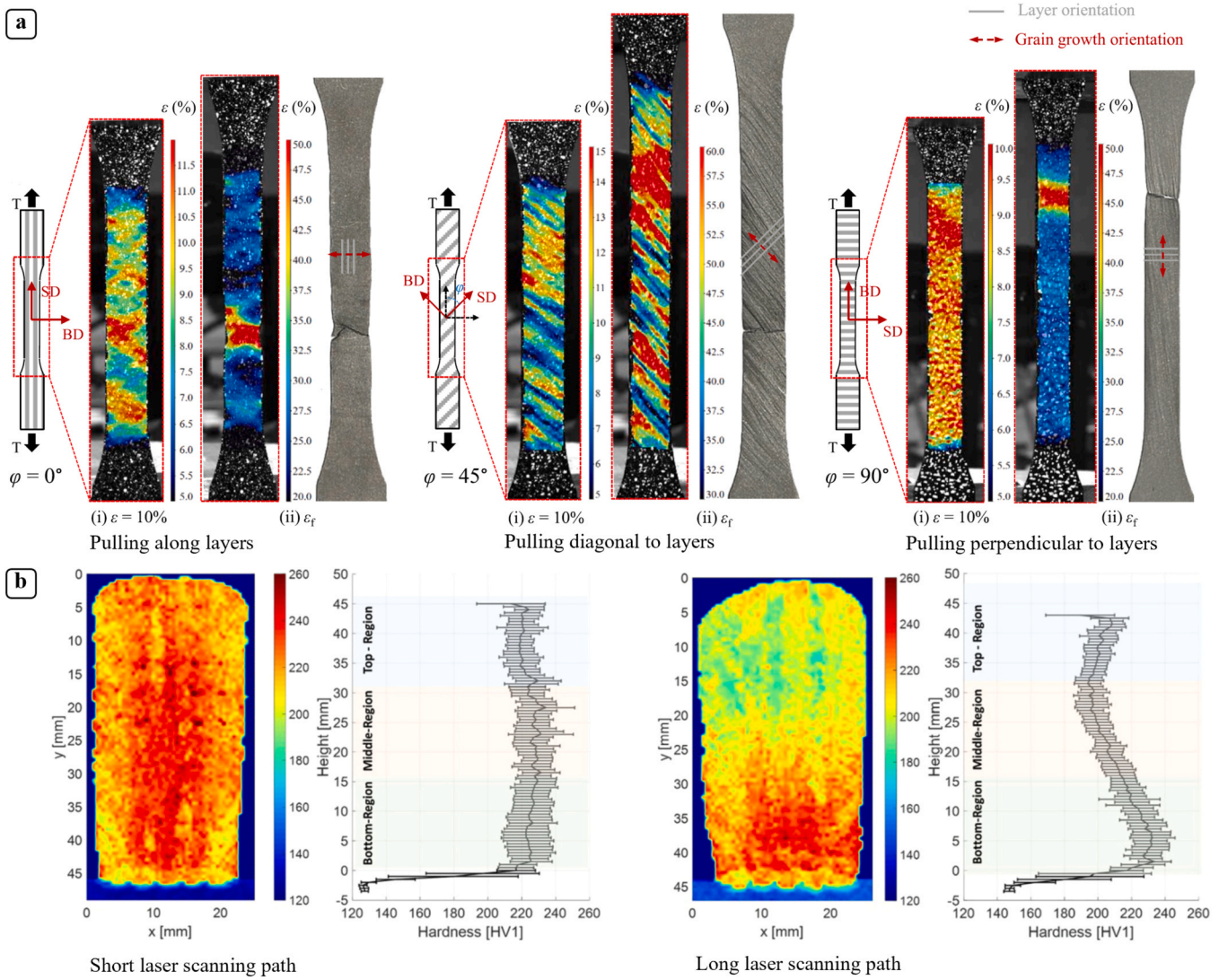


Fig. 11. Anisotropy of mechanical properties of LW-DED parts: (a) deformation profiles of thin (2 mm) tensile test samples with overlaid longitudinal strain fields at (*i*) 10% strain and (*ii*) at fracture, showing layer-dependent behaviour [231]; and (b) hardness distribution maps for different laser scan strategies, demonstrating the importance of controlled cooling [252].

structure during deposition itself, for instance via the laser scan strategy by Pixner et al. [252] or laser oscillation strategy by Mao et al. [146], which effectively reduced anisotropy by promoting equiaxed grains, yielding nearly equal horizontal and vertical strengths with a marginal difference in UTS of 2%. It is worth noting that this type of anisotropy is different from that observed in parts produced by other AM methods. In LPBF [254–257] and extrusion-based metal printing [258–262], parts are typically weaker along the build direction due to poorly bonded layer interfaces. Finally, the magnitude of anisotropy in LW-DED parts is relatively modest (up to 20% [235]) compared to other AM routes (up to 50% [258–262]), and in optimised processes with refined or equiaxed microstructures, it can become negligible (e.g., 2%) [146].

5.4. Benchmark geometry

No standardized benchmark artifact has currently been identified for this process. In contrast to LPBF, where more than 20 benchmark geometries and comprehensive qualification artifacts have been proposed to evaluate dimensional accuracy, geometric fidelity, surface quality, and process capability across hardware and material systems [263], no equivalent benchmark study was identified for LW-DED in the entire literature corpus reviewed. Beyond the literature, several industrial LW-DED system manufacturers were contacted directly regarding the existence of standardized benchmark build plates; none reported the use of a unified benchmark geometry for machine qualification or cross-platform comparison. Instead, the practical benchmark currently used in industrial LW-DED remains relatively simple and application-driven: a straight 5–10 mm thick wall, or occasionally simple cylindrical or square tube geometries (see Fig. 9d–f). These geometries are primarily used to verify deposition stability, wall continuity, bead appearance, dilution, and basic dimensional repeatability rather than to interrogate the broader geometric capabilities of the process. This gap is important because LW-DED fundamentally differs from LPBF in both scale and process physics. LPBF benchmark artifacts were developed around millimetre-scale precision manufacturing [263], where the primary concerns include feature resolution, overhang capability, hole circularity, thin walls, lattice fidelity, and micro-dimensional tolerances. LW-DED, in contrast, operates in a fundamentally different manufacturing regime characterized by high deposition rates, large melt pools, strong thermal accumulation, multi-axis kinematics, and near-net-shape manufacturing of large components. Consequently, simply transferring LPBF benchmark artifacts into LW-DED is inappropriate and often of limited relevance. Many LPBF benchmark features, such as sub-millimetre lattices or unsupported micro-overhangs, lie entirely outside the practical operating window of LW-DED. A dedicated LW-DED benchmark artifact should therefore target the actual geometric and thermomechanical challenges unique to high-deposition-rate processes. Based on the analysis performed in this review, several geometry classes should be included. First, vertical and inclined walls of varying thickness are required to evaluate bead stability, layer stacking consistency, heat accumulation, and wall waviness. Second, cylindrical and square tube geometries are necessary because they represent dominant industrial LW-DED strategies. Third, multi-axis deposition paths and freeform surfaces are essential to evaluate robotic kinematics, toolpath synchronization, and orientation-dependent geometric fidelity. Fourth, large-mass-to-thin-section transitions should be included because they strongly influence thermal history, distortion, and residual stress evolution. Finally, reference datum features and standardized measurement surfaces are needed to enable quantitative comparison using coordinate metrology, optical scanning, and deviation mapping. Importantly, the purpose of such a benchmark should not be micron-level dimensional qualification, as commonly pursued in LPBF, but rather the evaluation of geometric stability under industrially relevant deposition conditions. The benchmark must therefore reflect the true operational domain of LW-DED: large-scale, high-throughput, thermally dynamic manufacturing rather than small-scale precision prototyping.

6. Numerical modelling in LW-DED

Modelling of LW-DED is inherently a multiphysics simulation problem involving multiple coupled physical phenomena, whose solution facilitates understanding of the effects of process parameters on temperature profiles, melt pool geometry, and solidification behaviour, ultimately leading to prediction and mitigation of microstructural defects and residual stresses. Accurate simulation of the process requires simultaneous consideration of thermal, fluid flow, and mass transport phenomena, all of which are strongly coupled through the dynamics of the laser–material interaction (Fig. 12). To capture the evolution of residual stresses and their impact on mechanical properties, full-field solid mechanics equations must be solved, while also accounting for the influence of grain size and grain boundary characteristics on the part's elastic–plastic behaviour. This section outlines the fundamentals and recent progress in LW-DED finite element analysis (FEA), computational fluid dynamics (CFD), phase-field (PF) methods, and integrated multiphysics frameworks reinforced with machine learning. We start with heat transfer and fluid flow, then proceed to mechanics and finally to microstructure simulations to provide a structured understanding of deposition process modelling. For clarity, Table 3 summarises the main modelling approaches along with their advantages and limitations.

6.1. Heat transfer and melt flow

Heat transfer and thermo-mechanical behaviour in LW-DED are often simulated using CFD and FEA. In these simulations, laser input is modelled as a moving heat source with spatial and temporal distribution. These simulations predict thermal histories, cooling rates, and temperature gradients, which are essential for identifying zones of rapid solidification or reheating [264]. Wei et al. [265] accounted for the interaction between substrate, liquid metal, and gas to predict the temperature profile and molten metal flow in the melt pool and heat-affected zone. The model was validated against experimental results obtained on steel samples, showing the capability to capture the size of the fusion zone and heat-affected zone accurately (Fig. 13a).

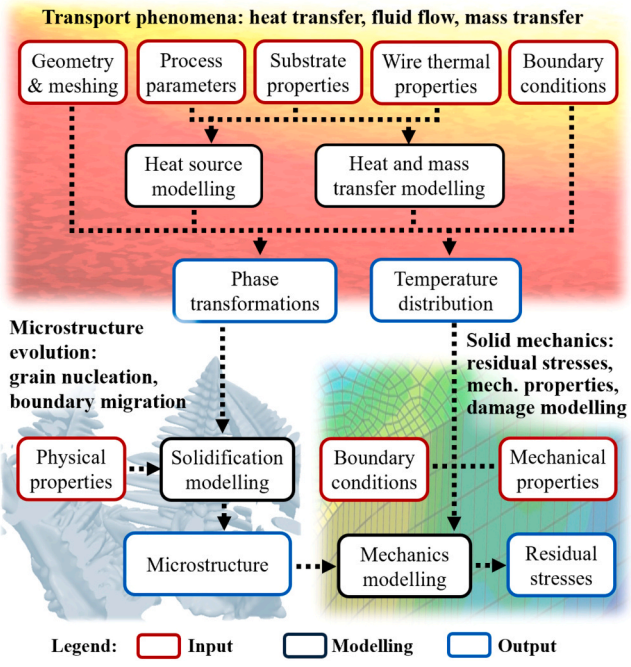


Fig. 12. Multiphysics simulation workflow of LW-DED process including thermal, mechanical, and microstructure modelling.

Table 3
Summary of strengths, challenges and applications of FEA, CFD, PF, ML, and analytical modelling approaches for the LW-DED process.

Refs	Strengths	Challenges	Applications in LW-DED
Finite Element Analysis (FEA)			
[265], [267] [269], [271] [272], [273] [86] [277]	Efficient for large-scale and multiscale thermo-mechanical process modelling. Allows realistic geometries and boundary conditions. Couples heat transfer and solid mechanics. Allows multi-layer simulations.	Requires modelling of moving laser, wire, and melt pool. Limited resolution of melt pool dynamics. Oversimplifies microstructural effects. Relies on assumed heat sources and material properties. Needs fitting of convective heat transfer coefficient.	Predicts temperature profiles, thermal gradients, and cooling rates. Evaluates residual stress and distortion due to warping, cracking, or delamination. Simulates multi-track and multi-layer builds.
Computational Fluid Dynamics (CFD)			
[274] [215] [275] [276] [164] [282]	Effective for melt pool and flow dynamics. Allows tracking of gas bubbles within the melt pool. Captures the Marangoni effect in the melt pool. Can be coupled with solidification modelling for microstructure analysis.	Expensive computation time. Often limited to single-layer simulation. Highly sensitive to boundary conditions. Limited coupling with solid mechanics for distortion and damage analysis.	Analyses melt pool dynamics and stability. Models wire-melt pool interaction. Bead shape and penetration depth. Spattering and porosity prediction.
Phase Field Modelling (PFM)			
[284] [70] [286] [83] [287] [288]	Captures complex microstructures. Couples microstructure with thermal analysis. Handles moving phase boundaries. Enables analysis of microstructure heterogeneity.	High computation cost, especially for 3D models of fine microstructure. Valid only for small parts (μm to mm scale). Requires boundary definition from CFD. Sensitive to difficult-to-find input parameters.	Grain growth and boundary evolution. Linking process parameters to microstructure heterogeneity. Tracks liquid metal to solid phases. Models dendritic structures and arm spacing.
Machine learning (ML)			
[289] [290] [291] [292]	Low computational cost after training. Suitable for highly nonlinear problems. Enables multi-step simulation from heat transfer to mechanics and microstructure prediction.	Requires a large amount of training data. Difficult integration in larger scale production. Needs validation for each change of process parameter to avoid overfitting.	Fast process parameter optimisation. Microstructure to properties correlation. Integration with sensors for on-line process control.
Analytical modelling			
[278] [293] [250] [294] [295]	Minimal computation costs. Minimal software requirements. Simple boundaries and material input. Suitable for initial parametric studies to decouple effects of process parameters.	Limited accuracy especially when considering multi-layer process. Limited coupling between thermal, mechanical, and microstructure predictions. Difficult to simulate dynamic effects.	Prediction of melt pool depth and geometry. Parametric studies to identify safe operating conditions. Useful for early-stage process design and prototyping.

Their results demonstrated that the melt pool surface exhibited a distinctive Marangoni-driven outward flow, from the centre towards the periphery and downwards to the bottom of the melt pool (Fig. 13b), which affects cladding formation. Cross-sectional views at various time steps (Fig. 13c) demonstrate that the deposition rate initially increases but then slightly decreases, resulting in geometrically uneven deposition [265]. This Marangoni flow affects the deposition geometry. Within the Marangoni effect region, the surface tension gradients tend to drive a radial outflow from the centre to the boundary of the melt pool, which increases the width, while a rear-to-front flow in the trailing region of the melt pool tends to suppress the effect of recoil force and reduce the build height [266]. Hu et al. [267] combined heat transfer with fluid flow in a 3D model considering wire feeding speed and validated the results via cross-sectional microscopy measurements of the deposited track (Fig. 13d). With velocities averaging around 1.5 m/s and peaking at 4 m/s in the cavity region, liquid transfer from the wire tip to the melt pool is dominated by a so-called “liquid bridge” (Fig. 13e), driven by strong recoil pressure in the cavity centre (around 3100 K).

Low recoil pressure results in slower wire melting, weaker convection, and unstable wire–substrate liquid bridging [268]. The model by Nie et al. [248], incorporating a heat conduction coefficient, found that heat convection through the liquid bridge was 3–5 times greater than that of liquid metal in the static state (Fig. 13 f). The CFD model by Gu and Li [269], with material temperature-dependent physical properties for LW-DED in space, revealed that, at low gravitational force, the liquid metal tends to form a sphere that results in an unstable melt pool and irregular shape of the track, especially in subsequent layers due to accumulated substrate heating and a larger melt pool compared to the first layer. When the laser strikes the substrate and melts the material at the start of the operation, the temperature rises quickly [270,271]. Consequently, the melt pool temperature gradient increases, modifying the surface tension accordingly. A spherical-shaped bulge forms to minimise the surface energy, as the system tends to reduce the free surface energy difference between the substrate and the melt pool. Li et al. [272,273] simulated bulge formation by balancing gravitational force and surface tension and validated the results by optical microscopy of cross-sections of the solidified melt pool and CMM measurements of the bulge. For optimised process parameters that could be used in actual manufacturing conditions, their analytical model was able to predict the cladded shapes within 14% error. Sun et al. [274] performed process parameter optimisation for improved part quality based on temperature profiles. Other studies utilised CFD simulations to model the coaxial laser DED process to understand the effects of process parameters. Four lasers are coaxially aligned with the wire's central axis for a single wire feed [215]. CFD modelling supports the prediction of mass transfer, melt pool dynamics, and wire melting, which are otherwise challenging to comprehend through experimentation. Over the course of the deposition, a significant geometrical agreement between experimental and simulated thin walls was observed. The effects of various laser incidence angles on a single wire, wire-multiple laser interactions, and their cumulative influence on the deposition were investigated [215]. The evolution of melt pool formation at different stages of the process, together with the temperature distribution in the melt pool, shows that fluid flow is directed towards the substrate in the deposition direction, with the initial droplet transitioning into a bell-shaped geometry (Fig. 14a).

A wiggle deposition strategy was investigated using the Flow−3D software, which solves the governing equations of the mass transport problem using the finite volume method [275,276]. The simulations were performed by moving the substrate while continually applying heat and pressure to the fixed wire and were validated against experiments. The wiggle deposition approach generated a highly dynamic melt flow and oscillating heat gradient in the melt pool, influencing fluctuations in the preferred grain growth direction and crystallographic texture in the sample (Fig. 14b). A coupled discrete element method (DEM) and computational fluid dynamics (CFD) model was developed to analyse the in-flight filler dynamics and fluid flow characteristics within the melt pool during LW-DED process of a steel-SiC metal matrix composite [164] (Fig. 14c). They demonstrated that increasing the SiC weight fraction decreases the maximum fluid temperature in the melt pool due to the lower energy input required. Huang et al. [86] developed

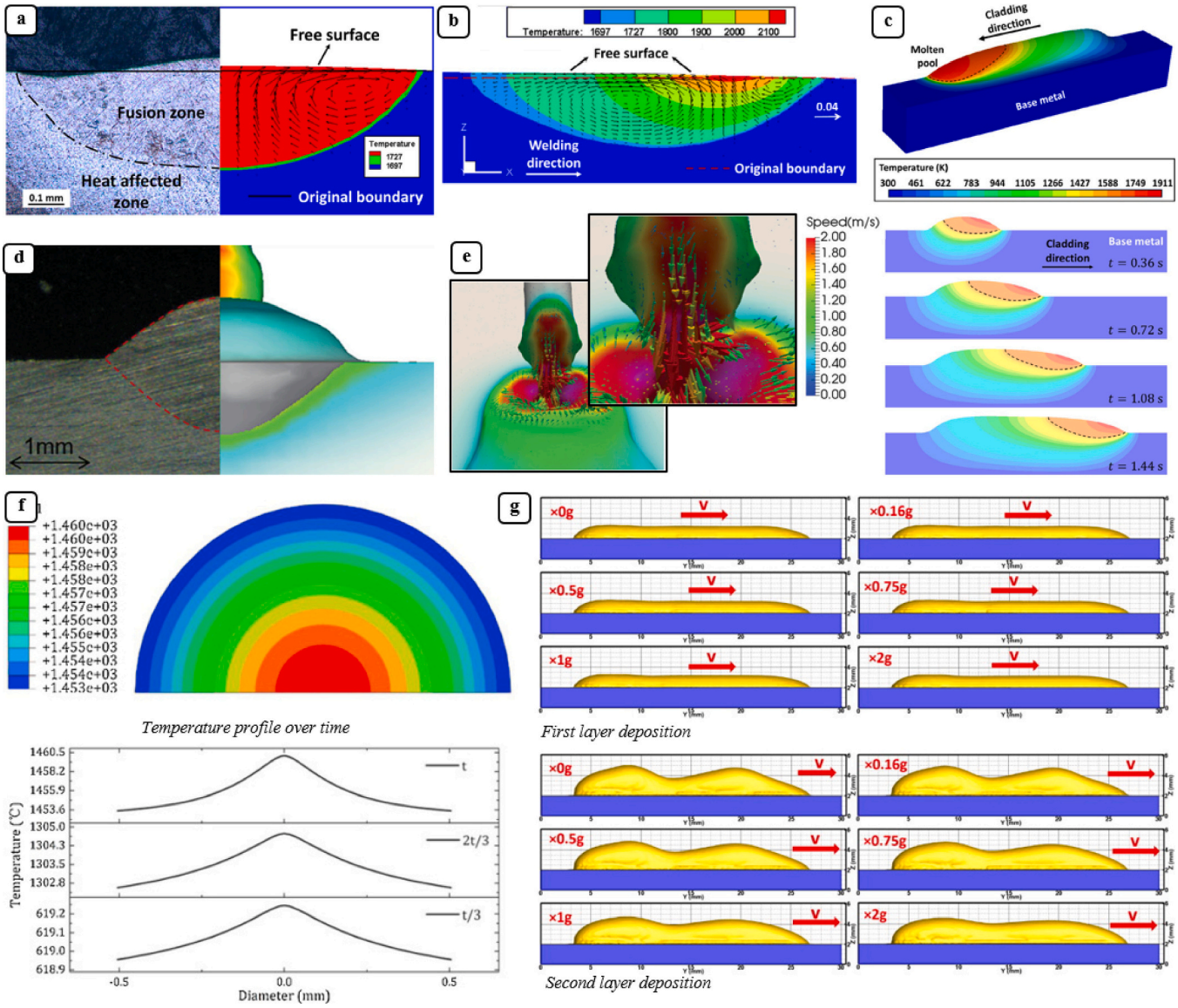


Fig. 13. CFD modelling of heat transfer and temperature evolution: (a) comparison of numerical prediction of the fusion zone and experimental results [265]; (b) temperature profile and flow pattern in the melt pool [265]; (c) morphology simulation and temperature distribution [265]; (d) experimental validation of melt pool size and shape [267]; (e) liquid transfer from the wire tip to the melt pool via a liquid bridge [267]; (f) temperature evolution over time [248]; (g) effect of gravitational force on first- and second-layer profiles [269].

a FE model to simulate the oscillating LW-DED process of aluminium, assuming an incompressible Newtonian fluid for the molten metal flow in the melt pool. Melt pool depth was found to be inversely related to oscillating frequency. They also revealed that circular oscillating lasers operating at 50 Hz and 150 Hz provide considerable preheating ahead of the melt pool, hence significantly improving the spreading and wetting characteristics of the liquid alloy (Fig. 14d).

6.2. Solid mechanics and residual stress

The simulated temperature profile can be used as input to a solid mechanics model to simulate residual stresses using the finite element method. High residual stresses are an inevitable consequence of the high energy input employed in DED, due to the large temperature gradients responsible for strain generation [277]. Because of the large difference between heat input and heat dissipation rates at the upper surface exposed to the laser beam, a significant temperature difference is created. The temperature difference between the current layer and previously deposited layers, combined with reduced material strength at elevated temperatures, leads to deformation as the number of layers increases. The top layer of the bead undergoes plastic deformation, causing compressive residual stresses. Upon cooling, this layer contracts, leading to bending of the structure. Nie et al. [248] simulated the complete LW-DED process using a multiphysics FE model and obtained residual stress profiles as a function of process parameters within a 25% error margin, and accurately predicted distortion at several positions. Liang et al. [278] developed a coupled FEA/CFD thermal-fluid-mecha nical model to demonstrate that the surface quality had a major impact on the highest residual stress at the deposit's root. Unlike most models, Bock et al. [279] ignored the dynamics of the melt pool and microstructural evolution while simulating LW-DED. Nevertheless, they concluded that residual stresses were increased when switching from a unidirectional to a bidirectional scanning technique. They also suggested reducing the interlayer waiting time to 10 s and increasing the substrate and environmental temperatures to achieve a significant reduction (27%) in both in-plane and out-of-plane stresses. Such simulations can be reinforced via experimental validation using recently proposed X-ray stress detection techniques [280]. Several important

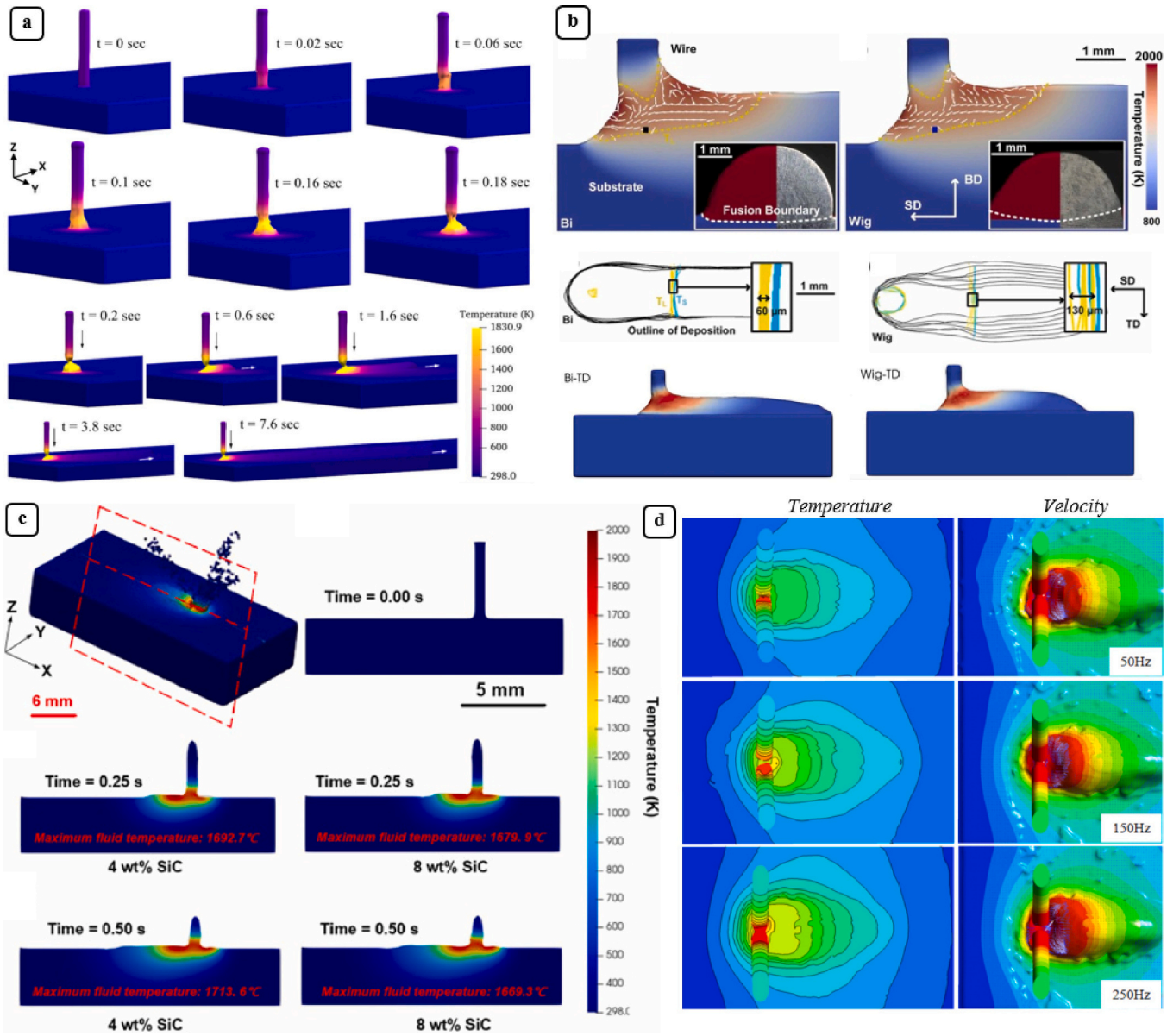


Fig. 14. Prediction of the temperature distribution using different DED approaches: (a) single-wire behaviour under multi-laser interaction [215]; (b) wiggle deposition process [276]; (c) LW-DED of metal matrix composites (MMCs) [164]; (d) oscillating LW-DED process [86].

findings were reported by Benmessaoud et al. [281], who investigated the effects of grain size and crystallographic texture on the cyclic and monotonic mechanical behaviour of Ti–6Al–4 V alloy. Grain size was shown to affect kinematic hardening behaviour and to decrease yield strength while increasing ductility. The mechanical characteristics of weakly textured microstructures were superior to those of substantially textured ones. At room temperature, all microstructures exhibited cyclic softening without any discernible strain rate sensitivity, regardless of grain size or texture. Slip trace analysis showed that the dominant slip system (basal, prismatic, or pyramidal) and favoured grain orientations have a significant impact on yield stress fluctuations. While incorporating implicit texture specification into model parameters successfully captured anisotropic yield strength variations arising from texture, a modified hardening model that directly incorporates grain size effects was shown to predict the material response across various microstructures without the need for repeated parameter recalibration [281].

6.3. *Phase field and microstructure*

Microstructure simulation of LW-DED parts remains limited in the literature due to the lack of solidification data required for modelling. The phase change of Ti–6Al–4 V during the LW-DED process has been examined using a density-based constituent phase simulation approach [282]. The model was validated through experiments on single- and multi-layer deposits, showing good agreement with experimental results. Four stages were identified by in situ analysis of phase transformation during cooling, including the transition from β to metastable α′. Increasing the temperature and decreasing the cooling rate were shown to reduce the fraction of α′ phase or even suppress its formation entirely. In another study, phase transformation kinetics and α-lath width evolution during the LW-DED process of Ti–6Al–4 V components were investigated and validated using an integrated process-microstructure numerical model. First, a heat transfer model of the LW-DED process was developed, addressing spatial multiscale

effects. Then, using a range of experimental data, an integrated microstructural evolution model was proposed, validated, and compared with existing models. This model accounts for the formation and dissolution of grain boundary α, Widmanstätten (basketweave) α, martensitic α′, and β phases, as well as the coarsening kinetics of Widmanstätten α laths. To examine the microstructural evolution during the LW-DED process of a Ti–6Al–4 V block, the thermal model is validated and then combined with an integrated microstructural evolution model [283,284]. Their results indicated that full transformation into stable phases may be achieved at 650 °C, given adequate annealing time; nevertheless, observable morphological evolution of the microstructure was only noted above a certain temperature, without alteration of the preceding β grain structure. Overall, these studies highlight that despite recent progress, current simulations of microstructural evolution in LW-DED remain heavily limited by scarce solidification data and insufficient predictive capability, underscoring the need for more comprehensive models and experimental validation to reliably capture phase transformations in various metals and alloys. Finally, the process has not been extensively explored using molecular dynamics simulation methods, which may offer another avenue for understanding melt pool consolidation and crystallographic orientation [285].

Although high-fidelity multiphysics simulations provide valuable mechanistic insight into melt pool dynamics and microstructure evolution, their direct application to predicting deposition outcomes for large industrial components remains limited by computational cost and model complexity. Consequently, current simulations are primarily used to guide process parameter optimisation and understand process trends, while reduced-order models, surrogate models, multi-scale modelling approaches, and hybrid simulation-machine learning frameworks are increasingly explored to enable scalable industrial predictions. Machine learning (ML) has been deployed to establish predictive relationships between process parameters and deposition outcomes. Liu et al. [289] demonstrated that ML-based frameworks can capture the complex process-geometry-microstructure-property relationships governing deposited beads, enabling hierarchical design of bead material properties and prediction of microstructural features from processing conditions. In their subsequent work [290], they further showed that ML models can effectively map the interdependence between process parameters, bead geometry, and resulting microstructure, providing a data-driven pathway to optimise deposition conditions. Complementing these efforts, Mbodj et al. [291] applied ML algorithms to predict bead geometry in LW-DED and demonstrated that trained models can estimate bead width and height with good accuracy based on processing parameters, thereby supporting process planning and control. Similarly, Yang et al. [292] deployed ML approaches to predict melt pool dimensions in wire-fed directed energy deposition, showing that data-driven models can reliably estimate melt pool size from key process variables. These studies indicate that ML models can efficiently capture nonlinear relationships between process inputs and deposition outcomes, offering promising tools for rapid prediction, parameter optimisation, and process design in LW-DED, although their reliability remains dependent on the quality and diversity of the training datasets. Despite this progress, ML models for LW-DED still suffer from limited generalisation when applied to new materials, machines, or process conditions outside the training dataset. Moreover, current closed-loop control systems lack a unified hierarchical architecture that effectively integrates real-time sensing, data processing, decision-making, and process actuation, highlighting the need for standardized intelligent manufacturing frameworks.

7. Process monitoring

Achieving high dimensional accuracy and structural integrity in LW-DED requires advanced in-situ sensing and monitoring frameworks that can capture the dynamic interactions between the laser heat source, wire feedstock, melt pool, and subsequent solidification process in real time. The LW-DED process is inherently complex due to the coupled thermal, fluid, and metallurgical phenomena, making it highly sensitive to process fluctuations. Without appropriate monitoring, defects such as lack of fusion, porosity, or geometric inaccuracies may arise, limiting adoption for high-value applications [296].

7.1. Sensing methods

A wide spectrum of sensor-based measurement approaches has been developed, which can be broadly categorised into direct and indirect sensing modalities (Fig. 15a). Direct measurements aim to quantify the physical geometry and microstructure of deposited features using techniques such as laser line scanners [90], line-section method [299], and operando synchrotron X-ray imaging [157,276]. These approaches provide high-fidelity insights into part shape, layer height, and even internal defect evolution, though often at the expense of higher system complexity. By contrast, indirect measurements focus on capturing physical signals that correlate with process states, such as optical emission, thermal radiation, or acoustic response, to infer melt pool stability, deposition efficiency, and defect formation mechanisms [84,149,244,298]. However, most indirect sensing approaches primarily monitor surface or near-surface phenomena and therefore have limited capability for direct detection of internal defects such as subsurface porosity or lack-of-fusion defects. Meanwhile, advanced direct sensing methods such as synchrotron X-ray imaging require highly specialised facilities and complex experimental setups, which restrict their applicability for industrial in-situ monitoring and real-time control. Consequently, increasing attention has been directed towards hybrid multi-modal sensing and data fusion strategies [300] that combine complementary sensing signals to improve defect detectability, monitoring robustness, and process understanding. Collectively, these sensing strategies not only enable real-time quality assurance but also provide the foundation for closed-loop process control, multi-sensor data fusion, and digital twin integration. Their application is critical for advancing LW-DED towards industrial deployment, where consistency, repeatability, and certification of AM parts remain key challenges.

7.1.1. Indirect measurement

Optical monitoring of the melt pool represents one of the most critical indirect sensing approaches in LW-DED, as the melt pool acts as the central mediator of energy absorption, material transfer, and solidification. The melt pool geometry, characterised by its width, length, depth, and surface oscillations, is strongly influenced by process parameters (Fig. 15d) such as laser power, wire feed rate, travel speed, and beam oscillation, and directly governs bead morphology and deposition quality [149,244]. High-speed cameras equipped with charge-coupled device (CCD) or complementary metal-oxide-semiconductor (CMOS) sensors are commonly deployed in either coaxial or off-axis configurations to capture the evolution of the melt pool in real time, allowing the tracking of key signatures such as pool area, thermal gradients, spatter dynamics, and plume intensity [84,300]. These measurable features serve as proxies for process stability, providing early indications of defects such as underfill or humping instabilities. Advanced image-processing and deep learning algorithms have further expanded the potential of melt pool monitoring, enabling automated detection, segmentation, and statistical analysis of pool dynamics to support anomaly detection and stability assessment [225,300]. Metrics such as melt pool size fluctuation, aspect ratio variation and bead width variance can provide quantitative indicators of deposition consistency and process robustness [89,300]. In particular, temporal fluctuations in melt pool geometry are often associated with unstable wire transfer, excessive thermal accumulation, or insufficient energy input during multi-layer deposition [252]. However, achieving repeatable monitoring results across different laboratories and equipment remains challenging due to variations in machine architecture, optical

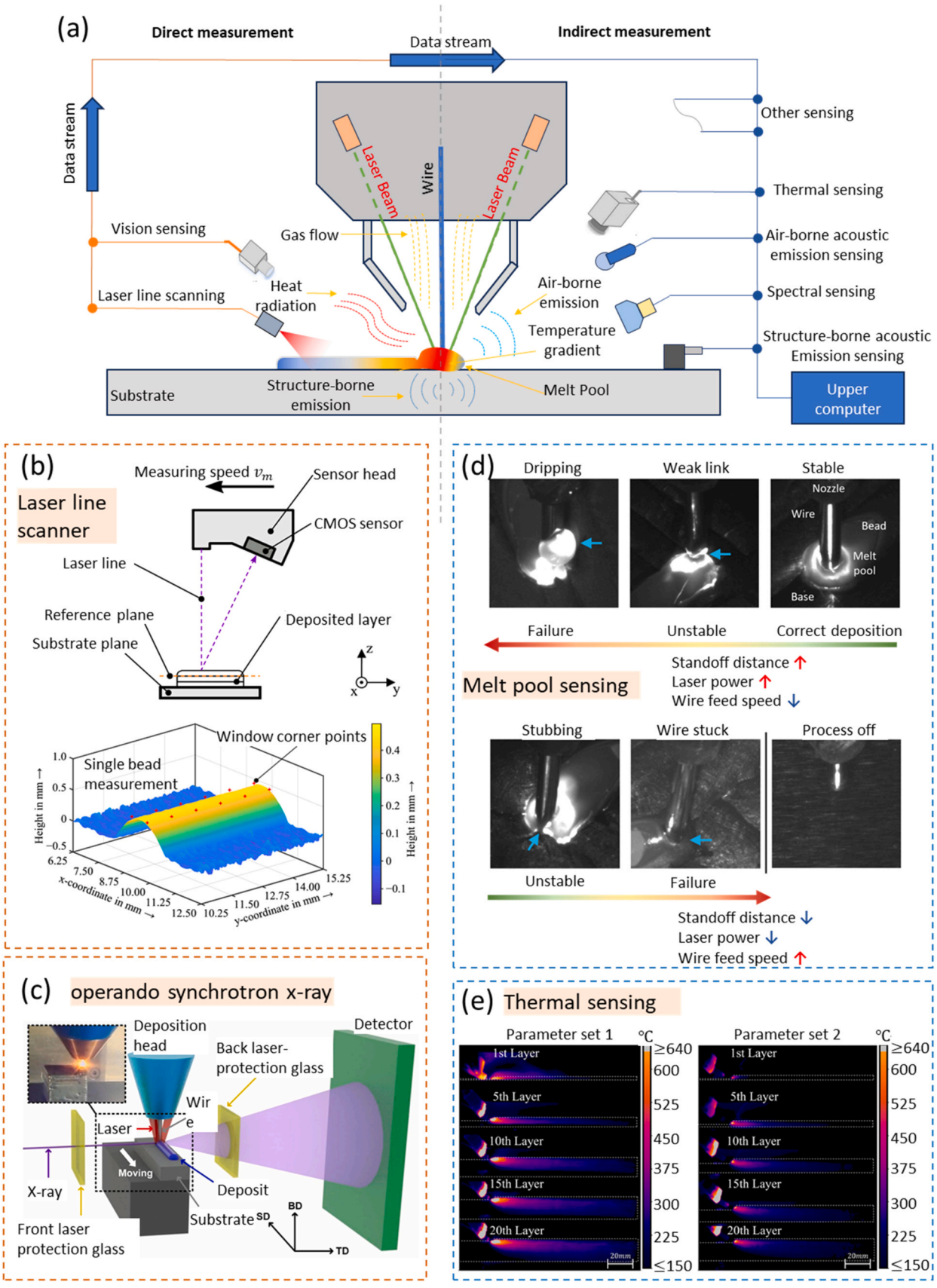


Fig. 15. Sensor-based in-situ measurement of the LW-DED process: (a) schematic of the overall process and measurement principles [296], which include direct measurement such as (b) laser-line scanner [90] and (c) operando synchrotron X-ray imaging [157], and indirect measurement such as (d) optical sensing of the melt-pool [297] and (e) thermal sensing of layer-wise temperature distribution [298].

configuration, sensor calibration, and shielding conditions. Therefore, standardised benchmark geometries, unified calibration procedures, and cross-platform validation strategies are important for improving the reproducibility and industrial applicability of LW-DED monitoring systems. From a process physics perspective, melt pool behaviour embodies a delicate balance between heat input, Marangoni convection, surface tension, and solidification kinetics. Oscillations in pool size or surface waves, for instance, can signal transitions between stable and unstable deposition regimes, while changes in pool aspect ratio may reveal insufficient energy coupling or improper wire feeding [89,225]. Monitoring these dynamics provides not only a real-time indicator of deposition quality but also a foundation for predictive modelling and closed-loop control schemes that adjust process parameters to maintain desired stability. However, despite its importance, optical monitoring faces inherent limitations: coaxial systems may suffer from plume interference and reflections that obscure the pool surface, while off-axis systems require geometric corrections and are sensitive to alignment errors [84,244]. Moreover, optical sensing is restricted to surface phenomena and cannot detect subsurface defects such as porosity or interlayer lack-of-fusion defects, highlighting the need for complementary sensing modalities.

Thermal sensing can complement optical information by capturing the temperature evolution of the melt pool, wire tip, and deposited layers (Fig. 15e). Infrared (IR) cameras, pyrometers, and thermographic sensors are widely employed to track local temperature distributions and cooling rates [298], which are closely linked to solidification microstructure, residual stress formation, and interlayer bonding quality [246]. For example, pyrometry-based monitoring has been used to characterise melt pool temperature and thermal cycling effects, offering insight into heat accumulation and microstructural transformations in multi-layer builds [252]. Similarly, Huang et al. [250] demonstrated that monitoring wire tip temperature during deposition enables real-time control of wire melting behaviour, reducing instability in the transfer process and improving deposition consistency. These thermal signatures provide a pathway for feedback control strategies that dynamically regulate laser power or wire feed rate to mitigate overheating, porosity, or poor bonding. Acoustic emission sensing, though more extensively studied in powder-based DED, can be explored as a means of detecting high-frequency vibrations from melting, solidification, and wire–substrate interactions. It offers the potential to identify internal defects such as cracking or delamination when optical access is limited [301]. Similarly, spectral sensing, widely used in powder-fed DED, relies on analysing plasma plume and optical emission spectra to infer melt pool chemistry and stability [302]. While its application in LW-DED remains underexplored, it is expected to provide complementary information on element vaporisation and contamination events. In addition to process control, these indirect sensing modalities strengthen process understanding by providing multi-physics perspectives beyond deposited geometry.

7.1.2. Direct measurement

Direct sensing techniques are increasingly adopted in LW-DED to measure the deposited geometry and even internal structure. Among these, laser line scanners and structured light projection are widely used for inter-layer inspection and dimensional verification. Mounted coaxially or off-axis to the deposition head, these sensors generate high-resolution point clouds of the deposited surface, enabling detection of geometric deviations such as bulging, under-deposition, or layer shifting. For instance, Bernauer et al. [90] developed a segmentation-based closed-loop layer height control system using a laser line scanner, thereby enhancing part dimensional accuracy (Fig. 15b). Similarly, Takushima et al. [299] applied a cross-line beam optical method for in-process height measurement, achieving micron-level accuracy in characterising layer growth. Such direct geometric feedback is critical for adaptive toolpath correction and prevention of cumulative errors in large structures. Further, Li et al. [303] combined a machine vision-based interlayer height controller (CMOS camera) and P-controller-based melt pool temperature controller (two laser-targeted infrared thermometers) to improve the vertical dimensional accuracy using deep learning. Operando synchrotron X-ray imaging has provided unprecedented insights into the fundamental physics of melt pool behaviour and solidification. Gao et al. [276] employed synchrotron-based diagnostics to investigate the effect of wire melting state on microstructural development, revealing strong correlations between deposition strategies and final material properties. Extending this work, Gao et al. [157] conducted time-resolved synchrotron studies that captured solidification front evolution and defect formation mechanisms (Fig. 15c). While synchrotron-based imaging is currently limited to laboratory-scale studies due to infrastructure demands, it remains an invaluable tool for validating models and developing predictive frameworks for process optimisation. Together, these direct sensing methods complement indirect monitoring by providing quantitative geometric data and fundamental insights into microstructure evolution. When integrated into the LW-DED workflow, they not only support inter-layer quality assurance but also serve as a foundation for hybrid monitoring frameworks that couple geometry, thermal history, and microstructural data for enhanced process control.

7.2. Integration of machine learning in process monitoring

The highly dynamic and multi-physical nature of LW-DED produces large volumes of complex sensor data, ranging from high-speed optical images to thermal profiles and temporal signals, that are difficult to interpret using conventional methods. Machine learning (ML) has therefore become a key enabler for in-situ monitoring, offering automated feature extraction and pattern recognition to transform raw signals into actionable information. Current research has mainly focused on two areas: regression models, which predict bead geometry and quality metrics from process signatures, and classification models, which identify process states and detect anomalies in real time, as summarised in Table 4. Together, these approaches provide the foundation for intelligent monitoring frameworks that support adaptive control and defect mitigation.

Regression-based applications in LW-DED monitoring primarily aim to establish predictive relationships between process signatures and bead quality metrics such as width, height, and fusion zone depth. These models are particularly valuable for real-time quality assurance and feedforward control. Jamnikar et al. [304] developed a multi-modality convolutional neural network (CNN) that combined melt pool images with temperature profiles to predict bead width, height, and fusion zone dimensions, demonstrating strong accuracy in capturing complex process–geometry interactions. Similarly, Yang et al. [292] employed random forest models to predict bead width and height from laser power, wire feed, and travel speed, highlighting the superior predictive capability of ML compared to lumped physics-based models. Furthermore, Gaussian process regression has also been adopted as a powerful non-parametric tool, enabling prediction of bead geometry and microstructure features such as α-lath thickness and β-grain length based on input process parameters [289]. These regression frameworks provide a pathway toward predictive monitoring and online parametric optimisation depending on part geometry.

Classification-oriented ML approaches have focused on detecting process states and anomalies, thereby improving process stability and defect prevention. Early works applied Naïve Bayes classifiers to distinguish bead quality categories such as smooth, rippled, or failed deposition based on input parameters [289]. With the availability of richer spatiotemporal data, deep learning architectures have become increasingly prominent. Assad et al. [84] integrated in-situ imaging with process-aware ML models to map process anomalies, while Asadi et al. [300] applied CNN-based methods for segmentation and statistical analysis of melt pool images. More advanced models, such as convolutional long short-term memory (Conv-LSTM) autoencoders [98] and

multi-layer CNN [297], have been used to analyse material transfer states, enabling detection of irregularities such as wire dripping, weak link, arcing, and stubbing. Chen et al. [305] developed a vision-based measurement method with contour extraction and spatial reconstruction to enable time-resolved, quantitative evaluation of wire stick-out under severe optical interference to capture the dynamic interaction between the feeding wire and the molten pool, addressing the challenge of maintaining stable layer height. These classifications expand the capability of LW-DED monitoring, moving from simple defect detection toward real-time stability assessment and intelligent fault prevention. Overall, the integration of ML into LW-DED monitoring allows transforming raw sensor signals into actionable feedback. Recent studies highlight the potential of multi-modal data fusion, where optical, thermal, and other sensor inputs are combined to enhance predictive accuracy and reliability [225,304]. Over time, these methods are expected to form the backbone of digital twin architectures and adaptive closed-loop control strategies, ultimately paving the way for fully autonomous LW-DED systems [296].

Despite the rapid progress of ML-assisted monitoring in LW-DED, important challenges remain regarding scalability and industrial deployment readiness. Many existing models are still trained and validated using relatively simple deposition geometries, such as single-track or thin-wall structures under controlled laboratory conditions [84,300], while their generalisation capabilities across complex multi-layer geometries, different deposition strategies, and varying material systems remain insufficiently demonstrated. In industrial environments, additional factors including thermal accumulation, plume interference, sensor contamination, calibration drift, and machine-to-machine variability may further reduce model robustness during long-duration manufacturing processes [306]. Recent reviews have also highlighted the limited availability of standardised datasets and the lack of cross-platform validation in current DED monitoring studies [296,307]. Therefore, future research should focus on improving model transferability, integrating physics-informed learning approaches, and establishing standardised multi-modal datasets and validation frameworks to facilitate reliable industrial deployment of intelligent LW-DED systems.

7.3. Closed-loop control of LW-DED process

Open-loop approaches cannot adequately handle the variability in heat input, material transfer, and geometric growth, as they rely solely on predefined parameters. Closed-loop systems integrate real-time sensing, feedback control algorithms, and actuation to detect deviations during deposition and adjust inputs such as laser power, wire feed rate, or scanning speed accordingly. As illustrated in Fig. 16a, two primary levels of control are distinguished: intra-layer control (Fig. 16b–c), which relies mainly on indirect measurements such as melt pool dimensions [244] or temperature measurements to regulate process stability within a single track or layer [89], and inter-layer control (Fig. 16d–e), which is typically based on direct geometric measurements such as layer height [308] or surface profile to correct accumulated deviations between successive layers [90]. Together, these control strategies form hierarchical systems in which intra-layer feedback maintains local melt pool consistency, while inter-layer corrections ensure global dimensional accuracy and structural integrity.

Intra-layer closed-loop control in LW-DED focuses on stabilizing the melt pool during track or layer deposition by dynamically tuning process parameters such as laser power, wire feed rate, or scanning speed. Since melt pool geometry directly governs bead morphology and bonding quality, it is often used as the primary feedback signal. Gibson et al. [244] demonstrated that multiple feedback modalities, including real-time adjustment of laser power and averaged control of melt pool size across a track, can significantly reduce dimensional fluctuations in Ti–6Al–4 V wire deposition. Building on this, Dehaghani et al. [89] introduced a parameter-signature-quality modelling framework that links melt pool width with deposition quality, enabling closed-loop regulation of laser power. Bernauer et al. [90] showed that coaxial monitoring of melt pool temperature allowed effective laser power modulation, reducing defect formation and improving microstructural homogeneity. Yet, intra-layer control is not without challenges. Direct monitoring of melt pool width or temperature is often sensitive to plume interference, calibration errors, or sensor noise, which can introduce delays or instability in feedback responses. Moreover, single-variable feedback strategies may fail under complex deposition conditions, such as sharp curvatures or multi-axis toolpaths. Achieving fast and reliable control across diverse geometries and materials remains a key limitation, underscoring the need for robust multi-sensor frameworks and adaptive controllers that can balance speed with precision.

Inter-layer closed-loop control addresses the gradual accumulation of geometric deviations between layers by incorporating direct measurements of the deposited surface into the feedback loop. Unlike intra-layer control, which relies on indirect process signatures, inter-layer strategies use explicit geometric data, such as layer height, bead width, or surface profile, captured through laser line scanners or vision systems. For instance, segmentation-based height control has been shown to adapt wire feed rates across individual segments within a layer, thereby mitigating uneven growth and improving dimensional stability in multi-layer builds [90]. Earlier approaches also employed iterative learning control, where deviations detected after each layer informed corrections to subsequent toolpaths, progressively correcting the build [308]. Recently, this has been extended to complex geometries, where adaptive path-planning methods dynamically adjust scanning speed or deposition inputs to accommodate curvature and overhanging features, preventing common issues such as corner bulging or thinning [309,310]. Vision-based detection and thermal feedback have also been combined to correct layer height while maintaining process stability, demonstrating that hybrid sensing approaches can simultaneously ensure dimensional accuracy and homogeneous microstructure [92]. However, inter-layer control also faces limitations in response speed. Sensor-based height measurements trade resolution for speed to remain viable for layer-by-layer feedback in real time, while data processing and correction algorithms introduce latency as well. Moreover, while effective for local corrections, current inter-layer methods lack integration with intra-layer feedback, leading to fragmented control architectures. Addressing these challenges will require hierarchical frameworks that couple local melt pool regulation with global geometry correction, enabling more consistent and autonomous deposition across entire builds. Despite recent progress, many existing closed-loop control systems in LW-DED are often designed for specific sensing configurations or individual process variables, limiting their scalability and interoperability across different manufacturing platforms. In most studies, sensing, prediction, and control modules are implemented independently, while unified hierarchical architectures integrating multi-modal sensing, real-time decision-making, and adaptive process control remain insufficiently developed. The strong coupling among thermal behaviour, melt pool dynamics, material transfer, and geometric evolution further increases the complexity of integrated control implementation [149,244]. Therefore, modular and hierarchical control frameworks are expected to play an important role in improving the robustness and industrial applicability of intelligent LW-DED systems.

8. Sustainability performance

Industry accounts for approximately one third of global GHG emissions, largely driven by energy use [311]. Circular and sustainable strategies based on the 6Rs framework (Reduce, Reuse, Recycle, Recover, Remanufacture, Redesign) could significantly improve both energy and resource efficiency [312]. LCA remains an essential approach for process evaluation and comparisons, even though recent ‘absolute sustainability’ approaches demand thresholds aligned with

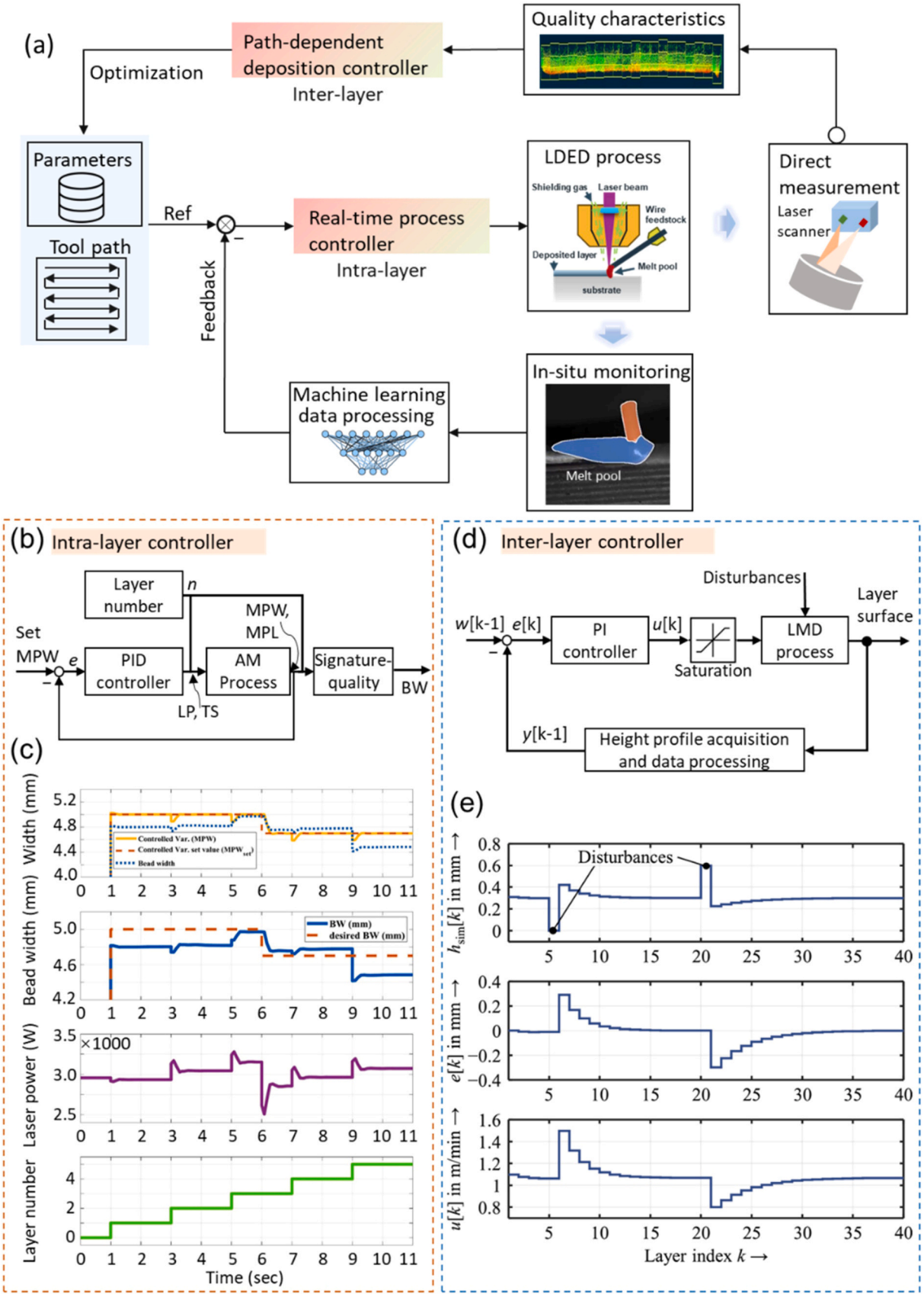


Fig. 16. Online LW-DED process control: (a) overview of two hierarchical control systems (adapted from [296]), comprising intra-layer control, including (b) melt-pool width control and (c) real-time regulation of laser power (adapted from [89]), and inter-layer control, including (d) layer height control and (e) tuning of wire feed rate for each layer (adapted from [90]).

planetary boundaries [313]. Integrating these concepts within the Triple Bottom Line (TBL) framework, encompassing the environmental, economic and social dimensions of sustainability, can enable manufacturing to transition from a major emitter to a driver of sustainable and circular transformation. This section reviews the sustainability implications of LW-DED based on the current body of literature. However, existing studies remain limited and fragmented, reflecting the early maturity of the field rather than a shortcoming of individual contributions. To address this, the section integrates direct evidence from LW-DED studies with indirect insights derived from adjacent wire-based DED technologies, while explicitly distinguishing transferable findings from technology-specific limitations. To better contextualise the available evidence, sustainability-related studies in LW-DED are categorised into three levels: (*i*) direct assessments explicitly addressing environmental, economic, or social impacts; (*ii*) indirect process-oriented studies reporting energy use, material efficiency, or defect mitigation; and (*iii*) proxy evidence derived from related wire-based DED processes, particularly WA-DED, where more extensive sustainability analyses are available. This approach allows the identification of current knowledge gaps while avoiding overgeneralisation from incomplete datasets.

8.1. Current research landscape on sustainability of LW-DED

Few studies have explicitly addressed the sustainability of LW-DED processes through dedicated investigations. This evidence has already been documented by Pusateri et al. [314], who recently reviewed 115 papers (84 original studies and 31 reviews) on metal AM published between 2003 and 2023 (85% in 2016–2023), finding powder-based AM technologies to be dominant (85%). Only 3 out of these 115 studies consistently applied the TBL approach, and these included only qualitative social impact assessments. Overall, 79% accounted for environmental aspects and 33% economic ones. Nonetheless, some of the technology-oriented studies on LW-DED can be considered relevant to sustainability (even if such assessments are not directly performed), including those focusing on energy consumption reduction, resource use minimisation, improved material efficiency, or defect/scrap mitigation, as summarised in Table 5. Despite the diversity of technological interventions, quantitative assessments of their sustainability impact remain scarce, preventing direct comparison across studies and highlighting the need for standardised reporting metrics.

Table 5
Technology-oriented LW-DED studies with indirect sustainability relevance.

Intervention area	Technological investigation (s)	Sustainable implication (s)
Process parameters	Tuning the laser-beam shape to reduce irradiance required for melt-pool formation from 480 to 190 W/mm² [315].	Reducing energy consumption (environmental impact and cost).
Auxiliary equipment	Preheating the wire with electrical resistance to stabilise the melt-pool [249].	Improving material properties; reducing scrap/material disposal.
Robotic build strategies	Optimising the toolpath and build-plate orientation for laser hot-wire DED with an 8-axis robot [310].	Reducing material waste by avoiding sacrificial supports and machine tools for cutting off the supports.
Wire feeding strategies	Investigating wire-feeding configurations in addition to coaxial and off-axis (frontal/lateral) approaches [81,247,316].	Reducing defects and scrap generation; enabling in-situ repair without component disassembly, with potential reductions in transportation requirements.
Modelling and simulation	Predicting thermal and microstructural evolution with phase-fraction forecasting at significantly reduced computational cost [83].	Providing a viable alternative to labour-intensive full-scale characterisation; improving material usage.
Real-time monitoring and closed-loop control	Modulating laser power in real-time to enhance melt-pool stability, increase deposition rates, and reduce inter-layer dwell times [244].	Converting heat accumulation from a limitation into a lever; lowering cooling-system energy use and cost.
Coating and repair	Cladding of protective coatings for part restoration and maintenance [317]. Underwater cladding for marine-component repair [318].	Reducing material usage and downtime via remanufacturing and extending service life of parts.

8.2. Energy consumption and emissions

Both deposition energy and material usage efficiency in wire-based DED processes are closely linked to the melt pool behaviour. Its formation, size, and cooling dynamics largely determine the energy demand and the amount of deposited material, which in turn affect the subsequent finishing operations [319]. Fig. 17a illustrates how melt pool control, process parameters, and equipment interact within the

Table 4
Machine learning application to LW-DED process monitoring.

ML algorithms	Experiment	Input	Output	Comments	Refs
Regression:					
Multi-modality convolutional neural network (CNN)	Single layer, single bead	Melt pool images and temperature	Bead width and height, fusion zone depth and area	Served as feedforward model for closed-loop control	[304]
Gaussian process regression	Single layer, single bead	Process parameters	Bead width, height, fusion zone, dilution and microstructure	Served for parameter optimisation in the material design framework	[289]
Random forest	Single layer, single bead	Process parameters	Bead width and height	Compared with lumped model (physics-based)	[292]
YOLOv8 + CNN	Single layer, single bead	Melt pool images	Bead width, height and area	YOLOv8 segmented melt pool serving as input for prediction	[84]
Artificial neural network (ANN)	Single and multi-bead	Melt pool size and temperature	Bead width	Signature-quality model is applied for closed-loop control	[89]
Classification:					
Naïve Bayes	Single layer, single bead	Process parameters	Bead overall quality: smooth, rippled, failed	Classification model is used to filter inappropriate parameters	[289]
Convolutional long short-term memory	Single and multi-bead	Melt pool video	Process flaws: wire dripping, arcing, stubbing, melt oscillation	Anomaly detection for regularity score	[98]
Logistic regression, support vector machine, K-nearest neighbors, ANN.	Thin-wall parts	Melt morphology	Process states: dripping, incomplete melting, stubbing	Benchmarked against computationally intensive CNN	[84]
CNN-based models (pre-trained network)	Thin-wall parts	Melt pool images	Process stability: intersection of laser beam, wire, and top layer	Can be used for deposition height prediction	[225]
CNN	Multi-layer and multi-bead	Melt pool images	Material transfer states: dripping, weak link, stable, stubbing, etc.	Yields a stability indicator for continuous deposition	[297]

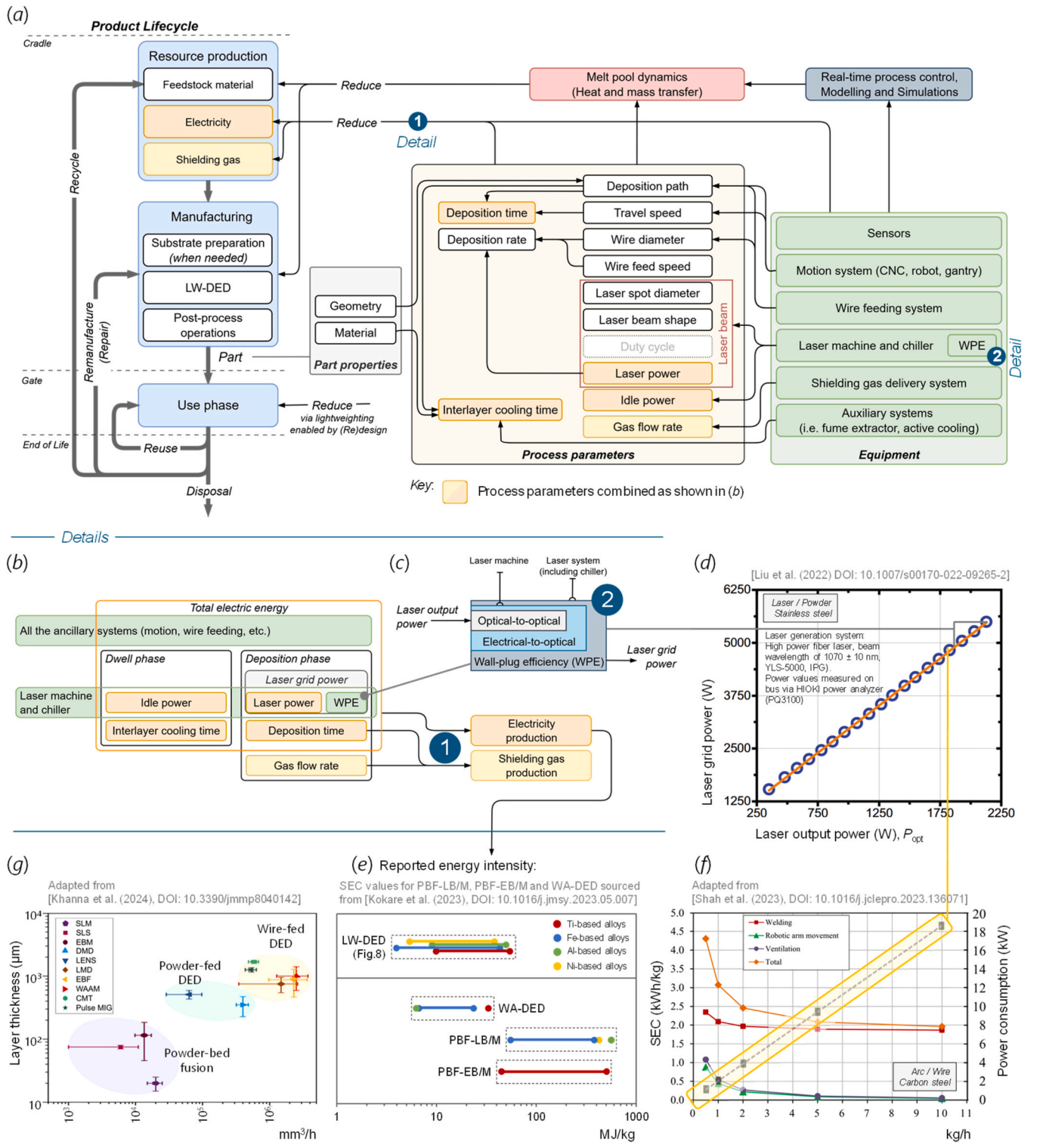


Fig. 17. Sustainability performance of laser wire directed energy deposition: (a) key process parameters and enablers for melt pool dynamics control; (b) combination of process parameters affecting electricity demand and shielding gas use; (c) efficiency hierarchy in the laser system; (d) relationship between laser input (grid) power and laser output power (in DED-LB/p) [290]; (e) comparative energy intensity across technologies, including specific deposition energy for LW-DED and literature-reported SEC values for other metal AM processes, and (f) SEC breakdown as a function of deposition rate (example for DED-Arc/w) [325]; (g) layer thickness for wire- and powder-fed DED processes and powder-bed fusion [348].

manufacturing stage (here framed in the product life cycle). Melt pool formation is primarily controlled by laser power and travel speed (*TS*); their ratio is commonly used as a simplified proxy for the heat input [84] and supports the development of operating maps that identify smooth rather than defective regimes [317]. The selected laser power depends on the material being processed (e.g., aluminium often requires higher power due to reflectivity and thermal conductivity [320]), and it is correlated to the laser spot size and wire-laser configuration [46]. The energy associated with the active deposition phase can be estimated from the average optical output power (P_{opt}), combined with the duty

cycle, where applicable, and deposition time (t_{dep}), while accounting for losses in the laser system, including the chiller subsystem (Fig. 17b). The laser grid power (P_{grid}) can be directly measured at the system inlet or estimated by using the wall-plug efficiency (WPE, defined as the P_{opt}/P_{grid} ratio, Fig. 17c-d [321]), noting that WPE varies with the nominal optical power (the higher the output power is, the higher the efficiency typically becomes). For example, varying P_{opt} from 400 to 800 W can lead to a 22.8% increase in laser efficiency [322] in a system that includes the generator plus the optical path. Additional electricity consumption from auxiliary systems (e.g., fume extraction, ventilation, motion) must also be considered. The active deposition time can be first approximated by the deposition path length (influenced by the part geometry) divided by *TS*, which in LW-DED typically ranges from 0.05 to 2.4 m/min [46].

To quantify the energy delivered to the material during deposition, deposition-oriented metrics such as Specific Energy Input (SEI) [323] and specific deposition energy have been proposed. Their values typically exhibit a non-linear decrease as the deposition rate (*DR*) increases. Moreover, factors such as the material and process setup can influence this trend [324]. For the sake of exemplification, Fig. 17 f decomposes total electricity consumption for WA-DED: as *DR* increases, energy required for ventilation falls because operating time is reduced [325]. Similar trends are likely to occur in LW-DED, which moreover generates lower fume levels [310]. By contrast, the deposition-energy share is less sensitive because higher deposition rate requires higher laser power (Fig. 17 f); in laser cells, chiller demand rises accordingly and may become comparable to the laser load [326]. Moreover, if, as observed for WA-DED processes, higher *DRs* result from a combination of process parameters that on the one hand shorten t_{dep} but on the other hand increase energy input, interlayer cooling time (or dwell time, t_{dwell}) may be prolonged. In such cases, the machine would operate longer at idle power (P_{idle}). Nonetheless, since P_{idle} is expected to be relatively low and deposition power is delivered over shorter times, the overall electricity consumption would generally tend to decrease [327]. In addition, if active cooling or alternative configurations were used, their extra energy should be included and justified by quantified benefits. Typical *DRs* are reported in the literature to be lower than 8.3 g/min for powder-laser DED, 1.5–48.0 g/min for LW-DED, 16.7–66.7 g/min for WA-DED, and lower than 330 g/min for EBW-DED [46]. As for the energy consumption during t_{dwell}, the idle power P_{idle} is generally lower than the power required in the active deposition phase and its contribution to the total power demand varies depending on system scale, equipment, and process parameters. For instance, while investigating a fibre laser by varying the output power from 100 W to 900 W, Urresti et al. [322] measured a corresponding deposition power demand of 0.9 and 3.6 kW, respectively. With a constant idle power of 0.38 kW, this corresponded to approximately 42% and 11% of the deposition power demand, respectively. The quantification of t_{dwell} is product-dependent, as it depends on the thermal energy involved, deposited material, deposition path, number of layers, and the presence or absence of active cooling [328]. Its estimation is case-specific and would require testing or simulation, while the choice of a fixed dwell time has direct implications for the resulting geometry [329].

While SEI and similar indicators provide useful information on the energy requirements during material deposition, they typically do not capture non-productive phases such as dwell time, auxiliary systems, and idle operation. For this reason, a more comprehensive metric, such as Specific Energy Consumption (SEC), can be used to account for the total energy demand of the unit process, as it integrates all energy contributions over the entire processing time. Together, these metrics provide a basis for evaluating not only energy efficiency but also economic performance, as they directly relate energy consumption to process throughput across different process configurations and technologies, particularly in terms of productivity–energy trade-offs. Fig. 17e compares literature-reported SEC values for selected metal AM technologies with the dataset presented in Fig. 8. A direct comparison across technologies remains challenging because different studies adopt different system boundaries and energy accounting approaches. Reported values may refer to machine electricity demand, deposition- or process-level energy consumption, or more comprehensive metrics incorporating upstream energy contributions. However, even if data available across different material classes remain scattered, reflecting variations in equipment, process configurations, and operating parameters, the reported data generally place wire-based DED processes in a lower energy-intensity region than powder-bed fusion technologies. It is worth remarking that, in wire-based DED processes, non-productive phases such as interlayer dwell time, idle operation, shielding gas delivery, auxiliary equipment, thermal management strategies, and active cooling can contribute significantly to the overall energy demand. Consequently, the total SEC depends not only on process parameters but also on component geometry, deposition strategy, thermal history, and machine configuration. Therefore, the lack of energy–deposition relationships or scaling laws across alloys represents a relevant research gap in the current LW-DED literature and highlights the need for standardised methodologies to enable cross-study comparison.

Once total electricity consumption (in kWh) is obtained, CO_2-equivalent emissions can be calculated by applying a country-specific grid-emission factor that reflects the electricity mix of renewable and non-renewable sources. For the EU−27 (2023), the European Environment Agency (EEA) provided an average value of 0.207 $kgCO_2$-eq/kWh (ranging from 0.008 $kgCO_2$-eq/kWh in Sweden to 0.594 $kgCO_2$-eq/kWh in Poland) [330]. Electricity prices are also geography dependent. Average values for EU non-household (500–2000 MWh/year) in 2024 ranged from 0.16 €/kWh to 0.19 €/kWh [331], while typical values in literature are within the 0.11–0.15 €/kWh range [332,333]. Regarding the shielding gas used to prevent oxidation in the melt zone, it contributes to both environmental and economic impacts [46]. Although often overlooked, shielding gas consumption can represent a non-negligible share of impact and operating cost, particularly in long-duration builds, and should therefore be explicitly included in techno-economic assessments. Pure argon (99.99%) is typically used on a once-through basis (i.e., not recovered), and vented at a constant flow of 15 L/min [197], 20–25 L/min [79,84,142], and sometimes reaching 28–40 L/min [87]. Our survey of gas flow rates used in approximately one hundred of LW-DED studies published in 2024–2025 [52,63,70–80,82–86,88–91,98,139–149,151,152,154–157,163–165,170,186,187,193–234] shows that nearly half of the studies report argon flow rates above 20 L/min. Under constant gas-flow conditions, the impact of shielding gas use is expected to be proportional to the active deposition time [334]. To put it into perspective, at a consumption rate of 20 L/min a typical 40-litre gas bottle at 150 bar containing 6000 litres of argon lasts for nearly 300 min (~5 h) of deposition. The cost of argon is approximately 2.3 €/m^3 [335]. Thus, approaches to reduce gas consumption can have a tangible impact. Aditya et al. [72] used a dual gas flow, one to protect the melt pool at 12 L/min and another to protect the laser optics at 3 L/min. Other authors, instead, employ an airtight processing chamber to shield the processing zone [213]. While shielding gas costs have been shown to exceed electricity costs in WA-DED [336] (e.g., representing 48% versus 44% of the total impact, respectively [334]), the corresponding contribution in LW-DED processes remains unknown, despite the high energy consumption expected from the laser system. A conservative argon carbon footprint was assumed to be 0.18 ± 10% $kgCO_2$/kg [337], including the effects of gas storage and transportation in a cradle-to-gate quantification. Other authors have reported different values; for instance, Lavery et al. [338] assumed an energy requirement of 0.1 kWh/kg (i.e., 0.37 MJ/kg) for argon production, while the value of 0.69 MJ/kg considered by Kamps et al. [335] would correspond to a carbon footprint lower than 0.05 $kgCO_2$/kg based on the European electricity mix. In this context, life-cycle assessments explicitly accounting for shielding gases and their optimisation are still lacking, particularly for industrial scenarios in different regions, where variations in electricity mix and gas production infrastructure can

significantly affect the overall impact.

8.3. Life-cycle oriented analysis

In sustainable development, the role of manufacturing processes is increasingly assessed within the broader life cycle of products rather than in isolation. This perspective is well established in the scientific literature, as environmental, economic, and social impacts can shift across life-cycle stages. This is typically operationalised for AM-based manufacturing routes through frameworks such as Life Cycle Assessment (LCA), including cradle-to-gate and cradle-to-grave approaches, as well as complementary methodologies such as Life Cycle Costing (LCC) and Social Life Cycle Assessment (S-LCA) [314]. Adopting an LW-DED process has sustainability implications both upstream (material consumption) and downstream (post-processing, use phase performance, maintenance, repair, and end-of-life strategies). Laser-based DED produces a small, localised melt pool thanks to the high energy density of the laser, enabling precise heat-input control and the deposition of intricate geometries with limited distortion [50]. This precision also affects allowances: they are expected to be lower than in WA-DED yet higher than in powder-based routes, unless the wire diameter is reduced, as in laser micro-wire deposition [339] or cladding [340]. Thermal behaviour is further driven by geometric complexity, which influences deposition quality and the extent of post-processing (heat treatment, HIP, finish machining, grinding) [341]. Favi et al. [342] report specific primary energy values for the manufacturing phase across different processes, showing wide variability for AM. Beyond material and parameter effects, the variability observed in SLM (65–670 MJ/kg deposited) reflects differing laser sources and build-chamber sizes. In PBF, chamber occupancy changes per-part allocation and thus per-kg values. DED processes, including wire- and powder-fed variants, show a range of 30–605 MJ/kg deposited. Overall, the manufacturing phase of metal AM often remains energy-intensive relative to conventional manufacturing despite material-efficiency gains. When extending the analysis to the full life cycle, impact drivers (materials, energy/consumables, equipment, labour) shift with the production route. From the environmental perspective, material often dominates cradle-to-gate impacts per kg (e.g., 41–45% for steel) in WA-DED [325, 332]; in SLM, electricity represents a major impact contributor, due to energy-intensive powder production, laser and chiller use, chamber reheating, and powder spreading at each layer (20–120 μm, Fig. 17 g) [343]. This positions LW-DED within a fundamental trade-off between the low embodied energy and high material efficiency of wire feedstock, on the one hand, and the operational energy demand of laser-based systems, on the other; this balance remains insufficiently quantified in the current literature.

The impact of feedstock materials transformed by LW-DED processes is strongly influenced by three main factors. First, process-intrinsic efficiency, where near−100% is achievable in wire-based processes [46]. Part geometrical configuration and complexity also play a key role [344], and similar advantages are expected for LW-DED. Secondly, impacts depend heavily on primary versus secondary sourcing. For Ti–6Al–4 V, embodied energy decreases from nearly 700 MJ/kg for primary material production to 580 MJ/kg with 49% secondary content, and CO_2-equivalent emissions decrease from nearly 42–28 $kgCO_2/kg$. For AISI 316 L (with 35% secondary content), embodied energy decreases from 86 to 66 MJ/kg, and CO_2-equivalent emissions from nearly 7.5–5.5 $kgCO_2/kg$ [345]. Finally, repair strategies, enabled by LW-DED, can markedly reduce impacts by preserving embedded value [346], even across multi-repair loops [347].

From an economic standpoint, material prices usually rank below machine time and labour, though increased competition and maturing supply chains should reduce prices [348]. Indicative prices for titanium, Inconel 718 and 316 L steel from the 2024-market were 79, 98 and 34 €/kg for wire, respectively, and 368, 170 and 115 €/kg for powder [348], corresponding to a powder-to-wire price ratio of approximately 1.7–4.7. The effective cost advantage of wire feedstock can further increase when material utilisation is considered, since wire-based processes avoid powder overspray and recovery losses. Further, wire avoids energy-intensive atomisation, easing manufacture and recycling and aligning with circular-economy principles [349]. Metal wire can even be produced as a by-product from other processes like stationary shoulder friction stir channelling [350]. As for operational costs, typical equipment charges are 12 €/h for WA-DED, 20 €/h for SLM, and 6 €/h for CNC [351], while labour ranges from 15 €/h [351] to 22 €/h ± 15% [327]. Consequently, longer processing and operator involvement increase costs, typically higher in SLM than in WA-DED. To quantify LW-DED costs, trade-offs must be found considering that laser-based DED systems generally cost more than WA-DED cells, but less than commercial PBF machines. Moreover, because wire-based cells do not require powder-handling hardware, they allow more open, lower-cost architectures and easier retrofits for hybrid use, potentially reducing capital expenditures [352]. Finally, hourly LW-DED costs should be weighed against *DR*s that are typically higher than in powder-based processes but lower or comparable to that of WA-DED [46]. To provide a holistic economic picture, environmental externalities can also be monetised via shadow prices, as shown by Gouveia et al. [333] using environmental prices adjusted for inflation. From a techno-economic perspective, LW-DED can be positioned within a three-dimensional trade-off space defined by (*i*) material efficiency, (*ii*) energy consumption, and (*iii*) capital and operational costs. Compared to powder-based processes, LW-DED can offer higher material efficiency and lower feedstock cost, while compared to WA-DED it can provide higher precision at the expense of increased energy demand and equipment cost. The lack of comprehensive environmental and economic assessment studies specifically addressing LW-DED remains a critical limitation for industrial adoption, as it prevents robust benchmarking against alternative manufacturing routes. Future work should prioritise the development of standardised LCA/LCC frameworks tailored to large-scale DED processes.

From a social perspective, available evidence up to 2023 for metal AM is limited but broadly positive; potential downsides include the need for specialised personnel and automation-related job losses, especially in emerging economies [314]. These considerations extend to LW-DED. A Social Life Cycle Assessment (S-LCA) of WA-DED found negative impacts on local communities from $PM_{2.5}$ and NO_x linked to material production, positive impacts for workers, society, and suppliers, and neutral for consumers. Key issues identified included weak technology transfer, gender gaps, employment disparities, and air-quality concerns; recommended actions included diffusion to low-tech firms/emerging economies, removal of entry barriers, training, and air-quality monitoring near material-production sites [353]. Lastly, wire feedstock generally offers cleaner shop-floor conditions than powder, reducing operator-exposure and dust-explosion risks and simplifying handling and logistics [352]. However, the scalability of these social benefits remains uncertain, particularly in highly automated industrial settings where workforce requirements may decrease.

9. Capabilities and applications

Like most technologies in an early stage of development, LW-DED is surrounded by significant hype, often misleading researchers about its actual value to industry. In preparing this section, we analysed applications in hundreds of sources such as academic papers, websites of private labs, DED equipment producers and AM service providers, and even applied large language models, such as ChatGPT and Scopus AI, to cross-check these resources and verify whether any proven prospect of LW-DED was missed. The identified applications ranged from biomedical implants [143] to pedestrian bridges [45], yet deeper analysis showed that only a fraction of applications in that range could present a commercial case. Many printed components, although impressive, are more demonstrative than practical for industrial adoption, e.g., printing

bollards, wheel disks, and other simple shapes without added value over casting. Accordingly, this section aims to showcase meaningful uses of LW-DED. It starts by mapping LW-DED capabilities among other AM technologies, highlighting its competitive edges in the manufacturing technology market, and then classifies LW-DED applications, not exhaustively but focusing on the most recent and commercially viable ones in the high-value manufacturing sector. Such demonstrators primarily highlight technical feasibility and should be interpreted with caution when considering full life-cycle costs and industrial implementation. While a wide range of applications have been demonstrated for LW-DED, their industrial relevance must still be critically assessed in light of process cost, scalability, and lifecycle performance, which remain key factors for sustainable deployment and are not yet consistently quantified in the current literature.

9.1. *Benchmarking versus other AM technologies*

LW-DED is not intended to compete with other AM technologies, but to extend the size scale, productivity, and material selection range. In brief, while offering larger print size, productivity, and material range than other AM processes, it exhibits lower performance in part accuracy, surface roughness, and design complexity, as visually compared in Fig. 18. The print size and productivity of LW-DED are among the highest compared to other AM systems because of considerably greater volumetric deposition rates and almost unlimited build envelope. The LW-DED systems can be configured over a wide size range, spanning from several decimetres to several metres. At larger scales, LW-DED systems are used to fabricate aerospace engine casings and ship propellers, or even pedestrian bridges, as exemplified further. The typical deposition rate averages around one kilogram per hour [80], but was shown to deliver up to 3 kg/h [80], in cases where the print accuracy is largely irrelevant, such as filling the internal space of a part or for "soft" metals (e.g., aluminium bronze), where extensive CNC post-processing can be justified. The deposition rate can be limited in small parts by insufficient heat dissipation, which leads to melting, stress build-up, and part warping, thus requiring long tool paths for intermediate cooling of hot zones [143,153] in addition to thermal treatment for stress relaxation [85,148,155,235], which increases processing time.

The print accuracy of LW-DED is perhaps the least competitive among all AM technologies (Fig. 18a). The minimum feature size and surface roughness of LW-DED parts are inferior to those achievable with PBF techniques [354–356], and nearly an order of magnitude larger than those of parts produced with binder jetting [357–359] and photopolymerisation-based methods [360–364] (Fig. 18b). Several studies have shown that LW-DED can deposit a standalone wall as thin as 3 mm, even if the wire is three times thinner [70] (Fig. 18c). The extreme case for accuracy in LW-DED, so far, is a nearly 300 μm thick wall produced with a 200 μm wire [340], but this achievement came at productivity rates far below those typical of LW-DED. For comparison, fused deposition modelling allows printing 1.0–2.0 mm thick walls [258,365–367], SLM systems produce 0.3–0.5 mm walls [354–356], while binder jetting and lithography metal additive manufacturing (LMAM) can achieve 0.2 mm [357–359] and 0.1 mm [362,363] thick walls, respectively (with some limitations [368]). Similarly, for surface roughness, LW-DED parts are characterised by a submillimetre surface waviness, while SLM and LMAM can produce surfaces with average height of the profile (R_a) as low as 10 μm [369,370] and 1 μm [362,363], respectively. The accuracy and roughness in LW-DED can be improved by using a smaller wire and laser beam [74,224], yet at the expense of productivity to an extent where both would not be competitive with those of SLM.

The design space for LW-DED has many geometrical limitations regarding what can be meaningfully printed from technical and economic perspectives. The printable geometry is limited by the self-supporting angle, the ability to access its surface with CNC tools, and sometimes by the substrate (as it is often an integral part of the

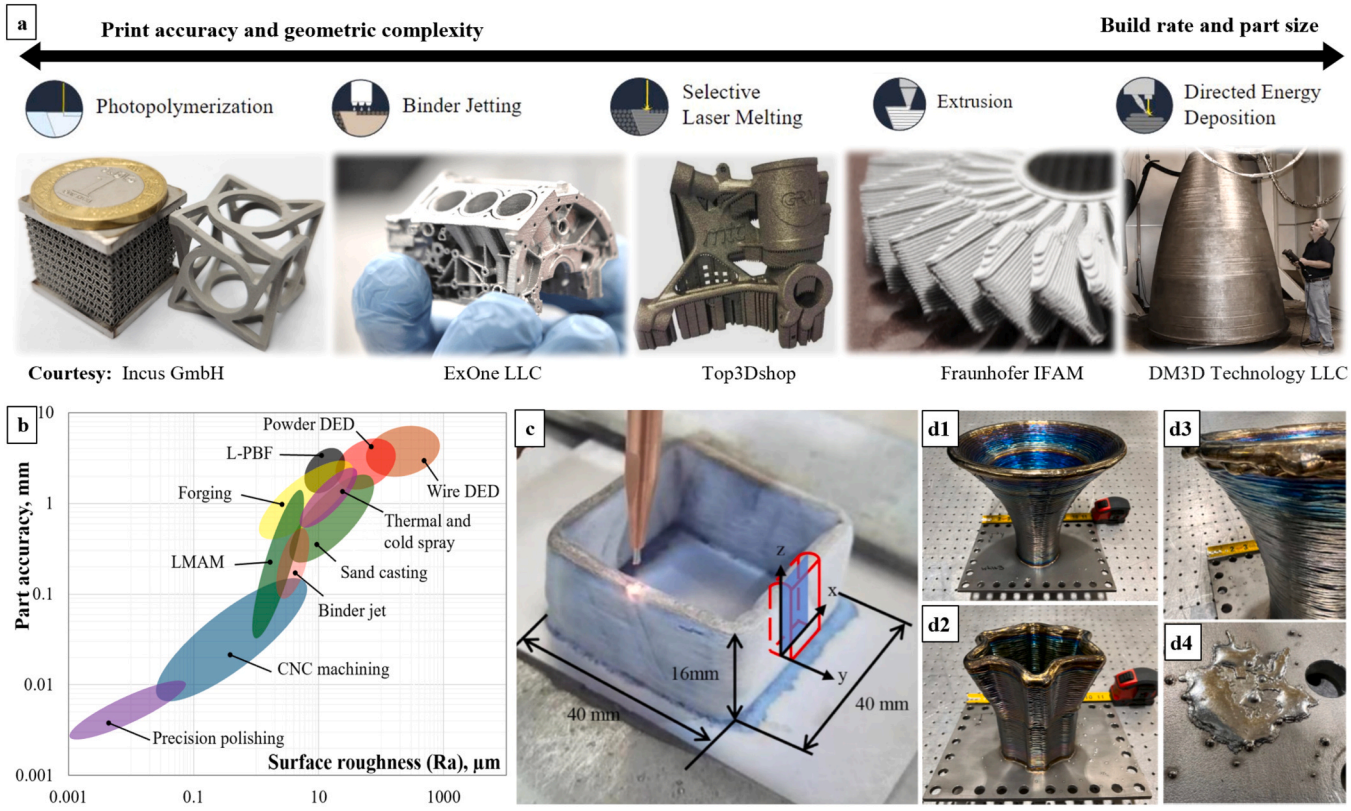


Fig. 18. Benchmarking capabilities of laser wire directed energy deposition (DED) versus other metal AM technologies: (a) print size and complexity [361], [57]; (b) part accuracy and surface roughness [362]; (c) minimal wall thickness [70]; (d1-d4) maximum unsupported overhang and associated defects [310].

component). Generally, LW-DED does not use support structures, because they would be monolithic and difficult to remove, thus the geometry of the part is restricted to curved surfaces with limited overhangs, without fine internal features. Unsupported overhangs were successfully deposited at 35° without the build plate tilt, beyond which the molten metal flows down, forming geometrical defects or dripping of molten material on the platform beside the part (Fig. 18d) [310]. LW-DED systems with five or more degrees of freedom can build more complex geometries by tilting the part relative to the deposition head to maintain consistent deposition orientations relative to gravity [310]. Some improvements in design freedom can also be achieved through parametric optimisation and by changing deposition orientation [371]. To expand the design space, hybrid LW-DED/CNC systems can be configured to intermittently perform CNC machining during printing to reach internal cavities that become enclosed in the final part [170].

The post-processing of LW-DED-produced structures includes heat treatment for stress relaxation [253] and CNC machining to reach final tolerances. This motivates hybrid process integration of additive and subtractive processes in a single unit to achieve a net shape geometry. The versatility and length-scale compatibility of LW-DED are driving significant industrial growth, especially for hard-to-machine, extensive-to-machine, high-temperature, and lightweight alloyed components in high-value manufacturing sectors. Industrial adoption of LW-DED requires explicit recognition of accuracy-throughput-reliability trade-offs. High-accuracy deposition (e.g., using fine wires, closed-loop melt pool control, or coaxial heads) reduces post-processing but lowers deposition rates and introduces system complexity that can compromise reliability in shop-floor environments. Conversely, prioritising throughput (via higher power and wire mass feed rates) achieves kg/h productivity but yields rougher as-built surfaces ($R_a = 50–150$ μm) and shape deviations, necessitating heavier CNC finishing. For many large-scale applications, especially where the roughness is not functional, accepting lower as-printed accuracy in favour of high deposition efficiency is economically justified. The key is matching application requirements: precision-critical features (sealing surfaces, thin walls) justify slower, monitored deposition, whereas bulk filling or geometrically tolerant parts benefit from maximum throughput. Future cost models should quantify these trade-offs using metrics like $/kg per unit surface roughness or post-processing hours per kg deposited, enabling users to select LW-DED configurations aligned with product requirements.

9.2. Competitive edges

LW-DED is not intended to replace existing manufacturing processes across all applications, but rather to address specific niche and emerging use cases. Beyond current commercial expectations, there are only a few niches where LW-DED can be competitive. The first niche for LW-DED is to replace casting, forging, welding, and CNC machining of non-serial large complex components consisting of difficult-to-machine superalloys. The production of such parts, taking casting as an example, requires an entire workshop for making single-use sand/gypsum moulds, a heavy part manipulation platform and a CNC machine dedicated to that exact part, as well as loading mechanisms and peripheral facilities. LW-DED aims to create a compact, cheaper, and faster production alternative. It is particularly beneficial for the production of superalloy parts where the raw material is expensive and difficult to process, such as titanium, tungsten, and nickel-based alloys among others. The production of large titanium forgings has conventionally required extensive material removal. Because titanium is a limited resource, finding a manufacturing option using less raw material is economically beneficial. Thus, LW-DED could be a competitive alternative to reduce the equipment and labour costs for components that have been manufactured conventionally for decades or even a century, e.g., ship propellers and jet engine nozzles, as exemplified further. Typically, AM technologies cannot compete with those production processes, and therefore it is a notable advantage of LW-DED.

The second potential niche for LW-DED is the production of parts whose design and functionality do not exist today, such as functionally graded and multi-material components. Changing feedstock (wire) in LW-DED during printing is simpler than in any other AM technology, creating interesting opportunities for multi-metallic parts, where some areas of the part are made of two, three, or more different alloys to address different local needs of the component, whether they are physical, mechanical, or chemical. Many studies have been conducted with LP-DED, and only recently (in the past few years) the topic has been explored with LW-DED, so far for different steels [240], steel-titanium [211], steel-aluminium alloy [82], steel-Inconel [75], and Inconel-copper alloy [212], targeting monolithic components with combined functionalities, such as load-bearing, with enhanced tribological and heat transfer capabilities, that were not previously considered manufacturable. Considering the current environmental trends in energy and mobility (e.g., the rise of electric vehicles), the production of lightweight parts that could perform functions typically associated with heavier components, for example, can have strong future potential.

Other competitive edges were claimed by researchers and LW-DED service providers, yet these are often specific cases. One of them is in situ local repair of difficult-to-access components, such as underwater components of nuclear plants [219,372,373], as elaborated in further subsections. In another case, a DED service provider in the Netherlands produced a customised crane hook, an order that metallurgical plants may decline due to the limited number of units requested. Furthermore, the high productivity of LW-DED can be used as a duplicate production method to ensure lead time reliability in case of logistics disruptions. In an industrial case, an automotive manufacturer used LW-DED to produce tow hooks for their vehicles to substitute cast components that were delayed in customs. LW-DED can also be used for the fabrication of heat exchangers; however, due to its low accuracy, not directly, but in combination with CNC machining or by adapting the process, for instance by depositing onto a fine metal tube that can circulate cooling fluid [223]. In short, due to its high productivity, LW-DED is useful for manufacturing in remote locations, for unique or time-critical parts, and where additional economic factors come into play.

9.3. Commercially viable applications

9.3.1. Difficult-to-machine superalloys components

Superalloys, such as highly alloyed steels as well as nickel-, chromium-, and molybdenum-based alloys, are difficult to machine into structurally functional components using conventional cutting processes, yet they are often needed for aerospace applications. To facilitate access to space for current and future missions, systems-level cost requirements are being flowed down to the component level to reduce associated design, development, and manufacturing costs while maintaining high performance. As a result, the space industry has embraced metal AM technologies, with PBF as the front runner so far, to reduce the production costs of hard-to-machine superalloy components [374]. However, PBF techniques are limited in scale (e.g., 32”×16”×20” max.). Electron beam-based DED offers larger area capability but is limited in build height (96” diameter × 48” height) and in the range of available metal alloys [191,375]. High-power WA-DED allows high build rates and large build sizes, yet at the cost of process resolution and significant distortions in the part [375,376]. This is where LW-DED becomes advantageous. To exemplify, DM3D Technology LLC, jointly with NASA, produced the 2.5 m-large and 2.8 m-tall RS−25 engine nozzle liner for the Artemis II moon rocket core stage (Fig. 19a–b). The RS−25 nozzle liner was printed with JBK−75 stainless steel, an age-hardenable superalloy. JBK−75 has high thermal conductivity, high-temperature strength, and resistance to hydrogen embrittlement, making it a widely used material for nozzle liners, hot gas sections, structural jackets, and hot gas manifolds in rocket engines. They tailored a DED system comprising a 3-metre build envelope with a rotary tilting table,

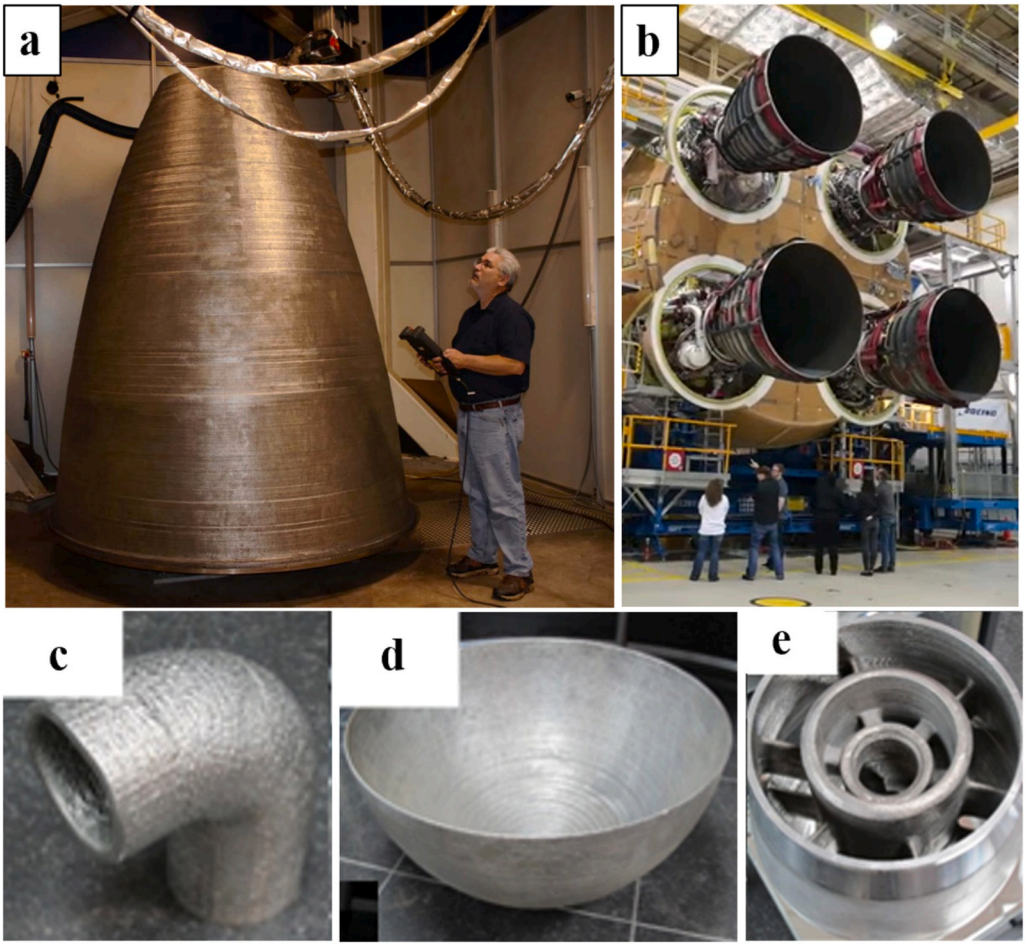


Fig. 19. Hard-to-machine superalloy parts for aerospace applications: (a) full-scale RS−25 nozzle liner upon completion of the build and (b) installed in the core stage of the Artemis II rocket [57], (c) hollow elbow, (d) hemisphere, and (e) turbine engine part [206].

two simultaneously depositing coaxial nozzles, and feedstock preheating. Replacing conventional manufacturing with the DED setup for this component resulted in up to 50% reduction in lead time and cost [57]. Further, DED has enabled new engine designs and materials that are difficult to process using traditional techniques. Beyond nozzle liners, DED capability has been estimated to halve the lead time and costs of combustion chambers, elbows, valve cups, turbine parts, and other components of liquid rocket engines [374] (Fig. 19c–e). Considering multiple military programs that use such engines, wider adoption of DED technologies by the space industry is likely to increase [374]. Besides alloys, LW-DED can build metal-carbide composite parts that would be quite impractical to produce by milling. Zhao et al. [142] incorporated hot-wire-fed laser deposition and remelting for repairing stainless steel with WC-Ni composite multilayers reinforced with homogeneously distributed dual-scale tungsten carbide particles. Based on the partial dissolution of WC/W2C particles and the temperature variation of the melt pool, micro-sized WC particles were successfully synthesised in situ around the large WC/W2C particles. The wear resistance of the deposited layer was nearly 50 times higher than that of the steel substrate [142]. The thermal spray coating can also achieve similar results, yet the added advantage of LW-DED consists in the possibility of producing such composite parts in full shape rather than as a surface coating only.

9.3.2. *Components requiring extensive processing*

Unlike commonly CNC-turned and milled parts, such as shafts, pins, bushings, and connectors, some components require considerably longer processing using expensive multi-axis CNC machines, wasting large amounts of material and cutting tools to transform a cylindrical billet into a net shape part. Turbine blades and centrifugal compressor impellers are renowned for their complex design, intricate surface characteristics, and high economic value in manufacturing. The conventional method of making an impeller is casting followed by machining [377,378], which is labour-intensive and leads to high costs [379]. Impellers can be fabricated by PBF [380], yet at higher costs than casting and still requiring machining to achieve final surface roughness. Karade et al. [170] demonstrated the possibility of manufacturing impellers using an LW-DED/CNC hybrid process. They first deposited an 18 cm large hub using 1.2 mm mild steel wire, then CNC machined it to a net shape, on which the impeller blades were deposited and CNC milled to the final shape (Fig. 20). Different slicing techniques and hybridisation levels were explored to improve process efficiency and accuracy. Compared to conventional manufacturing, the hybrid approach reduced the impeller production time by 4.5 times (from 60 h to 13 h) and material waste by 8 times (from 74% to 9%). Karade et al. [170] concluded that hybridisation of LW-DED with CNC is key to cost-efficient production of geometrically complex parts.

9.3.3. *Lightweight components*

Several LW-DED developers and service providers have showcased the possibility of producing thin-walled titanium and aluminium components. GKN Aerospace AM division, jointly with Oak Ridge National Laboratory, built an LW-DED system with a flip/tilt fixture for the substrate, adding two additional degrees of freedom to the robot-mounted deposition head for complex overhangs and double-sided deposition [58]. Further, they optimised process parameters for

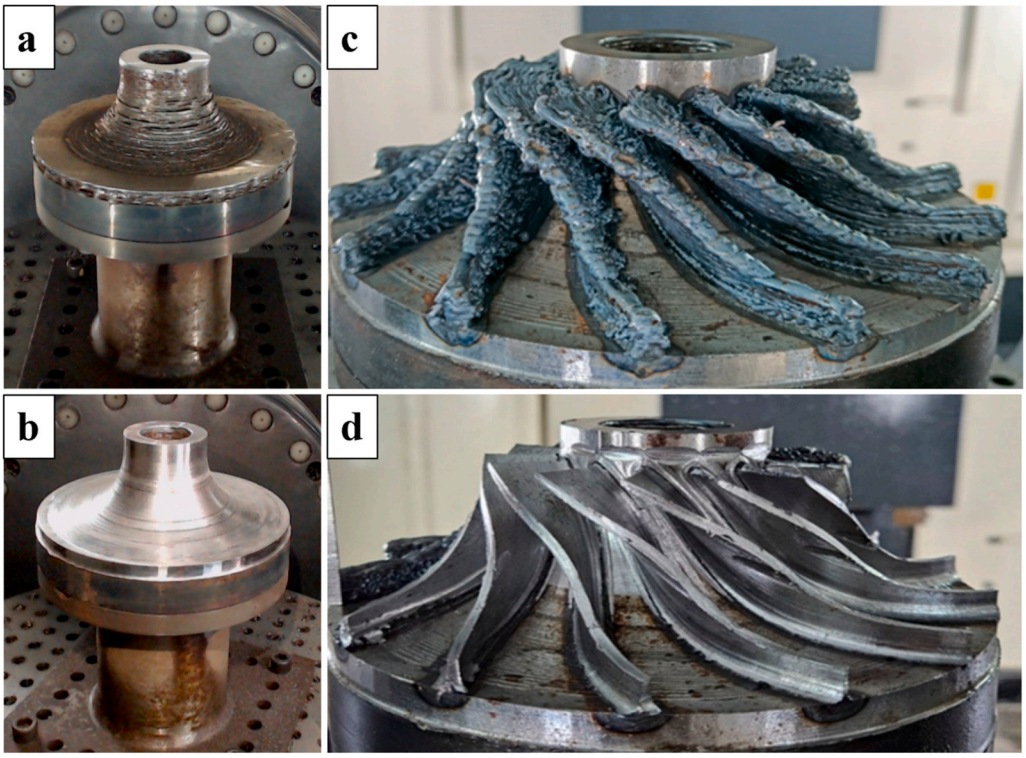


Fig. 20. Manufacturing stages of a centrifugal compressor impeller using an LW-DED/CNC hybrid process [170]: (a) as-deposited hub; (b) machined hub; (c) as-deposited blades; (d) machined blades.

printing titanium components with walls as thin as 3 mm. The Oak Ridge National Laboratory team used this process to produce a 1.3-m long fin-shaped titanium component with diamond-shaped openings, as shown in Fig. 21a. The double-sided deposition is helpful in preventing distortions and is particularly suitable for building symmetric parts with minimal CNC milling allowance to achieve net shape (Fig. 21b). Big Metal Additive, a company in Colorado, used a multi-axis LW-DED/CNC hybrid system to produce generatively designed thin-walled aluminium components as a monolith without support structures despite 45° overhangs and converging/diverging structures (Fig. 21c–e). The study of Zapata et al. [187] was motivated by the lightweighting of aluminium components in electric vehicles. They developed a methodology for LW-DED of thin-walled (3 mm) AlSi10Mg alloy parts, widely applied in the automotive sector. Huang et al. [86] introduced an oscillating laser dual-wire DED process to address the issues of low wire melting efficiency and poor forming quality of 5A06 aluminium alloy. Other examples of lightweight components, as well as a detailed comparison between wire-arc and wire-laser DED of titanium and aluminium alloys, are given in [50].

9.3.4. *High-temperature components*

Plasma-facing components in nuclear fusion reactors are exposed to extreme operational conditions. The combination of pressure and thermal loads, erosive wear, as well as neutron-induced damage, limit the number of materials suitable for this application. Tungsten is foreseen as the most suitable plasma-facing material for the demonstrational and fully operational power plants in the future, due to its exceptionally high melting point (3422 °C), excellent thermal conductivity (160 W/mK), and low tritium retention during plasma exposure [381,382]. The erosive wear (thickness reduction) of tungsten armour is expected to be as low as 0.3 mm per full power year [383]. Small armour layer thicknesses are desirable to enhance cooling; however, even if only small areas of the armour reach the end of their service life, the entire component must still be replaced. In situ local deposition of tungsten by means of AM could increase the service life of fusion reactors. However, most AM technologies, including PBF [384,385], are not suitable for in situ repairs, except the cold spray AM, which unfortunately does not work for tungsten and other refractory metals [241]. On the other hand, DED processes are particularly effective for local metal deposition [386], but this application imposes several constraints. The uncontrolled deposition of tungsten within the reactor can significantly cool the plasma through Bremsstrahlung and radiation losses [387]; therefore, the occurrence of loose material residues should be strictly avoided, excluding WA-DED. Furthermore, loose or incompletely melted tungsten powder particles can contaminate the fusion reaction, thereby excluding powder-based DED processes [48] and thermal spray [388]. In addition, the repair process should take place within the constrained space of the reactor vessel in vacuum, as this reduces possible contamination. LW-DED does not produce welding spatter or powder residues, has sufficient accuracy for thin wall repair, and the laser source can be positioned outside the vessel and guide light via fibre-optic cables to the repair location. There are few studies on the processing of tungsten by DED [389,390] or WA-DED [391,392]. Among them, the surface regeneration concept presented by Tweer et al. [221] offers an opportunity to deposit thin tungsten armour on plasma-facing components of fusion reactors using an LW-DED processing head attached to a robotic arm operating inside the vessel. The deposition of tungsten was possible on a tungsten substrate as well as on freshly deposited tungsten layers, by remelting and stacking them one upon another, delivering surface waviness below 100 μm. In the following study, Tweer et al. [154] showed that it is possible to repair damaged tungsten armour (due to thermally induced cracks) of plasma-facing components with LW-DED coating or remelting. These coatings were then successfully tested under fusion-relevant thermal loads [239]. In situ repair could significantly reduce the cost of commercial operation of fusion reactors by avoiding or delaying the replacement of damaged components. Future studies should investigate how the deposited layers perform under the conditions expected in fusion reactors.

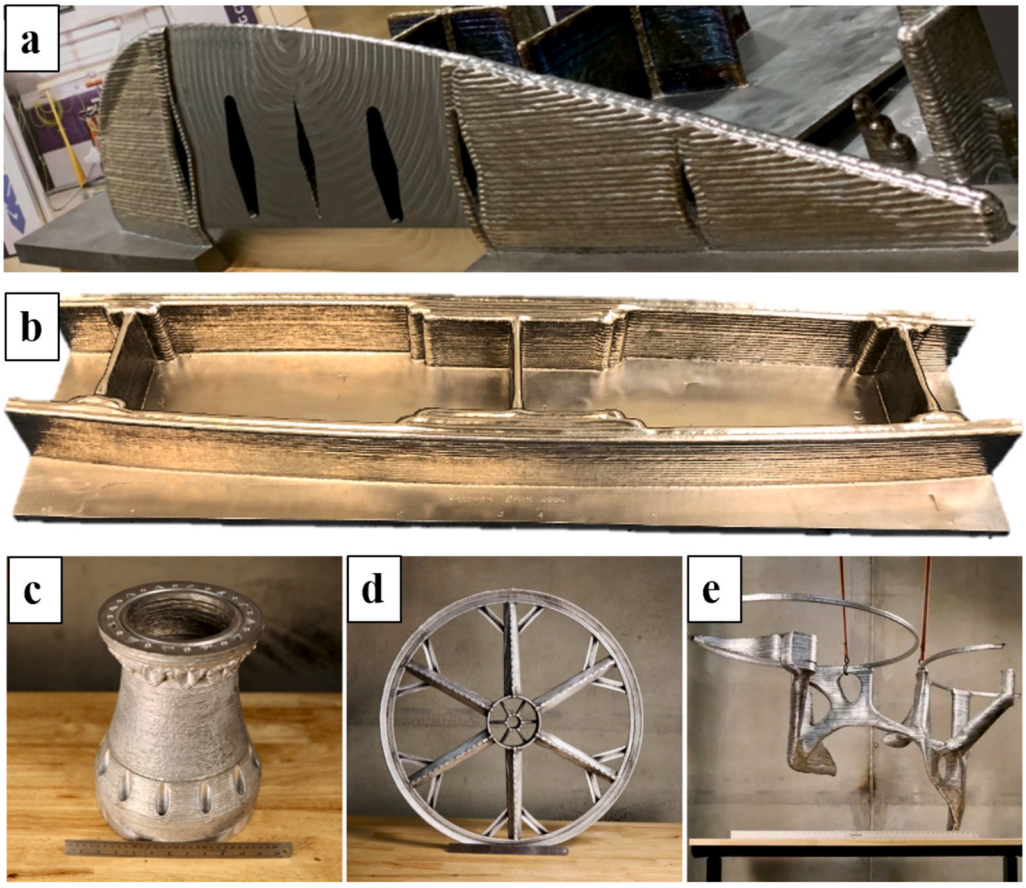


Fig. 21. Laser-wire DED of lightweight titanium and aluminium components: (a) partially machined fin-shaped titanium part (source: Oak Ridge National Laboratory Manufacturing Demonstration Facility); (b) double-sided deposition of a symmetric titanium part (source: GKN Aerospace); (c–e) free-formed aluminium shell structures (source: Big Metal Additive).

9.3.5. Large hollow components

Ship propellers are high-value manufacturing products. Large propellers are conventionally manufactured by casting molten metal into manually made single-use sand moulds to produce a near-net shape part, which then needs milling and grinding in a custom-made large CNC machine, followed by weeks of manual surface finishing, all of which require the use of heavy-duty lifting and positioning equipment, contributing to substantial costs for propellers [393]. DED presents a promising alternative to conventional manufacturing of ship propellers by offering reduced material utilisation, lead time, equipment, and overall production costs [394,395]. Notably, there is no functional requirement for ship propeller blades to be solid throughout their thickness; on the contrary, hollow propeller blades would be lighter and require less energy to operate. Moreover, a hollow blade would create an opportunity to incorporate wireless strain sensors during printing, enabling early detection of potential failure. In 2017, RamLab, jointly with Autodesk, propeller designers, a certification bureau, and a Dutch shipyard, manufactured and installed on a ship the world's first class-approved 3D printed propeller using WA-DED [396] (Fig. 22a). The propeller was 1.3 m large, weighed 180 kg, and did not require the support structures to be removed after printing. The post-processing took three days for finishing of blade surfaces using hand-held abrasive tools (Fig. 22d). In 2021, defence contractor Naval Group used wire-DED to manufacture a propeller for a French Navy ship, with a 2.5-meter span and five individual 200 kg blades, reportedly the largest thruster of its kind to be 3D printed [393]. Other examples of WA-DED propellers can be found on websites of large-scale DED providers [45] [396]. However, the structural integrity of blades produced with WA-DED remained problematic due to the risk of cracks. Further, WA-DED may lack sufficient accuracy for printing thin-walled hollow propeller blades of smaller size. Compared with WA-DED, LW-DED has a higher cooling rate and can produce finer microstructures with higher geometrical accuracy [397,398]. Deng et al. [148] experimented with LW-DED of nickel-aluminium bronze, which is a high-strength and corrosion-resistant alloy extensively employed for marine propellers, and argued for the superiority of its structural and geometrical integrity when produced by oscillating LW-DED (Fig. 22b–c). The as-fabricated bronze specimen exhibited fine equiaxed grains without porosity or cracking defects. After the normalising heat treatment (675 ℃ for 6 h), the ultimate tensile strength increased by 12% (626 MPa) and hardness by 13% (182 HV), attributed to the large increase in fine κ-phase precipitates [148]. Their study demonstrated that oscillating LW-DED, combined with appropriate heat treatment, offers a more geometrically accurate and mechanically stronger alternative solution for fabricating nickel-aluminium bronze propellers.

9.3.6. Local repair

LW-DED can be used for in-service repair of underwater components, such as maritime and offshore facilities, and nuclear power plants. This has been recently demonstrated for duplex stainless steel and titanium alloys. Duplex stainless steel is widely used in the nuclear industry, including as steel liners for spent fuel pools, refuelling pools, and primary coolant pipelines submerged under water [399]. These steel liners suffer from high-temperature radiation conditions, causing stress corrosion cracking, pitting, thermal aging, radiation damage, and creep [400]. These defects pose a risk of nuclear waste liquid leakage [401]. The conventional repair methods for these steel liners involve stopping the reactor, draining the liquid medium from the spent fuel pool, and

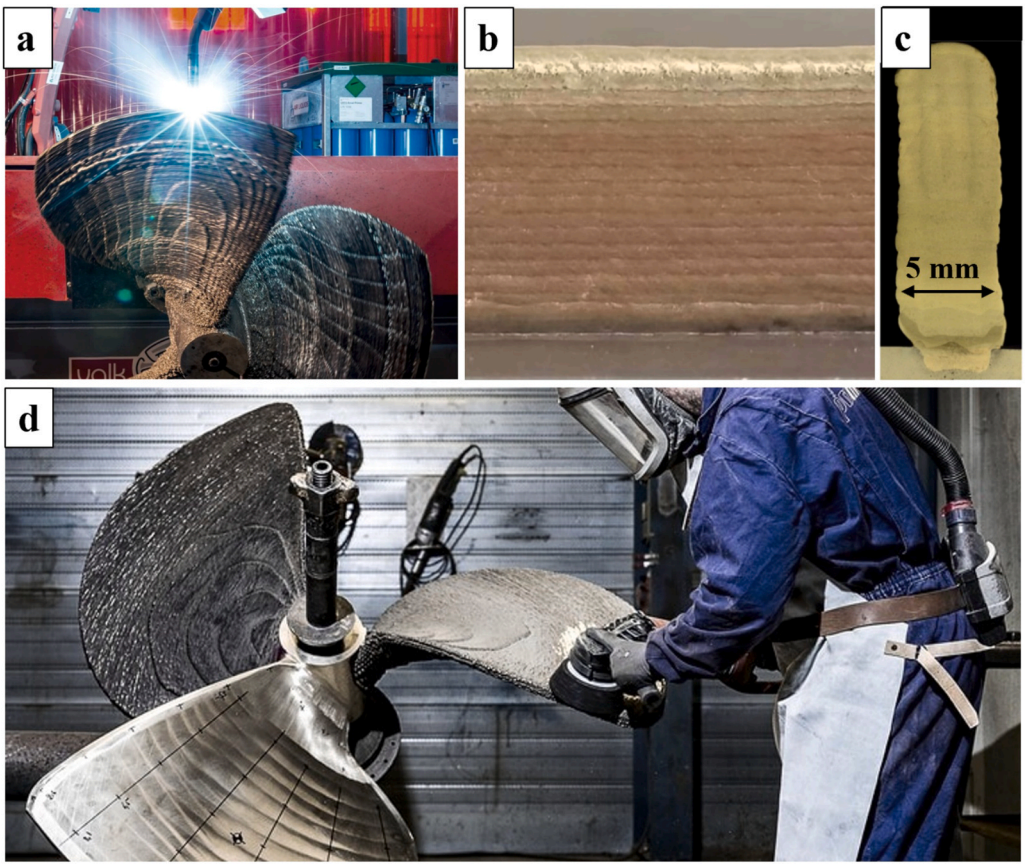


Fig. 22. DED-based fabrication of ship propellers: (a) surface morphology deposited by wire-arc DED [396]; (b) surface morphology and (c) cross-sectional accuracy of nickel-aluminium bronze (a typical alloy for propellers) deposited by oscillating laser-wire DED [148]; (d) surface post-processing of wire-arc deposited propeller [396].

welding the damaged locations in a dry environment. This repair approach is time-consuming and costly. Repairing steel liners during operation, directly underwater, would considerably improve maintenance efficiency and economy [318]. Li et al. [219] developed an LW-DED system in which all actuating components can operate in underwater environments (Fig. 23). The system was fitted with an underwater laser head and a coaxial camera, enabling remote positioning of the repair location, as well as an onshore wire feeder for continuous and stable wire filling within 20 m from the deposition location. Laser heat input needed adjustment to compensate for the smaller melt pool due to the heat loss in the water-cooled substrate, which could explain why underwater cladding layers demonstrated superior mechanical properties and corrosion resistance compared to air cladding [219].

Cai et al. [223] analysed microstructure and texture evolution of duplex steel in underwater LW-DED and showed that the rapid cooling effect of the underwater environment on the melt pool inhibits the ferrite-to-austenite transformation. Since ferrite has a lower surface energy, most of it was precipitated along the dense-packed α planes. The cyclic reheating by LW-DED not only changes the microstructure and texture but also affects the grain size and the proportion of special grain boundaries, which are beneficial for improving corrosion resistance [223]. Fu et al. [372,373] developed another underwater LW-DED system and confirmed its operation for Ti–6Al–4 V by evidencing the metal mass transfer within a locally created dry cavity around the deposition zone. In further studies, Fu et al. [155] performed in-situ X-ray high-speed imaging of mass transfer behaviours within a stable local dry cavity underwater. Three distinct mass transfer modes were identified: droplet transfer, liquid bridge transfer, and spreading transfer modes, the control of which allowed enhancement of the formability of the metal deposits. Confirming the studies referred to above, Fu et al. [155] also pointed out that the inherent heat treatment effects of the LW-DED process provide a unique opportunity to tailor microstructures and mechanical properties in situ. Overall, LW-DED can be customised for underwater deposition over in-service metal components with properties comparable to those obtained in workshop environments.

9.3.7. Manufacturing in space

Although futuristic, manufacturing in space is a strategic and mission-enabling autonomy problem [402]. The long-term viability of lunar bases, orbital infrastructure, and deep-space missions will depend on the ability to manufacture and repair metallic components in situ, reducing dependence on Earth-supplied spare parts. This challenge is closely linked to In-Situ Resource Utilization (ISRU), where local resources are converted into useful products. The most credible lunar astrometallurgy routes, such as molten regolith electrolysis and related extraction technologies, are attractive because oxygen production is coupled to metallic co-products [403]. However, these technologies still leave a critical downstream question unresolved: how to convert extracted or recycled metals into a feedstock that can be stored, manipulated, and robotically deposited with high material utilisation and deterministic mass flow. In this regard, LW-DED occupies a unique position, acting as a potential bridge between resource extraction and the fabrication of mission-critical spare parts, repair patches, brackets, thermal-management hardware, and scientific equipment.

The attractiveness of LW-DED originates primarily from its wire feedstock. Relative to powder-, droplet-, and jet-based processes, wire is already a consolidated feedstock with deterministic mass flow and low exposed surface area. Unlike powders, which require atomisation and tightly controlled particle-size distributions, metallic wire can be produced directly from extracted or recycled metals through comparatively

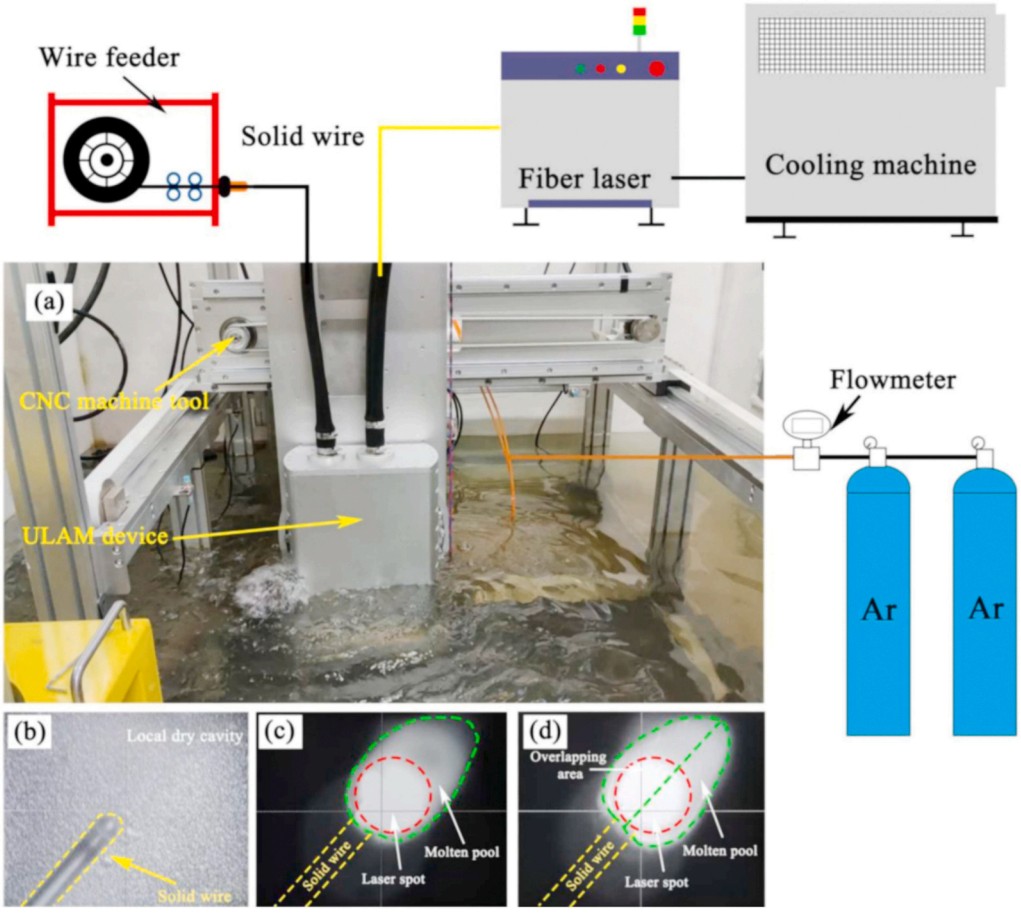


Fig. 23. Experimental system for underwater laser wire directed energy deposition [219]: (a) submerged LW-DED head; (b) wire in a local dry cavity; (c) real-time melt pool observation at first contact; (d) real-time melt pool control during overlay deposition.

simple thermomechanical processing routes. Furthermore, wire is transported mechanically (feeding) rather than ballistically (e.g., spray, flowing), meaning deposition does not depend on gravity settling, powder recoating, dispersion, or management of unconsolidated particles. These distinctions become particularly important in vacuum, low-gravity, and dusty planetary environments. Powder-based AM systems proposed for space have required dedicated compression-and-release architectures simply to make feedstock transport gravity-independent, indicating that powder systems are not naturally compatible with off-Earth operation [404]. Historically, NASA's EBF3 concept reached a similar conclusion for orbital manufacturing, identifying solid wire as the most controllable inventory format for metal AM in vacuum environments [405].

Beyond feedstock logistics, recent studies suggest that the fundamental physics of LW-DED remain compatible with extraterrestrial conditions. The CFD analysis by Abadi et al. [406] showed that, compared with terrestrial conditions, near-vacuum and zero-gravity environments can increase metal vapour generation sufficiently to modify the curvature of the melt-pool free surface, while remaining insufficient to trigger a transition into keyhole melting. The same study demonstrated that microgravity alters the force balance within the liquid-metal bridge between the wire tip and melt pool, producing only modest changes in melt-pool geometry and temperature distribution [406]. Although the liquid bridge becomes thinner and therefore somewhat less stable, material transfer remains governed primarily by capillary and surface-tension forces rather than gravity. Consequently, LW-DED can operate under near-vacuum and microgravity conditions without losing process stability or transitioning into unstable melting modes [406]. Together, these characteristics make LW-DED one of the few metal AM technologies capable of forming a complete ISRU-to-component production chain, linking resource extraction, feedstock preparation, repair, and fabrication within a single autonomous manufacturing ecosystem.

10. Critical outlook, challenges and future roadmap

In this section, we outline a paragraph for each of the previous sections to critically summarise the work completed and future directions, to some extent subjectively but based on the consensus of the co-authors who shaped this review. This analysis aims to provide a consolidated perspective to help guide the future direction of the field.

10.1. A lesson from history – knowledge integration

The history of LW-DED shows that its central challenge today is knowledge integration. Welding-based deposition proved the concept of high productivity but brought distortions and poor precision. Lasers were expected to correct this in the 1980s, yet wire feeding stayed unreliable, with misalignment, incomplete fusion, and irregular beads still common. Later advancements like coaxial feeding, oscillating beam, blue lasers, or hybrid systems improved consistency but added cost and complexity. The rapid increase in publications after 2024 signals more a proliferation than consolidation, as research is split into isolated tracks: new alloys, control systems, simulations, or hardware tweaks that are rarely connected to one another. Most studies do not consider deposition rates at scales that would be appropriate for industry, or large geometries, or standardised testing, so results cannot be compared, upscaled, or transferred to practical application. The field still lacks agreed

benchmarks for deposition efficiency, defect tolerance, or mechanical properties, which slows adoption. To enhance the industrial relevance of academic research, a future priority must be the integration of alloy design, modelling, monitoring, and property analysis under common validation frameworks.

10.2. Technical and economic viability

The technical simplicity often attributed to LW-DED can be misleading: while in principle the process resembles laser welding with wire, in practice the tool is not always stable, cost-effective, or standardised. Lateral wire feeding is indeed low-cost but produces significantly asymmetric geometries. Coaxial feeding, though often marketed as a solution for accuracy, is considerably more expensive and likely too bulky to produce complex and delicate geometries. Even the newest multi-laser coaxial systems suffer from optical drift, complex calibration, and frequent maintenance, restricting reproducibility outside controlled settings. The supposed flexibility of robotic arms compared to CNC systems is undermined by unresolved path planning problems: most studies still produce simple walls or cylinders, while true 3D deposition without collisions remains proprietary and software-intensive. Auxiliary systems, such as wire preheating, substrate vibration, oscillating beams, and real-time sensors, are often highlighted in academic studies, with little to no techno-economic analyses to justify their added cost and complexity in industrial contexts, where reliability and throughput matter more than incremental gains in grain refinement. Hybrid approaches present similar challenges: powder-wire systems reintroduce powder-related issues, laser-arc combinations lose precision, and dual-wire deposition promises compositional flexibility but introduces toolpath complexity. Overall, the field lacks a technically and economically coherent route forward: instead of converging on robust platforms, research continues to expand auxiliary solutions and hybrid configurations. We therefore consider that further consolidation and translational research are needed.

10.3. Transferable materials data

Material-related discoveries and conclusions are often not directly transferable, which in turn creates a significant opportunity. Despite clear differences in absorptivity, melting range, and thermal conductivity across alloys, most studies ignore reporting these fundamentals. In fact, half of the papers published in 2024–2025 did not even specify the laser wavelength (which can be 2–10 times less efficient for Al, Cu, etc.), making their data difficult to replicate. Sometimes even wire diameter and feed rate were omitted. The authors contacted contributors of reviewed works individually to clarify their parameters and choices, noticing considerable scatter and a lack of a consistent approach. The calculated deposition rates and energy consumption are equally scattered: Al and Ti alloys often consume nearly twice the energy per gram as steels or Ni alloys, but this trend is blurred by suboptimal parameter choices due to diverse research goals across studies. Studies still emphasise what worked well in each lab setup rather than establishing transferable energy-deposition maps. As a result, materials are treated case by case with little cross-alloy insight. We strongly encourage future reports to include standardised tables of process parameters, including calculated energy-per-mass and deposition rates. Furthermore, inter-laboratory studies (e.g., "round-robin" tests) depositing standardised materials (e.g., SS316L, Ti–6Al–4 V, Inconel 718) into the same geometries under fixed conditions could provide a valuable, consolidated dataset that outweighs years of uncoordinated global efforts.

10.4. From microstructure to component performance

Microstructure evolution is well understood for single-track deposits and simple multilayer geometries such as walls, cubes, or rectangular blocks, but limited understanding exists for actual parts with complex geometries, which involve complex thermal gradients and multiple phase transformations. The same is true for mechanical properties; most studies machine tensile samples from a deposited straight wall to capture stress-strain response. Although useful from a fundamental perspective, this may not be representative of the mechanical response of actual parts. Overall, existing studies have explored the microstructure and properties of stand-alone samples rather than those of actual parts. Future efforts could move beyond repeating fundamental studies toward a broader examination of microstructure–performance relationships in real parts under real service conditions, e.g. functional geometries under long-term thermal exposure, fatigue and creep under cyclic loading, and corrosive environments in component-in-the-loop arrangements. Further, the microstructural control via laser scan path, which is possible for thick builds, may appear impractical for thin-walled components – a highly promising application for LW-DED. While microstructural anisotropy remains a detectable signature of LW-DED, the mechanical property anisotropy averages around 20% (in thin samples, and less in larger parts) and approaches already exist to manage anisotropy within 2%. Thus, while scientifically interesting, it appears largely resolved from an engineering standpoint. A critical assessment should be made as to whether further grain refinement has tangible value. An alternative direction would be developing scalable methods and tools for depositing large parts with tailored anisotropic properties.

10.5. Integrating multiphysics domains

Modelling of the LW-DED process is not necessarily simpler or faster than experimental characterisation; however, it provides fundamental insight into the underlying physical mechanisms governing the process. Despite significant progress, two major challenges remain. First, most current models treat the three physical domains involved in this process, heat transfer, solid mechanics, and microstructural evolution, independently, underplaying or overlooking the interdependence between them. In particular, solid mechanics and microstructure evolution strongly influence each other; for instance, residual stresses not only influence distortion and cracking but also interact with phase transformation pathways and grain growth, which determine local mechanical performance. Second, the predictive accuracy of microstructure models is limited due to the scarcity of experimentally validated solidification data, which are essential inputs for robust simulation frameworks. Comprehensive models that consider the full process, from heat transfer through microstructure and residual stresses to final mechanical properties, are still lacking. Future research should focus on developing fully coupled multiphysics and multiscale frameworks that integrate thermo-mechanical fields with microstructural evolution models, enabling accurate process–structure–property predictions. In parallel, systematic experimental studies must be conducted to acquire reliable solidification and transformation data for model validation and calibration. The deployment of hybrid FE and CFD models, together with ML models, will enable training of ML models using large datasets generated from high-fidelity numerical simulations, leading to faster and more cost-effective predictive tools for process optimisation.

10.6. From supervised monitoring to autonomous production

Monitoring and control strategies in LW-DED still have a long way to go before reaching industrial maturity, despite the abundance of optical, thermal, and acoustic studies. Most sensing strategies map the surface but miss important subsurface defects, such as porosity, delamination, or cracking. These remain invisible to indirect methods, which are also highly vulnerable to plume interference and alignment errors. Direct techniques like synchrotron X-ray imaging, although invaluable for controlling geometries and internal defects, are impractical beyond laboratory demonstrations, underscoring the gap between academic innovation and factory-floor applicability. Machine learning has been

rapidly embraced, yet existing models are overtrained on narrow datasets (single beads, thin walls), lack interpretability, and fail to generalise across materials, geometries, and machines. This raises doubts about their reliability, especially for expensive parts where LW-DED is best positioned for. Claimed "closed-loop" architectures are equally fragmented, with intra-layer melt pool regulation and inter-layer geometric correction seldom unified into coherent hierarchies, while latency, noise, and data-processing overheads compromise feedback stability. No framework to date has convincingly scaled to large, multi-axis components in production environments, nor addressed certification, redundancy, or fail-safe operation. In general, AM monitoring is academically impressive but industrially fragile, and without scalable, certifiable control it risks remaining a laboratory showcase. What is urgently needed is a paradigm shift toward multi-modal sensor fusion with spatial registration, defect-specific and physics-informed features, adaptive and uncertainty-aware learning, and hierarchical control that couples fast melt-pool stabilisation with predictive geometry correction. Such an integrated framework could help move LW-DED from an overly supervised demonstrator to an autonomous production line.

10.7. Sustainability and technoeconomics

Sustainable industrialisation of LW-DED requires a coherent framework and technoeconomic evidence at scale. A review of recent studies reveals wide, often unexplained, variations in the use of consumables (e.g., shielding gas) and energy requirements, suggesting a need for optimisation based on first principles. A key trade-off lies between minimizing material waste from extensive trial-and-error tests and performing the essential deposition activities required for model validation, sensor calibration, and data gathering for higher-level digital models. The sustainability implications of LW-DED need to be assessed within the broader framework of LCA/LCC, which is methodologically mature but still poorly applied to this specific case [314]. A critical first step is to address the urgent need for transparent functional units and geometry-aware comparisons to ensure meaningful benchmarking [334]. In addition, different industrial scenarios (including country-specific ones) should be analysed, also within the context of absolute sustainability boundaries. Finally, social sustainability assessment and broader coverage of Sustainable Development Goals (SDGs) are essential. Linking LCA to SDGs reinforces the holistic nature of this approach. This area has recently attracted attention from companies such as PRé Sustainability B.V. (Netherlands) and 2.0 LCA Consultants ApS (Denmark), which are developing methods for life cycle SDG screening and assessment. However, closer collaboration with LW-DED technical experts is required. In addition to technological advancements, the development of LW-DED requires the establishment of standardised performance metrics and benchmarking approaches to enable consistent evaluation across studies and industrial scenarios. From a sustainability perspective, future developments should also consider the transition from laboratory-scale demonstrations to industrial adoption, where cost, scalability, and lifecycle performance become critical decision factors.

10.8. Prioritizing case studies in a search of value

Future demonstrations of LW-DED applications should prioritise independent cost-benefit analysis. Applications of LW-DED are often presented with optimistic expectations, and further research is needed to explicitly distinguish realistic claims from overstatements. Demonstrations of bridges, bollards, or caterpillars add publicity but have limited industrial justification. Even in high-value sectors, the gap between promise and reality remains. Aerospace and space programs showcase rocket engine nozzles and chambers, yet these are exceptions backed by extraordinary budgets, not scalable proof of commercial readiness. Claims of cost or lead-time reductions are rarely benchmarked against full life-cycle costs, including post-processing, inspection, and certification, which usually dominate. Lightweight and thin-wall components are often presented as a niche, but the geometrical limits, surface waviness, and need for CNC can dilute the productivity advantage. Ship propellers and other large hollow structures are presented as high-impact use cases, but laser-based systems have yet to compete with electric arc-based processes in this area. Even "exotic" scenarios like underwater repair or in-space printing are technically intriguing but need case studies to demonstrate economic feasibility. The risk is that LW-DED becomes a collection of one-off demonstrations with limited industrial uptake. Future work should prioritise independent cost-benefit studies, with standardised metrics (kg/h, cost/kg, post-processing time, defect rates) across benchmark parts, to separate hype from genuinely viable applications.

10.9. Roadmap for future research

As LW-DED evolves, its future will depend not only on technical breakthroughs but also on the community's ability to align its efforts. To support further research and provide a common reference point, we outline below a set of research priorities that define the field's most pressing knowledge gaps.

Short-term priorities (1–2 years) – standardisation and optimization, high feasibility:

1) Establish benchmark geometries for consistent comparison of print outputs across DED systems. This was done for LPBF two decades ago [407] and has been refined regularly since then [263,408–414]. No build plates have been proposed for DED methods. Resources: development of dedicated CAD models and interlaboratory testing.
2) Optimise process parameters to minimize post-processing and production costs. This review shows that up to 5 times less energy and gas can be used per kg of deposit (Fig. 8). Resources: existing lab equipment and multiple independent parametric studies with productivity metrics.
3) Define geometry-dependent build strategies and process windows for tall walls, thin ribs, large cross-sections, and thermally massive builds across alloys. Resources: pilot experiments and a multi-partner consortium for validation.

Medium-term priorities (3–5 years) – generalization and upscaling, moderate feasibility:

4) Expand the material portfolio to include refractory and high-entropy alloys, metal-matrix composites, bimetallic structures, and functionally graded deposits. Resources: feedstock materials costs and characterisation expenses.
5) Develop unified deposition metrics to map processability windows and energy requirements across alloy families. Resources: improved reporting standards to consolidate outputs into a shared database for cross-comparison.
6) Translate high deposition rates achieved on simple blocky samples to geometrically complex, thin-walled, or shell-like components. Resources: adding more degrees of freedom or a robotic arm to existing setups.
7) Move beyond sample-based characterisations toward component-level performance testing under realistic service conditions. Resources: industry partnerships.

Long-term priorities (5–10 years) – transformation and integration, lower feasibility:

8) Couple thermal, mechanical, and microstructural modelling into a unified framework, enabling a digital thread from process parameters to part properties. Resources: multi-institution software initiatives.
9) Integrate optical, thermal, and acoustic monitoring into a multi-sensing control system with melt pool-, bead shape-, and

geometry-level feedback. Resources: large collaborative research centres.

10) Conduct technoeconomic case studies quantifying cost/kg, post-processing load, and LCA metrics to create a comprehensive assessment framework of LW-DED competitiveness across part families. Resources: initial scoping studies in the short term, with full framework development requiring medium-term data and continuous updates.

Finally, we attempted to categorise and illustrate these ten priorities through the roadmap shown in Fig. 24, which aims to bring greater coherence and direction to research in the field and to enable the scalable and industrially viable deployment of LW-DED. A parallel task that cuts across all stages of LW-DED development for its adoption is not the technology, but the lack of certification standards. Although AM standards are no longer absent, the available framework remains only partially fit for LW-DED. Generic AM documents in the ISO/ASTM 529xx family, ASTM F3413, SAE AMS DED specifications, and ASME Y14.46/Y14.47 establish terminology, procurement logic, design guidance, and digital product definition [415], but they do not by themselves qualify the LW-DED process with its unique melt-pool regimes, high deposition rates, multi-axis toolpaths, and geometry-dependent heat accumulation, all of which shift part morphology, residual stress, and defect populations relative to small qualifying samples. NASA-STD−6030 [416] shows what a mature route can look like for wire-fed DED: wire feedstock traceability, witness specimens printed alongside (or even adjacent to) components, qualified in-situ monitoring that may complement but not replace NDE, and 99/95 statistical material allowables, while DNV-ST-B203 adds procurement controls, process qualification, and DED-focused inspection. In simple words, wire-fed DED requires not only demonstrating acceptable mechanical properties, but also a set of factors that collectively demonstrate the process can repeatedly produce conforming parts with the same properties rather than a single successful build. The relevant list of standards today would include ISO/ASTM 52900, 52901, 52904; NASA-STD−6030; DNV-ST-B203. Yet these frameworks are not LW-DED-specific and keep the hardest translation issues open: geometry-class-specific witness strategies, repair qualification, defect acceptance criteria, and qualification by non-destructive testing [415]. Literature precedents mainly consist of WAAM marine hardware and DNV-certified AM repair cases, whereas equivalent LW-DED aerospace qualification frameworks have yet to be demonstrated. Practical progress should therefore come from inter-laboratory round-robins on benchmark LW-DED geometries, common protocols for data accumulation, and proof that in-situ monitoring signals can reliably predict defects and component performance, ideally under tiered NASA control-plan logic, API criticality levels, and ABS/DNV cradle-to-grave documentation [415].

11. Conclusions

The main message of this review is that LW-DED will not advance meaningfully through incremental studies alone. The technology is limited not by fundamental physics but by knowledge fragmentation. What has often been framed as "*laser 3D welding*" is, in practice, a deeply interdependent manufacturing ecosystem where optics, metallurgy, heat transfer, motion planning, sensing, simulation, and cost all collide. The literature demonstrates excellence in each of these areas, but rarely the integration required for scalable deployment. Without convergence, industrial uptake will remain slow and difficult beyond isolated success stories in aerospace and energy programs.

Further LW-DED research shall therefore (1) establish shared benchmark geometries, (2) define geometry-dependent process windows, (3) optimise parameters to reduce post-processing and energy use, (4) expand the material palette, particularly to refractory metals, high-entropy alloys, and bimetallic compositions, (5) unify deposition metrics across alloys, (6) scale high-rate deposition to complex industrial geometries, (7) validate real-component performance rather than samples, (8) integrate fully coupled digital-thread modelling, (9) deploy multi-modal closed-loop control, and (10) ground performance claims in transparent technoeconomic evidence – together enabling LW-DED to shift from niche, high-budget demonstrators to a broadly reliable and industrially competitive manufacturing route.

CRediT authorship contribution statement

Guoda Chen: Writing – review & editing, Supervision, Funding acquisition, Formal analysis, Data curation. **Priarone Paolo Claudio:** Writing – review & editing, Supervision, Formal analysis, Data curation, Conceptualization. **Samanta Piano:** Writing – review & editing, Validation, Methodology, Formal analysis. **Chengzhe Zhang:** Writing – original draft, Visualization, Formal analysis, Data curation. **Catalano Angioletta:** Writing – original draft, Visualization, Investigation, Data curation. **Ahmed Wagih:** Writing – original draft, Visualization, Formal analysis, Data curation. **Long Ye:** Writing – original draft, Validation, Investigation, Formal analysis, Data curation. **Ruslan Melentiev:** Writing – review & editing, Writing – original draft, Visualization, Project administration, Methodology, Formal analysis, Data curation, Conceptualization. **Nan Yu:** Writing – review & editing, Supervision, Resources, Project administration, Funding acquisition. **Fangda Xu:** Writing – review & editing, Resources, Formal analysis, Data curation.

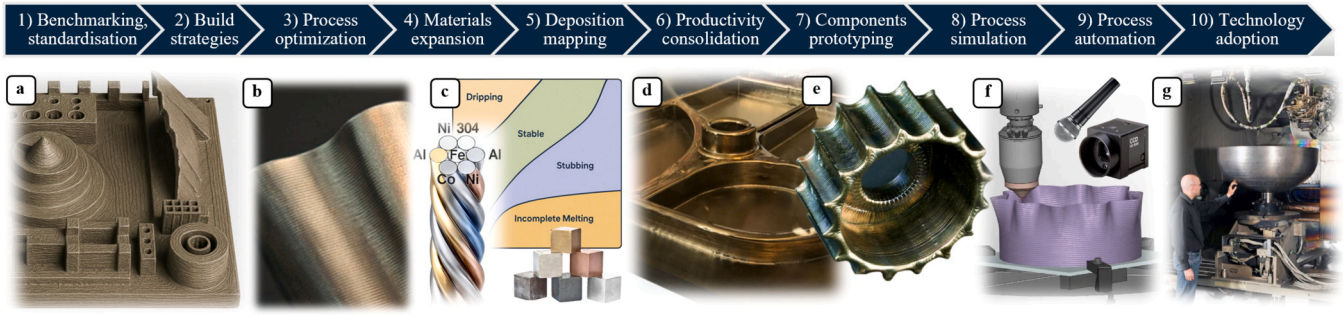


Fig. 24. Roadmap for future laser wire DED (LW-DED) development. Further progress can begin with (1) establishing benchmarking standards inspired by mature AM systems (a), (2) enabling geometry-dependent optimisation of build strategies and (3) refined process parameters that reduce post-processing (b). Broader adoption requires (4) expanding the material palette and (5) mapping deposition regimes across alloy families (c), followed by (6) consolidating high-productivity conditions on larger, thermally challenging geometries (d) and (7) demonstrating reliability on commercial-scale components (e). The final stage involves (8) developing predictive simulation frameworks and (9) multi-modal closed-loop monitoring (f), converging toward (10) fully autonomous LW-DED manufacturing. Graphics
Adapted from: (a) Gradl et al. [408]; (b) Rongsu Tech; (c) Assad et al. [84]; (d) GKN Aerospace; (e) Rongsu Tech; (f) BeAM Machines; (g) Sciaky (electron beam wire DED).

Christos Spitas: Writing – review & editing, Validation, Formal analysis, Conceptualization.

Declaration of Competing Interest

The authors declare that they have no known competing financial interests or personal relationships that could have appeared to influence the work reported in this paper.

Acknowledgements

This work was supported by the State Key Laboratory of Materials Processing and Die & Mould Technology, Huazhong University of Science and Technology (Grant No. P2025-003) and by the National Natural Science Foundation of China (Grant No. 52475494). P.C. Priarone acknowledges the support received from the FACILE project (ID: 765–260), funded by the Piedmont Region (Italy) under the program P. R. F.E.S.R. 2021/27 – Bando SWIch: Support of the Whole Innovation Chain – Action I.1i.1. R. Melentiev acknowledges financial support of High Tech zone of Ningbo municipality and Zhejiang Provincial Talent Scheme.

Data availability

This is a review article based on already published data.

References

[1] K. Zhang, P. Chermprayong, F. Xiao, D. Tzoumanikas, B. Dams, S. Kay, B. B. Kocer, A. Burns, L. Orr, C. Choi, D.D. Darekar, W. Li, S. Hirschmann, V. Soana, S.A. Ngah, S. Sareh, A. Choubey, L. Margheri, V.M. Pawar, R.J. Ball, C. Williams, P. Shepherd, S. Leutenegger, R. Stuart-Smith, M. Kovac, Aerial additive manufacturing with multiple autonomous robots, Nature 609 (2022) 709–717, https://doi.org/10.1038/s41586-022-04988-4.

[2] S. Graziosi, J. Faludi, T. Stanković, Y. Borgianni, N. Meisel, S.I. Hallstedt, D. W. Rosen, A vision for sustainable additive manufacturing, Nat. Sustain. 7 (2024) 698–705, https://doi.org/10.1038/s41893-024-01313-x.

[3] C. Panwisawas, Y.T. Tang, R.C. Reed, Metal 3D printing as a disruptive technology for superalloys, Nat. Commun. 11 (2020) 1–4, https://doi.org/10.1038/s41467-020-16188-7.

[4] S. Gao, Z. Li, S. Van Petegem, J. Ge, S. Goel, J.V. Vas, V. Luzin, Z. Hu, H.L. Seet, D. F. Sanchez, H. Van Swygenhoven, H. Gao, M. Seita, Additive manufacturing of alloys with programmable microstructure and properties, Nat. Commun. 14 (2023), https://doi.org/10.1038/s41467-023-42326-y.

[5] U.M. Dilberoglu, B. Gharehpapagh, U. Yaman, M. Dolen, The role of additive manufacturing in the era of industry 4.0, Procedia Manuf. 11 (2017) 545–554, https://doi.org/10.1016/j.promfg.2017.07.148.

[6] A. Papacharalampopoulos, P. Foteinopoulos, P. Stavropoulos, Integration of Industry 5.0 requirements in digital twin-supported manufacturing process selection: a framework, Procedia CIRP 119 (2023) 545–551, https://doi.org/10.1016/j.procir.2023.06.197.

[7] B. Bigliardi, E. Bottani, E. Gianatti, L. Monferdini, B. Pini, A. Petroni, Sustainable additive manufacturing in the context of industry 4.0: a literature review, Procedia Comput. Sci. 232 (2024) 766–774, https://doi.org/10.1016/j.procs.2024.01.076.

[8] T.T. Wohlers, Wohlers report 2025: 3D printing and additive manufacturing global state of the industry, Wohlers Assoc. (2025). https://scholar.google.com/scholar_lookup?title=Wohlers. Reports&publication_year=2018&author=T. Wohlers.

[9] C. Market, Global manufacturing market size, share, trends, and growth analysis, 2024–2032, Coherent Mark. Insights (2025) 160. https://www.coherentmarketinsights.com/industry-reports/global-manufacturing-market?.

[10] L. Love, B. Post, M. Noakes, A. Nycz, V. Kunc, There's plenty of room at the top, Addit. Manuf. 39 (2021), https://doi.org/10.1016/j.addma.2020.101727.

[11] J. Han, S. Wang, W. Ge, H. Chen, Y. Sun, Y. Ai, W. Yuan, S. Ruan, W. Niu, H. Yang, S. Yin, W. Yan, X. Lin, Non-contact ultrasound to assist laser additive manufacturing, Nat. Commun. 16 (2025), https://doi.org/10.1038/s41467-025-62803-w.

[12] C. Vidler, M. Halwes, K. Kolesnik, P. Segeritz, M. Mail, A.J. Barlow, E.M. Koehl, A. Ramakrishnan, L.M. Caballero Aguilar, D.R. Nisbet, D.J. Scott, D.E. Heath, K. B. Crozier, D.J. Collins, Dynamic interface printing, Nature 634 (2024) 1096–1102, https://doi.org/10.1038/s41586-024-08077-6.

[13] S.J. Ahn, H. Lee, K.J. Cho, 3D printing with a 3D printed digital material filament for programming functional gradients, Nat. Commun. 15 (2024) 1–11, https://doi.org/10.1038/s41467-024-47480-5.

[14] T. Ma, Y. Li, H. Cheng, Y. Niu, Z. Xiong, A. Li, X. Jiang, D. Park, K. Zhang, C. Yi, Enhanced aerosol-jet printing using annular acoustic field for high resolution and minimal overspray, Nat. Commun. 15 (2024) 1–13, https://doi.org/10.1038/s41467-024-50789-w.

[15] V. Sukhotskiy, A.J. Pascall, J.R. Jeffries, Enabling multi-resolution droplet-on-demand metal jetting through tailored pulsing, Npj Adv. Manuf. 2 (2025) 1–11, https://doi.org/10.1038/s44334-025-00029-w.

[16] J.C. Griffis, K. Shahed, K. Meinert, B. Yilmaz, M. Lear, G. Manogharan, Multi-material laser powder bed fusion: effects of build orientation on defects, material structure and mechanical properties, Npj Adv. Manuf. 2 (2025) 1–11, https://doi.org/10.1038/s44334-025-00020-5.

[17] V. Karthikeyan, J.U. Surjadi, X. Li, R. Fan, V.C.S. Theja, W.J. Li, Y. Lu, V.A.L. Roy, Three dimensional architected thermoelectric devices with high toughness and power conversion efficiency, Nat. Commun. 14 (2023), https://doi.org/10.1038/s41467-023-37707-2.

[18] J. Zhang, M. Xiao, L. Gao, A. Alù, F. Wang, Self-bridging metamaterials surpassing the theoretical limit of Poisson's ratios, Nat. Commun. 14 (2023), https://doi.org/10.1038/s41467-023-39792-9.

[19] P. Jiao, J. Mueller, J.R. Raney, X. (Rayne) Zheng, A.H. Alavi, Mechanical metamaterials and beyond, Nat. Commun. 14 (2023), https://doi.org/10.1038/s41467-023-41679-8.

[20] J.U. Surjadi, B.F.G. Aymon, M. Carton, C.M. Portela, Double-network-inspired mechanical metamaterials, Nat. Mater. (2025), https://doi.org/10.1038/s41563-025-02219-5.

[21] S.K. Saha, D. Wang, V.H. Nguyen, Y. Chang, J.S. Oakdale, S.C. Chen, Scalable submicrometer additive manufacturing (80-.). Science 366 (2019) 105–109, https://doi.org/10.1126/science.aax8760.

[22] J.U. Surjadi, C.M. Portela, Enabling three-dimensional architected materials across length scales and timescales, Nat. Mater. 24 (2025), https://doi.org/10.1038/s41563-025-02119-8.

[23] M.S. Ummah, Rapid, continuous additive manufacturing by volumetric polymerization inhibition patterning, Sci. Adv. 11 (2019) 1–14. http://scioteca.caf.com/bitstream/handle/123456789/1091/RED2017-Eng-8ene.pdf?sequence=12&isAllowed=y%0Ahttps://doi.org/10.1016/j.regsciurbeco.2008.06.005%0Ahttps://www.researchgate.net/publication/305320484_SISTEM_PEMBETUNGAN_TERPUSAT_STRATEGI_MELESTARI.

[24] S. McConnell, Y. Beshay, K. Kourousis, D. Tanner, Increasing productivity for laser powder bed fusion of Ti–6Al–4V parts through increased layer thickness, Prog. Addit. Manuf. 10 (2025) 7891–7909, https://doi.org/10.1007/s40964-025-01079-4.

[25] S. Kokare, J.P. Oliveira, R. Godina, Life cycle assessment of additive manufacturing processes: a review, J. Manuf. Syst. 68 (2023) 536–559, https://doi.org/10.1016/j.jmsy.2023.05.007.

[26] P. Wang, G. Robertson, B.T. Gibson, C.M. Fancher, J. Reynolds, M. Borish, J. R. Cruz, P. Chesser, B. Stump, A. Jackson, E. Macdonald, Improved productivity with multilaser rotary powder bed fusion additive manufacturing, 3, D. Print. Addit. Manuf. 11 (2024) 231–241, https://doi.org/10.1089/3dp.2022.0288.

[27] T.A. Yeshiwas, A.B. Tiruneh, M.A. Sisay, A review article on the assessment of additive manufacturing, J. Mater. Sci. Mater. Eng. 20 (2025), https://doi.org/10.1186/s40712-025-00306-8.

[28] D.S. Thomas, S.W. Gilbert, Costs and cost effectiveness of additive manufacturing: a literature review and discussion, Addit. Manuf. Costs Cost. Eff. Ind. Econ. (2015) 1–96.

[29] U. Auyeskhan, G. Turysbekov, S.P. Roshaven, A. Perveen, D. Talamona, Decision-making framework supported by techno-economic analysis of laser powder bed fusion: a novel approach using Retrieved Augmentation Generation (RAG), Prog. Addit. Manuf. 10 (2025) 9099–9115, https://doi.org/10.1007/s40964-025-01173-7.

[30] B. Karaş, A. Shokrani, Activity-based costing of laser powder-bed additive manufacturing incorporating discrete event simulation, Npj Adv. Manuf. 2 (2025), https://doi.org/10.1038/s44334-025-00036-x.

[31] S. Das, E. Rasouli, T. Ziev, N. Lamprinakos, J. Seo, A. Rollett, P. Vaishnav, V. Narayanan, Design and techno economic optimization of an additively manufactured compact heat exchanger for high temperature and high pressure applications, Appl. Therm. Eng. 245 (2024) 122778, https://doi.org/10.1016/j.applthermaleng.2024.122778.

[32] P. Burggräf, G. Bergweiler, S. Kehrer, T. Krawczyk, F. Fiedler, Mega-casting in the automotive production system: expert interview-based impact analysis of large-format aluminium high-pressure die-casting (HPDC) on the vehicle production, J. Manuf. Process. 124 (2024) 918–935, https://doi.org/10.1016/j.jmapro.2024.06.028.

[33] M. Shah, D. R.Patel, S. Pande, Additive manufacturing integrated casting- a review, Mater. Today Proc. 62 (2022) 7199–7203, https://doi.org/10.1016/j.matpr.2022.03.413.

[34] T. Lehmann, D. Rose, E. Ranjbar, M. Ghasri-Khouzani, M. Tavakoli, H. Henein, T. Wolfe, A. Jawad Qureshi, Large-scale metal additive manufacturing: a holistic review of the state of the art and challenges, Int. Mater. Rev. 67 (2022) 410–459, https://doi.org/10.1080/09506608.2021.1971427.

[35] C.M.S. Vicente, M. Sardinha, L. Reis, A. Ribeiro, M. Leite, Large-format additive manufacturing of polymer extrusion-based deposition systems: review and applications, Prog. Addit. Manuf. 8 (2023) 1257–1280, https://doi.org/10.1007/s40964-023-00397-9.

[36] L. Li, A. Tirado, I.C. Nlebedim, O. Rios, B. Post, V. Kunc, R.R. Lowden, E. Lara-Curzio, R. Fredette, J. Ormerod, T.A. Lograsso, M.P. Paranthaman, Big area additive manufacturing of high performance bonded NdFeB magnets, Sci. Rep. 6 (2016) 1–7, https://doi.org/10.1038/srep36212.

[37] G.D. Goh, K.K. Wong, N. Tan, H.L. Seet, M.L.S. Nai, Large-format additive manufacturing of polymers: a review of fabrication processes, materials, and

design, Virtual Phys. Prototyp. 19 (2024) 1–34, https://doi.org/10.1080/17452759.2024.2336160.
[38] A. Roschli, K.T. Gaul, A.M. Boulger, B.K. Post, P.C. Chesser, L.J. Love, F. Blue, M. Borish, Designing for big area additive manufacturing, Addit. Manuf. 25 (2019) 275–285, https://doi.org/10.1016/j.addma.2018.11.006.
[39] D. Vanerio, M. Guagliano, S. Bagherifard, Emerging trends in large format additive manufacturing processes and hybrid techniques, Prog. Addit. Manuf. 10 (2024) 1945–1972, https://doi.org/10.1007/s40964-024-00771-1.
[40] A. Roschli, B.K. Post, P. Wang, P. Chesser, A.K. Barnes, A. Stevens, J. Heineman, V. Kunc, J. Vaughan, C. Atkins, A. Jackson, M. Borish, The cost of scaling up in large-format additive manufacturing, D. Print. Addit. Manuf. 3 (2025), https://doi.org/10.1089/3dp.2023.0112.
[41] A.A. Hassen, M. Noakes, P. Nandwana, S. Kim, V. Kunc, U. Vaidya, L. Love, A. Nycz, Scaling Up metal additive manufacturing process to fabricate molds for composite manufacturing, Addit. Manuf. 32 (2020) 101093, https://doi.org/10.1016/j.addma.2020.101093.
[42] D.M. Wirth, C.C. Li, J.K. Pokorski, H.K. Taylor, M. Shusteff, Fundamental scaling relationships in additive manufacturing and their implications for future manufacturing and bio-manufacturing systems, Addit. Manuf. 84 (2024) 104081, https://doi.org/10.1016/j.addma.2024.104081.
[43] D. Dubey, S.P. Singh, B.K. Behera, A review on recent advancements in additive manufacturing techniques, Proc. Inst. Mech. Eng. Part. E J. Process. Mech. Eng. (2024), https://doi.org/10.1177/09544089241275860.
[44] D.E.P. Klenam, F. McBagonluri, T.K. Asumadu, S.A. Osafo, M.O. Bodunrin, L. Agyepong, E.D. Osei, D. Mornah, W.O. Soboyejo, Additive manufacturing: shaping the future of the manufacturing industry – overview of trends, challenges and opportunities, Appl. Eng. Sci. 22 (2025) 100224, https://doi.org/10.1016/j.apples.2025.100224.
[45] Tim Heston, 2023, Test. World'S. first 3D-Print. Metal. Bridge10(Webpage)https://www.thefabricator.com/thefabricator/article/additive/testing-the-worlds-first-3d-printed-metal-bridge.
[46] D.G. Ahn, Directed energy deposition (DED) process: state of the art, Korean Soc. Precis. Eng. (2021), https://doi.org/10.1007/s40684-020-00302-7.
[47] ASTM F2792, Standard terminology for additive manufacturing technologies, ASTM Int. (2015) 1–3, https://doi.org/10.1520/F2792-12.
[48] K.L. Terrassa, J.C. Haley, B.E. MacDonald, J.M. Schoenung, Reuse of powder feedstock for directed energy deposition, Powder Technol. 338 (2018) 819–829, https://doi.org/10.1016/j.powtec.2018.07.065.
[49] R. Chen, H. Yin, I.S. Cole, S. Shen, X. Zhou, Y. Wang, S. Tang, Exposure, assessment and health hazards of particulate matter in metal additive manufacturing: a review, Chemosphere 259 (2020) 127452, https://doi.org/10.1016/j.chemosphere.2020.127452.
[50] A.P. Nagalingam, M. Shamir, E.B. Tureyen, A.R.C. Sharman, O. Poyraz, E. Yasa, J. Hughes, Recent progress in wire-arc and wire-laser directed energy deposition (DED) of titanium and aluminium alloys, Int. J. Adv. Manuf. Technol. 136 (2025) 2035–2073, https://doi.org/10.1007/s00170-024-14967-w.
[51] N. Ghanadi, S. Pasebani, A review on wire-laser directed energy deposition: parameter control, process stability, and future research paths, J. Manuf. Mater. Process. 8 (2024), https://doi.org/10.3390/jmmp8020084.
[52] R.S. Tanwar, S. Jhavar, Multi-wire additive manufacturing: a comprehensive review on materials, microstructure, methodological advances, and applications, Results Eng. 26 (2025) 104814, https://doi.org/10.1016/j.rineng.2025.104814.
[53] D. Svetlizky, B. Zheng, A. Vyatskikh, M. Das, S. Bose, A. Bandyopadhyay, J. M. Schoenung, E.J. Lavernia, N. Eliaz, Laser-based directed energy deposition (DED-LB) of advanced materials, Mater. Sci. Eng. A 840 (2022) 142967, https://doi.org/10.1016/j.msea.2022.142967.
[54] ESAB, The story of ESAB is the story of welding, ESAB Corp, 2025. https://esab.com/us/nam_en/about/history/.
[55] N. Sosnin, S. Ermakov, P. Topolianski, 2013, Plasma Technol. Guide Eng. (Russ.) http://scioteca.caf.com/bitstream/handle/123456789/1091/RED2017-Eng-8ene.pdf?sequence=12&isAllowed=y%0Ahttps://doi.org/10.1016/j.regsciurbeco.2008.06.005%0Ahttps://www.researchgate.net/publication/305320484_SISTEM_PEMBETUNGAN_TERPUSAT_STRATEGI_MELESTARI.
[56] Neal Singer, Clint Atwood, Randy Montoya, Creating a complex metal part in a day is goal of commercial consortium, Sandia Natl. Lab. Lab. (1997).
[57] H.H.B. Dutta, M. Lewan, V. Singh, R. Fortuna, F. Ghadamli1, P. Gradl, R. Hickman, J. Fikes, M. Ogles, K. Wheeler, V. Hafiychuk, Rapid large scale additive manufacturing of full-scale RS-25 engine nozzle liner, DM3, D. Technol. 8 (2015).
[58] L. Ely, 2021Met. 3D Print.Met. 3D Print.Build. Blocks Dir. Energy Depos. Des.https://3dprint.com/280804/the-building-blocks-of-directed-energy-deposition-design/.
[59] R. Brooks, DoD assigns Pratt to develop AM repair capability, Am. Mach. (2023).
[60] A.N. Laboratory, A deeper look into wire-laser directed energy deposition, U. S. Dep. Energy Off. Sci. Use Facil. (2024).
[61] Global Directed Energy Deposition (DED) Manufacturing Market Professional Survey by Types, Applications, and Players, with Regional Growth Rate Analysis and Development Situation, from 2023 to 2028, Mark. Res. (2024) 105. https://www.marketresearch.com/Maia-Research-v4212/Global-Directed-Energy-Deposition-DED-36938424/.
[62] D. Ding, Z. Pan, D. Cuiuri, H. Li, Wire-feed additive manufacturing of metal components: technologies, developments and future interests, Int. J. Adv. Manuf. Technol. 81 (2015) 465–481, https://doi.org/10.1007/s00170-015-7077-3.
[63] Q. Liu, H. Mi, L. Feng, W. Guo, B. He, A critical overview of welding and directed energy deposition with flux-cored wires, J. Manuf. Process. 142 (2025) 231–268, https://doi.org/10.1016/j.jmapro.2025.03.097.
[64] H. Yi, F. Jiao, H. Cao, J. Zhang, Y. Zou, Numerical simulations of molten pool dynamics in wire-arc directed energy deposition processes: a review, J. Manuf. Process. 134 (2025) 970–997, https://doi.org/10.1016/j.jmapro.2025.01.022.
[65] Z. Li, S. Sui, X. Ma, H. Tan, C. Zhong, G. Bi, A.T. Clare, A. Gasser, J. Chen, High deposition rate powder- and wire-based laser directed energy deposition of metallic materials: a review, Int. J. Mach. Tools Manuf. 181 (2022), https://doi.org/10.1016/j.ijmachtools.2022.103942.
[66] B. Guan, L. Qin, G. Yang, Y. Ren, X. Wang, Laser polishing of directed energy deposition metal parts: a review, Addit. Manuf. Front. 3 (2024) 200174, https://doi.org/10.1016/j.amf.2024.200174.
[67] A. 52900:2015, Standard terminology for additive manufacturing – general principles – terminology, ASTM Int. i, 2015, pp. 1–9. http://compass.astm.org/EDIT/html_annot.cgi?ISOASTM52900+15.
[68] N. Benardos, S. Olszewski, 1887, Process. Appar. Work. Met. Direct Appl. Electr. Curr..
[69] C.L. Coffin, 1890, Method. Appar. Weld. Electr..
[70] X. Liu, Y. Di, G. Wang, Q. Yuan, Y. Rong, The thermal-flow dynamics of hydrogen bubbles in coaxial laser wire directed energy deposition of Al-Mg-Sc alloy, Addit. Manuf. 98 (2025), https://doi.org/10.1016/j.addma.2025.104649.
[71] C. Wang, X. Liu, F. Xing, G. Xu, H. Bian, W. Liu, Microstructure and mechanical properties of TiC/Ti6Al4V composite fabricated by concurrent wire-powder feeding laser-directed energy deposition, Opt. Laser Technol. 181 (2025) 111836, https://doi.org/10.1016/j.optlastec.2024.111836.
[72] Y.N. Aditya, J. Vincic, M.J. Benoit, Effects of wire feeding direction on the deposition characteristics of 316L stainless steel in laser-directed energy deposition, Manuf. Lett. 43 (2025) 27–32, https://doi.org/10.1016/j.mfglet.2024.11.006.
[73] W. Guo, L. Wang, L. Su, X. Ma, J. Wang, S. Hou, B. He, Microstructure evolution and mechanical properties of Q690D steel repaired by wire based laser directed energy deposition, Virtual Phys. Prototyp. 19 (2024), https://doi.org/10.1080/17452759.2024.2375108.
[74] B. Xu, J. Zhao, S. Geng, M. Song, P. Jiang, New insight into enhancing SiCp/Al composites: designing "interlocking + high entropy" interfacial microstructure via oscillating laser directed energy deposition, Mater. Sci. Eng. A 927 (2025), https://doi.org/10.1016/j.msea.2025.148011.
[75] S. Tyagi, S.K. Balla, M. Manjaiah, C. Aranas, Microstructure and mechanical properties of stainless steel 316L-Inconel 625 bimetallic structure fabricated by laser wire direct energy deposition, J. Mater. Res. Technol. 33 (2024) 8361–8371, https://doi.org/10.1016/j.jmrt.2024.11.130.
[76] G. Su, Y. Shi, G. Li, G. Zhang, Y. Xu, Highly-efficient additive manufacturing of Inconel 625 thin wall using hot-wire laser metal deposition: process optimization, microstructure, and mechanical properties, Opt. Laser Technol. 175 (2024) 110763, https://doi.org/10.1016/j.optlastec.2024.110763.
[77] F.C. Peng, C. Guo, F. Jiang, D. Yuan, H. Yin, Q. Sun, H. Zhang, T. Dong, D. Guo, S. Konovalov, Microstructure evolution and mechanical properties of Ti-6Al-4V alloy fabricated by directed energy deposition assisted with dual ultrasonic vibration, Mater. Sci. Eng. A 925 (2025), https://doi.org/10.1016/j.msea.2025.147934.
[78] X. Orue, J.L. Iñarrairaegi, E. Tabares, M. Abasolo, C. Soriano, I. Quintana, Comparative analysis of direct energy deposition parameters for Ti-6Al-4V using laser beam and coaxial wire (DED-LB/CW), Procedia CIRP 124 (2024) 205–209, https://doi.org/10.1016/j.procir.2024.08.100.
[79] A. Barroi, N. Schwarz, J. Hermsdorf, S. Kaierle, Additive manufacturing of Ti-6Al-4V with laser-wire DED and local shielding gas protection. in: Procedia CIRP, Elsevier B.V, 2024, pp. 254–256, https://doi.org/10.1016/j.procir.2024.08.111.
[80] G. Su, Y. Shi, M. Zhu, G. Zhang, Application of hot wire laser directed energy deposition for efficient fabrication of large nickel-based alloy components: Process, microstructure, and mechanical properties, J. Mater. Process. Technol. 338 (2025), https://doi.org/10.1016/j.jmatprotec.2025.118789.
[81] Y. Jia, S. Sun, J. Gu, Z. Yao, Z. Huang, H. Gao, W. Huang, R. Zeng, P. Zhang, Influence of follow-up wire feeding strategy on aluminum alloy laser wire additive manufacturing forming, Opt. Laser Technol. 192 (2025) 113457, https://doi.org/10.1016/j.optlastec.2025.113457.
[82] J. Preis, S.B. Lawson, I. Lee, M. Kawasaki, B.K. Bay, S. Manoharan, B.K. Paul, S. Pasebani, Influence of travel speed on microstructure and mechanical behavior of Inconel 625 fabricated using wire fed laser directed energy deposition, J. Mater. Process. Technol. 330 (2024), https://doi.org/10.1016/j.jmatprotec.2024.118464.
[83] Y. Lee, P. Nandwana, B. Gibson, P. Mhatre, J. Ortega Rojas, B. Prabhune, A. Thornton, J. Vaughan, S. Simunovic, Integrated top-down process and voxel-based microstructure modeling for Ti-6Al-4V in laser wire direct energy deposition process, Mater. Des. 247 (2024), https://doi.org/10.1016/j.matdes.2024.113434.
[84] A. Assad, B.D. Bevans, W. Potter, P. Rao, D. Cormier, F. Deschamps, J. D. Hamilton, I.V. Rivero, Process mapping and anomaly detection in laser wire directed energy deposition additive manufacturing using in-situ imaging and process-aware machine learning, Mater. Des. 245 (2024), https://doi.org/10.1016/j.matdes.2024.113281.
[85] X. Tao, J. Sun, Y. Huang, J. Yu, Y. Guo, Y. Xu, L. Yi, G. Wu, W. Liu, Ultra-light Mg-Li alloy with high modulus prepared by cold metal transfer-based directed energy deposition, Addit. Manuf. 97 (2025), https://doi.org/10.1016/j.addma.2024.104617.
[86] W. Huang, H. Zhong, X. Li, Y. Jia, S. Sun, N. Wu, Numerical and experimental investigation of heat transfer and flow in oscillating laser dual-wire deposition, Int. J. Therm. Sci. 211 (2025), https://doi.org/10.1016/j.ijthermalsci.2025.109741.

[87] X. Chen, M. Yao, Y. Fu, F. Kong, Applying multi-sensor fusion strategy for enhanced predictions of clad hardness and dilution in laser hot-wire cladding process by an ensemble machine learning model, J. Manuf. Process. 133 (2025) 211–225, https://doi.org/10.1016/j.jmapro.2024.11.052.
[88] C. Bernauer, S. Thiem, P. Garkusha, C. Geiger, M.F. Zaeh, Real-time monitoring and control of the layer height in laser metal deposition with coaxial wire feeding using optical coherence tomography, J. Laser Appl. 36 (2024), https://doi.org/10.2351/7.0001545.
[89] M. Rahmani Dehaghani, A. Sahraeidolatkhaneh, M. Nilsen, F. Sikström, P. Sajadi, Y. Tang, G.G. Wang, System identification and closed-loop control of laser hot-wire directed energy deposition using the parameter-signature-quality modeling scheme, J. Manuf. Process. 112 (2024) 1–13, https://doi.org/10.1016/j.jmapro.2024.01.029.
[90] C. Bernauer, P. Leitner, A. Zapata, P. Garkusha, S. Grabmann, M. Schmoeller, M. F. Zaeh, Segmentation-based closed-loop layer height control for enhancing stability and dimensional accuracy in wire-based laser metal deposition, Robot. Comput. Integr. Manuf. 86 (2024), https://doi.org/10.1016/j.rcim.2023.102683.
[91] M. Yao, J. Sheng, F. Kong, W. Tong, A multi-sensor based online monitoring system for laser hot-wire surface cladding process, Opt. Laser Technol. 177 (2024), https://doi.org/10.1016/j.optlastec.2024.111074.
[92] Y. Li, Z. Wang, C. Liu, F. Chen, G. Bi, A.M. Frontiers, Z. Wang, C. Liu, F. Chen, G. Bi, From geometric precision to performance: improved online monitoring system for thin-walled parts by fine wire laser directed energy deposition, Addit. Manuf. Front. 4 (2025), https://doi.org/10.1016/j.amf.2025.200201.
[93] M. Bodnariuk, R. Melentiev, Bibliometric analysis of micro-nano manufacturing technologies, Nanotechnol. Precis. Eng. 2 (2019) 61–70, https://doi.org/10.1016/j.npe.2019.05.001.
[94] R. Melentiev, M. Melentieva, N. Yu, Top 10 directions in lithography 3D printing, Bioprinting 40 (2024) e00343, https://doi.org/10.1016/j.bprint.2024.e00343.
[95] S. He, Z. Zhang, H. Li, T. Zhang, X. Lu, J. Kang, Multi-objective optimization for forming quality of laser and CMT-P arc hybrid additive manufacturing aluminum alloy using response surface methodology, Actuators 13 (2024), https://doi.org/10.3390/act13010023.
[96] E. Govekar, A. Jeromen, A. Kuznetsov, M. Kotar, M. Kondo, Annular laser beam based direct metal deposition, Procedia CIRP 74 (2018) 222–227, https://doi.org/10.1016/j.procir.2018.08.099.
[97] C. Lei, S. Ren, C. Yin, X. Liu, M. Chen, J. Wu, C. Han, Manipulating melt pool thermofluidic transport in directed energy deposition driven by a laser intensity spatial shaping strategy, Virtual Phys. Prototyp. 19 (2024), https://doi.org/10.1080/17452759.2024.2308513.
[98] B. Abranovic, S. Sarkar, E. Chang-Davidson, J. Beuth, Melt pool level flaw detection in laser hot wire directed energy deposition using a convolutional long short-term memory autoencoder, Addit. Manuf. 79 (2024), https://doi.org/10.1016/j.addma.2023.103843.
[99] L. Feng, H. Mi, S. Liao, P. You, Q. Liu, J. Wang, J. Lu, W. Guo, B. He, Advanced laser directed energy deposition of Q690D high-strength steel using flux-cored wire: microstructure evolution and mechanical performance, J. Mater. Process. Tech. 344 (2025) 119029, https://doi.org/10.1016/j.jmatprotec.2025.119029.
[100] M. Taghizadeh, Z.H. Zhu, A comprehensive review on metal laser additive manufacturing in space: modeling and perspectives, Acta Astronaut. 222 (2024) 403–421, https://doi.org/10.1016/j.actaastro.2024.06.027.
[101] M. Abuabiah, N.G. Mbodj, B. Shaqour, L. Herzallah, A. Juaidi, R. Abdallah, P. Plapper, Advancements in laser wire-feed metal additive manufacturing: a brief review, Mater. (Basel) 16 (2023) 1–23, https://doi.org/10.3390/ma16052030.
[102] H.C. Möhring, D. Becker, R. Eisseler, T. Stehle, T. Reeber, Influence of the manufacturing parameters of an AlMg5 wire–based hybrid production process on quality and mechanical properties, Int. J. Adv. Manuf. Technol. 119 (2022) 2445–2460, https://doi.org/10.1007/s00170-021-08106-y.
[103] I. John Solomon, P. Sevvel, J. Gunasekaran, P. Tanushkumaar, A review on additive manufacturing of alloys using laser metal deposition, Mater. Today Proc. 64 (2022) 44–50, https://doi.org/10.1016/j.matpr.2022.03.510.
[104] J.L. Su, F.L. Jiang, J. Teng, L.Q. Chen, G. Requena, M. Yan, L.C. Zhang, Y. M. Wang, I.V. Okulov, H.M. Zhu, G.W. Bo, Y.X. Chew, C.L. Tan, Laser additive manufacturing of titanium alloys: process, materials and post-processing, Rare Met. 43 (2024) 6288–6328, https://doi.org/10.1007/s12598-024-02685-x.
[105] N. Jamnikar, 2021, Compr. Model. Process. -Molten Pool. Cond. -Prop. Correl. Wire-Feed. Laser Addit. Manuf.http://scioteca.caf.com/bitstream/handle/123456789/1091/RED2017-Eng-8ene.pdf?sequence=12&isAllowed=y%0Ahttps://doi.org/10.1016/j.regsciurbeco.2008.06.005%0Ahttps://www.researchgate.net/publication/305320484_SISTEM_PEMBETUNGAN_TERPUSAT_STRATEGI_MELESTARI.
[106] W. Huang, S. Chen, J. Xiao, X. Jiang, Y. Jia, Laser wire-feed metal additive manufacturing of the Al alloy, Opt. Laser Technol. 134 (2021) 106627, https://doi.org/10.1016/j.optlastec.2020.106627.
[107] M. Sattari, A. Ebrahimi, M. Luckabauer, G. willem R.B.E. Römer, The effect of the laser beam intensity profile in laser-based directed energy deposition: a high-fidelity thermal-fluid modeling approach, Addit. Manuf. 86 (2024), https://doi.org/10.1016/j.addma.2024.104227.
[108] A. Zapata, C. Bernauer, M. Celba, M.F. Zaeh, Studies on the use of laser directed energy deposition for the additive manufacturing of lightweight parts, Lasers Manuf. Mater. Process. 11 (2024) 109–124, https://doi.org/10.1007/s40516-023-00233-6.
[109] F. Weng, G. Bi, Y. Chew, S. Sui, C. Tan, Z. Du, J. Su, F.L. Ng, Robust interface and excellent as-built mechanical properties of Ti–6Al–4V fabricated through laser-aided additive manufacturing with powder and wire, Int. J. Miner. Metall. Mater. 32 (2025) 154–168, https://doi.org/10.1007/s12613-024-3003-8.
[110] M. Abuabiah, T.C. Weidemann, M.A. Elahi, B. Shaqour, R. Day, P. Plapper, T. Bergs, Investigating the impact of process parameters on bead geometry in laser wire-feed metal additive manufacturing, J. Manuf. Mater. Process. 8 (2024), https://doi.org/10.3390/jmmp8050204.
[111] N. Chekir, 2018, Laser Wire Depos. Addit. Manuf. Ti-6Al-4V Aerosp. Ind..
[112] Y. Mao, H. Chen, J. Xiong, Research progress in laser additive manufacturing of aluminum alloys: microstructure, defect, and properties, J. Mater. Res. Technol. 30 (2024) 695–716, https://doi.org/10.1016/j.jmrt.2024.03.099.
[113] L. Ma, Z. Liu, C. Feng, B. Zhang, M. Pang, Q. Feng, Y. Wang, Investigation on forming process and product properties of laser wire-feed additive manufacturing for high-quality metal thin-walled parts, J. Mater. Eng. Perform. (2024), https://doi.org/10.1007/s11665-024-09947-w.
[114] J. Bi, L. Wu, S. Li, Z. Yang, X. Jia, M.D. Starostenkov, G. Dong, Beam shaping technology and its application in metal laser additive manufacturing: a review, J. Mater. Res. Technol. 26 (2023) 4606–4628, https://doi.org/10.1016/j.jmrt.2023.08.037.
[115] M. Bayat, R. Rothfelder, K. Schwarzkopf, A. Zinoviev, O. Zinovieva, C. Spurk, M. Hummel, A. Olowinsky, F. Beckmann, J. Moosmann, M. Schmidt, J.H. Hattel, Exploring spatial beam shaping in laser powder bed fusion: high-fidelity simulation and in-situ monitoring, Addit. Manuf. 93 (2024) 104420, https://doi.org/10.1016/j.addma.2024.104420.
[116] S.S.J.I. Shao-shan, L.I.U. Fan, FU Ge-yan, new forming method of coaxial wire feeding inside three beams laser cladding, China Acad. J. Electron. Publ. (2019) 285–293, https://doi.org/1001-3660.2019.04.040.
[117] C. Yan, R. Wang, 2024, Eff. Defocusing Var. Laser Wire Addit. Manuf. Morphol. Plasma Plume Change114.
[118] K. Marumoto, T. Horai, D. Morita, C. Oda, T. Fujii, T. Yuzawa, R. Koba, M. Yamamoto, Development of hot-wire laser additive manufacturing for dissimilar materials of stainless steel/aluminum alloys, J. Manuf. Mater. Process. 8 (2024), https://doi.org/10.3390/jmmp8030093.
[119] S. Ji, F. Liu, T. Shi, G. Fu, S. Shi, Effects of defocus distance on three-beam laser internal coaxial wire cladding (English Ed. Chin. J. Mech. Eng. 34 (2021) https://doi.org/10.1186/s10033-021-00560-9.
[120] H. Siva Prasad, F. Brueckner, J. Volpp, A.F.H. Kaplan, Laser metal deposition of copper on diverse metals using green laser sources, Int. J. Adv. Manuf. Technol. 107 (2020) 1559–1568, https://doi.org/10.1007/s00170-020-05117-z.
[121] E.W. Spisz, A.J. Weigund, R.L. Bowmun, J.R. Juck, 1969, Sol. absorptances Spectr. reflectances 12 Met. Temp. ranging 300 500 K.https://ntrs.nasa.gov/search.jsp?R=19690022517.
[122] Z. Tan, K. Yu, C. Zeng, X. Cai, Z. Wang, H. Wang, M. Yang, B. Qi, B. Cong, Porosity suppression and mechanical property improvement of wire-arc directed energy deposited TiCp/Al-Cu alloys joint by oscillating pulsed wave laser beam welding, J. Mater. Process. Technol. 329 (2024) 118458, https://doi.org/10.1016/j.jmatprotec.2024.118458.
[123] J. Xu, M. Pan, N. Liang, J. Kong, Y. Peng, Q. Zhou, K. Wang, Droplet transition behavior and compositional homogenization of TiAl alloys fabricated via dual-wire electron beam-directed energy deposition, J. Manuf. Process. 131 (2024) 270–282, https://doi.org/10.1016/j.jmapro.2024.09.026.
[124] A. Vidergar, A. Jeromen, E. Govekar, Influence of the laser-beam intensity distribution on the performance of directed energy deposition of an axially fed metal powder, J. Mater. Process. Technol. 327 (2024) 118360, https://doi.org/10.1016/j.jmatprotec.2024.118360.
[125] C. Roch, C. Tournier, S. Lavernhe, Process based modelling of power density for wire laser additive manufacturing using a coaxial head, Addit. Manuf. 73 (2023) 103648, https://doi.org/10.1016/j.addma.2023.103648.
[126] T. Zhao, Z. Yan, Y. Zhao, Y. Jia, S. Chen, Path planning in additive manufacturing with multi-robot collaboration based on structural primitive partitioning, Adv. Eng. Softw. 197 (2024) 103754, https://doi.org/10.1016/j.advengsoft.2024.103754.
[127] B. Huang, S.B. Singamneni, Curved layer adaptive slicing (CLAS) for fused deposition modelling, Rapid Prototyp. J. 21 (2015) 354–367, https://doi.org/10.1108/RPJ-06-2013-0059.
[128] D. Ding, Z. Pan, D. Cuiuri, H. Li, N. Larkin, S. Van Duin, Automatic multi-direction slicing algorithms for wire based additive manufacturing, Robot. Comput. Integr. Manuf. 37 (2016) 139–150, https://doi.org/10.1016/j.rcim.2015.09.002.
[129] G. Zhao, G. Ma, J. Feng, W. Xiao, Nonplanar slicing and path generation methods for robotic additive manufacturing, Int. J. Adv. Manuf. Technol. 96 (2018) 3149–3159, https://doi.org/10.1007/s00170-018-1772-9.
[130] A. López-Arrabal, Á. Guzmán-Bautista, W. Solórzano-Requejo, F. Franco-Martínez, M. Villaverde, Axisymmetric non-planar slicing and path planning strategy for robot-based additive manufacturing, Mater. Des. 241 (2024), https://doi.org/10.1016/j.matdes.2024.112915.
[131] B. Zhu, F. Xu, J. Zhi, X. Yang, S. Zhi, T. Yuan, Influence of laser power on microstructure and performance of Ti6Al4V fabricated through coaxial wire-laser directed energy deposition using six laser beams, Opt. Laser Technol. 192 (2025) 113901, https://doi.org/10.1016/j.optlastec.2025.113901.
[132] X. Zhang, D. Chu, X. Zhao, C. Gao, L. Lu, Y. He, W. Bai, Machine learning-driven 3D printing: a review, Appl. Mater. Today 39 (2024) 102306, https://doi.org/10.1016/j.apmt.2024.102306.
[133] T.S. Tamir, G. Xiong, X. Dong, Q. Fang, S. Liu, E. Lodhi, Z. Shen, F.Y. Wang, Design and optimization of a control framework for robot assisted additive manufacturing based on the stewart platform, Int. J. Control. Autom. Syst. 20 (2022) 968–982, https://doi.org/10.1007/s12555-021-0058-4.
[134] S. Rescsanski, R. Hebert, A. Haghighi, J. Tang, F. Imani, Towards intelligent cooperative robotics in additive manufacturing: past, present, and future, Robot.

Comput. Integr. Manuf. 93 (2025) 102925, https://doi.org/10.1016/j.rcim.2024.102925.
[135] P.M. Bhatt, R.K. Malhan, P. Rajendran, S.K. Gupta, Building free-form thin shell parts using supportless extrusion-based additive manufacturing, Addit. Manuf. 32 (2020) 101003, https://doi.org/10.1016/j.addma.2019.101003.
[136] T.S. Tamir, G. Xiong, Z. Shen, J. Leng, Q. Fang, Y. Yang, J. Jiang, E. Lodhi, F. Y. Wang, 3D printing in materials manufacturing industry: a realm of Industry 4.0, Heliyon 9 (2023) e19689, https://doi.org/10.1016/j.heliyon.2023.e19689.
[137] M.K. Micali, D. Dornfeld, Fully three-dimensional toolpath generation for point-based additive manufacturing systems, Solid Free. Fabr, Proc. 27th Annu. Int. Solid. Free. Fabr. Symp. - Addit. Manuf. Conf. SFF 2016 2016 (2016) 36–52.
[138] Y. Li, W. Fu, L. Meng, X. Wang, X. Liu, G. Zhang, Y. Zhou, Calibration of multi-robot coordinates for collaborative wire arc additive manufacturing using cross-source 3D point cloud models, Meas. J. Int. Meas. Confed. 242 (2025), https://doi.org/10.1016/j.measurement.2024.116294.
[139] W. Zhang, F. Ning, Y. Zhou, Directed energy deposition of Ti6Al4V wire with continuous layer varied laser power, Manuf. Lett. (2024). www.sciencedirect.com.
[140] Q. Cheng, N. Guo, Y. Fu, Y. Gao, X. Zhang, G. Zhou, Underwater additive manufacturing of 10CrNi3MoV high-strength low-alloy steel by wire-feed laser melting deposition: effect of microstructure evolution on mechanical properties, J. Mater. Res. Technol. 31 (2024) 2864–2875, https://doi.org/10.1016/j.jmrt.2024.07.044.
[141] R. Halder, S. Sahoo, J.T. Benzing, A.I. Saville, A.D. Rollett, Variant selection and macrozone in Ti-6Al-4V walls during laser hot wire direct energy deposition, J. Mater. Res. Technol. 33 (2024) 8289–8305, https://doi.org/10.1016/j.jmrt.2024.11.061.
[142] S. Zhao, G. Luo, L. Yang, M. Wang, J. Zhang, Y. Feng, Laser additive remanufacturing Ni-based multilayers reinforced with dual-scale tungsten carbides via a novel integrated strategy, Addit. Manuf. 84 (2024), https://doi.org/10.1016/j.addma.2024.104146.
[143] B. Yelamanchi, A. Alok, A. Prokop, H. Martin, B. Vuksanovich, E. Macdonald, M. Rodriguez, G. Knapp, Y. Lee, T. Feldhausen, P. Cortes, Influence of printing parameters on the mechanical behavior of 3D-printed SS316L parts manufactured using laser hot wire directed energy deposition, Int. J. Adv. Manuf. Technol. 134 (2024) 3281–3292, https://doi.org/10.1007/s00170-024-14308-x.
[144] Q. Wang, Y. Shi, K. Fan, S. Wang, Y. Li, Modeling of thermal evolution and fluid flow during synchronous induction-assisted laser wire deposition, Int. J. Heat. Mass. Transf. 238 (2025), https://doi.org/10.1016/j.ijheatmasstransfer.2024.126453.
[145] C. Bernauer, M.E. Sigl, S. Grabmann, T. Merk, A. Zapata, M.F. Zaeh, Effects of the thermal history on the microstructural and the mechanical properties of stainless steel 316L parts produced by wire-based laser metal deposition, Mater. Sci. Eng. A 889 (2024), https://doi.org/10.1016/j.msea.2023.145862.
[146] Y. Mao, H. Chen, J. Xiong, In-situ microalloying of Al-Cu-Sc alloy manufactured by beam oscillating wire laser directed energy deposition: Grain refinement and properties improvement, Addit. Manuf. 93 (2024), https://doi.org/10.1016/j.addma.2024.104419.
[147] Y. Mao, H. Chen, J. Xiong, Microstructural characteristics and mechanical properties of Al-Cu alloys fabricated via 8-shaped oscillating laser wire additive manufacturing, Mater. Sci. Eng. A 914 (2024), https://doi.org/10.1016/j.msea.2024.147101.
[148] Q. Deng, Y. Miao, Z. Yang, J. Liu, G. Hu, J. Chen, P. Wang, B. Wu, K-phase precipitation in nickel-aluminum bronze alloy fabricated by oscillating laser wire additive manufacturing, J. Alloy. Compd. 1012 (2025) 178484, https://doi.org/10.1016/j.jallcom.2025.178484.
[149] Y. Cai, Y. Wang, H. Chen, J. Xiong, Molten pool behaviors and forming characteristics in wire-laser directed energy deposition with beam oscillation, J. Mater. Process. Technol. 326 (2024) 118326, https://doi.org/10.1016/j.jmatprotec.2024.118326.
[150] M. Heidowitzsch, L. Gerdt, C. Samuel, J.-F. Maetje, J. Kaspar, M. Riede, E. López, F. Brueckner, C. Leyens, Grain size manipulation by wire laser direct energy deposition of 316L with ultrasonic assistance, J. Laser Appl. 35 (2023), https://doi.org/10.2351/7.0001090.
[151] V. Onuseit, S. Boley, D. Brinkmeier, A. Peter, T. Menold, C. Hagenlocher, T. Graf, A. Michalowski, Enhancing stability in thin-walled part production with L-DED wire using an adaptive controller, in: Procedia CIRP, Elsevier B.V, 2024, pp. 305–308, https://doi.org/10.1016/j.procir.2024.08.123.
[152] S. Rathor, R. Kant, E. Singla, Effect of laser energy density on bead characteristics in wire-DED, Sadhana 10 (2024), https://doi.org/10.1007/s12046-024-02472-5S.
[153] Y. Zhou, D. Jiang, A. Al-Akailah, F. Ning, Understanding the formation of laser-induced melt pools with both wire and powder feeding in directed energy deposition, Addit. Manuf. 89 (2024), https://doi.org/10.1016/j.addma.2024.104312.
[154] J. Tweer, R. Day, T. Derra, D. Dorow-Gerspach, S. Gräfe, M. Rasinski, M. Wirtz, C. Linsmeier, T. Bergs, G. Natour, Repair of heat load damaged plasma–facing material using the wire-based laser metal deposition process, Nucl. Mater. Energy 41 (2024), https://doi.org/10.1016/j.nme.2024.101787.
[155] Y. Fu, M. Yu, D. Wu, Z. Zhao, D. Wang, N. Guo, Fundamental investigation into mass transfer process and microstructural transformation pathways in Ti-6Al-4V via underwater wire-laser directed energy deposition, Virtual Phys. Prototyp. 19 (2024), https://doi.org/10.1080/17452759.2024.2374051.
[156] H. Choi, P. Bhowmik, T. Rimon, Y. Bandari, Y. Wang, S. Roy, Exploring the friction and wear mechanisms of nickel titanium alloy fabricated by laser powder and wire-based directed energy deposition, Tribol. Trans. 67 (2024) 522–537, https://doi.org/10.1080/10402004.2024.2358507.
[157] L. Gao, A.C. Chuang, P. Kenesei, Z. Ren, L. Balderson, T. Sun, An operando synchrotron study on the effect of wire melting state on solidification microstructures of Inconel 718 in wire-laser directed energy deposition, Int. J. Mach. Tools Manuf. 194 (2024), https://doi.org/10.1016/j.ijmachtools.2023.104089.
[158] M. Akbari, Y. Ding, R. Kovacevic, Process development for a robotized laser wire additive manufacturing, ASME 2017 12th Int. Manuf. Sci. Eng. Conf. MSEC 2017 Collocated JSME/ASME 2017 6th Int. Conf. Mater. Process. 2 (2017), https://doi.org/10.1115/MSEC2017-2951.
[159] H. Zhou, Y. Yang, C. Han, L. Liu, Z. Yan, Y. Wei, R. Jiang, X. Chen, D. Wang, Thin-Walled Structures Microstructure and mechanical properties of GH4169 thin-walled parts fabricated by ultrasonic vibration assisted laser directed energy deposition / milling hybrid process, Thin-Walled Struct. 205 (2024) 112349, https://doi.org/10.1016/j.tws.2024.112349.
[160] P. Stavropoulos, T. Souflas, H. Bikas, Hybrid Manufacturing Processes: an experimental machinability investigation of DED produced parts, Procedia CIRP 101 (2020) 218–221, https://doi.org/10.1016/j.procir.2020.11.010.
[161] Z. Jardon, G. Li, K. Vanmeensel, J. Sanchez-Medina, C. Snyers, M. Hinderdael, D. De Baere, L. Pyl, Optimization of hybrid directed energy deposition through production and microstructure assessment, Procedia CIRP 124 (2024) 324–330, https://doi.org/10.1016/j.procir.2024.08.127.
[162] J. Liu, J. Huang, Y. Zheng, S. Hou, S. Xu, Y. Ma, C. Huang, B. Zou, L. Li, Challenges in topology optimization for hybrid additive–subtractive manufacturing: a review, CAD Comput. Aided Des. 161 (2023) 103531, https://doi.org/10.1016/j.cad.2023.103531.
[163] M. Hoffmann, L. Heinrich, M. Paramanathan, K.B. Fillingim, A. Elwany, T. Feldhausen, Hybrid additive manufacturing of AISI 316L via asynchronous powder and hot-wire laser directed energy deposition, J. Manuf. Process. 127 (2024) 446–456, https://doi.org/10.1016/j.jmapro.2024.07.144.
[164] Y. Zhou, A. Shakibi, M. Grandhi, Z. Liu, F. Ning, Wire-influenced particle dynamics and fluid flow behaviors of melt pool in coaxial wire-powder fed directed energy deposition of metal matrix composites, J. Mater. Res. Technol. 36 (2025) 2909–2924, https://doi.org/10.1016/j.jmrt.2025.04.015.
[165] C. Wang, F. Xing, G. Xu, X. Liu, H. Bian, W. Liu, High addition content WC particle reinforced titanium matrix composites fabricated by concurrent wire powder feeding laser directed energy deposition, Opt. Laser Technol. 188 (2025) 113026, https://doi.org/10.1016/j.optlastec.2025.113026.
[166] T. Keller, Q. Campbell, D. Hayrikyan, K. Murphy, O. Fitchorova, J. Lesko, N. Post, A. Neils, Strength, microhardness, and microstructure analysis of 316L stainless steel manufactured via hybrid laser wire and laser powder bed additive, J. Manuf. Process. 150 (2025) 1–9, https://doi.org/10.1016/j.jmapro.2025.06.037.
[167] M.A. Rabalo, E.M. Rubio, B. Agustina, A.M. Camacho, Hybrid additive and subtractive manufacturing: evolution of the concept and last trends in research and industry, Procedia CIRP 118 (2023) 741–746, https://doi.org/10.1016/j.procir.2023.06.127.
[168] V.V. Popov, A. Fleisher, Hybrid additive manufacturing of steels and alloys, Manuf. Rev. 7 (2020), https://doi.org/10.1051/mfreview/2020005.
[169] Y. Yang, S. Yan, S. Qu, M. Yi, Z. Chen, T. Zhou, C. Xu, Microstructure of titanium alloy in additive/subtractive hybrid manufacturing: a review, J. Alloy. Compd. 1014 (2025) 178769, https://doi.org/10.1016/j.jallcom.2025.178769.
[170] S.R. Karade, S. Siddhartha, N.K. Gupta, G.G., K.P. Karunakaran, H. Zeidler, Hybridization in metal wire additive manufacturing: a case study of an impeller, Met. (Basel) 15 (2025), https://doi.org/10.3390/met15010071.
[171] R. Melentiev, F. Fang, Tailoring of surface topography for tribological purposes by controlled solid particle impacts, 444–445, Wear (2020) 203164, https://doi.org/10.1016/j.wear.2019.203164.
[172] R. Melentiev, F. Fang, Prediction of crater depth, surface roughness and erosion rate during abrasive jet machining of glass, 468–469, Wear (2021) 203596, https://doi.org/10.1016/j.wear.2020.203596.
[173] P. Gradl, Thin-Wall Internal Microchannels and Surface Enhancements for Rocket Nozzles using Laser Powder Directed Energy Deposition, in: NASA, NASA, 2025: p. 41. NASA.
[174] P. Gradl, A. Cervone, P. Colonna, Influence of build angles on thin-wall geometry and surface texture in laser powder directed energy deposition, Mater. Des. 234 (2023) 112352, https://doi.org/10.1016/j.matdes.2023.112352.
[175] D. Mudakavi, R. B Sreesha, R.S. Thanumoorthy, S. Anar, A. Krishnan R, S. Simhambhatla, S. Bontha, S. M Adinarayanappa, Sequential hybridisation of wire and powder-based additive manufacturing of Inconel 718: Mechanical and microstructural characterization, Mater. Sci. Eng. A 903 (2024) 146639, https://doi.org/10.1016/j.msea.2024.146639.
[176] R. Melentiev, F. Fang, S.K.R. Narala, Influence of different pretreatments on Ti-6Al-4V surface integrity and scratch-resistance of epoxy coating: Analysis of topography, microstructure, chemistry and wettability, Surf. Coat. Technol. 404 (2020) 126436, https://doi.org/10.1016/j.surfcoat.2020.126436.
[177] R. Melentiev, C. Kang, G. Shen, F. Fang, Study on surface roughness generated by micro-blasting on Co-Cr-Mo bio-implant, Wear 428429 (2019) 111–126, https://doi.org/10.1016/j.wear.2019.03.005.
[178] R. Melentiev, R. Tao, L. Fatta, A.K. Tevtia, N. Verghese, G. Lubineau, Towards decoupling chemical and mechanical adhesion at the electroplated metal/polymer interface via precision surface texturing, Surf. Interfaces 38 (2023) 102875, https://doi.org/10.1016/j.surfin.2023.102875.
[179] R. Melentiev, R. Tao, X. Li, A.K. Tevtia, N. Verghese, G. Lubineau, Mapping the coating failure modes of electroless plated metal on ABS polymer with micro-nano

structured interface, Int. J. Adhes. Adhes. 126 (2023) 103471, https://doi.org/10.1016/j.ijadhadh.2023.103471.
[180] R. Tao, L. Fatta, R. Melentiev, A.K. Tevtia, G. Lubineau, Contributions of chemical interactions and mechanical interlocking for the adhesion of electroplated copper to ABS in the Cr(VI) etching process, Int. J. Adhes. Adhes. 126 (2023) 103450, https://doi.org/10.1016/j.ijadhadh.2023.103450.
[181] R. Melentiev, A. Lagerweij, G. Lubineau, Multiprocess additive manufacturing via fused deposition modeling, chemical deposition, and electroplating with tough interfacial adhesion, Smart Mater. Manuf. 2 (2024) 100043, https://doi.org/10.1016/j.smmf.2023.100043.
[182] D. Chen, C. Su, T. Fang, Y. Wang, Study on the microstructure and properties of TC4-Cu functionally graded alloy fabricated by laser wire-powder synchronous additive manufacturing, Opt. Laser Technol. 192 (2025) 113781, https://doi.org/10.1016/j.optlastec.2025.113781.
[183] Y. Wang, X. Chen, Y. Huang, D. Chen, Y. Wang, A, Microstructure and properties of Ti6Al4V-xB alloys fabricated by concurrent wire-powder laser metal deposition additive manufacturing, Mater. Sci. Eng. A 946 (2025) 149085, https://doi.org/10.1016/j.msea.2025.149085.
[184] R. Melentiev, F. Fang, Investigation of erosion temperature in micro-blasting, Wear 420421 (2019) 123–132, https://doi.org/10.1016/j.wear.2018.12.073.
[185] Y. Otynshiyev, B. Sariyev, B. Golman, Y. Nie, C. Spitas, B. Golman, Wire- and powder-based direct energy deposition of NiTi-CuSn10-SS316L, Mater. Manuf. Process. 40 (2025) 1049–1058, https://doi.org/10.1080/10426914.2025.2491411.
[186] W. Huang, H. Zhong, X. Li, Y. Jia, S. Sun, N. Wu, Formation mechanism of hump defects in high-speed laser wire additive manufacturing, Opt. Laser Technol. 183 (2025), https://doi.org/10.1016/j.optlastec.2024.112239.
[187] A. Zapata, M. Spreitler, X.F. Zhao, C. Bernauer, M.F. Zaeh, Toward the rapid manufacturing of lightweight parts by laser directed energy deposition, Procedia CIRP 126 (2024) 579–584, https://doi.org/10.1016/j.procir.2024.08.243.
[188] P. Gao, J. Fan, M. Duan, W. Zhang, G. Chang, Microstructure and mechanical properties of micron-TiC reinforced novel martensitic high-strength steel via hybrid laser-arc directed energy deposition, Appl. Mater. Today 47 (2025) 102943, https://doi.org/10.1016/j.apmt.2025.102943.
[189] Y. Mao, H. Chen, J. Xiong, A novel pre-melted liquid filler laser directed energy deposition for Al alloy: process behaviors and filler transfer characteristics, Int. J. Heat. Mass. Transf. 252 (2025) 127431, https://doi.org/10.1016/j.ijheatmasstransfer.2025.127431.
[190] H. Lin, W. Zhai, Z. Li, M. Wang, Q. Chen, R. Zhou, Y. Fu, J. Huang, M. Liu, G. Zhao, G. Wang, R. Li, A.M.M. Ibrahim, H. Zhang, Enhanced fabrication and microstructure-property optimization of IN718 superalloy via laser rolling-assisted wire-arc directed energy deposition, Mater. Sci. Eng. A 944 (2025) 148890, https://doi.org/10.1016/j.msea.2025.148890.
[191] Z. Li, B. Chang, jiachen Wang, H. Zhang, Z. Liang, Z. Liao, L. Wang, C. Liu, D. Du, Dual-droplet transition control for improving forming quality and composition homogenizing in dual-wire additive manufacturing of Ti2AlNb alloy, Int. J. Mach. Tools Manuf. 195 (2024) 104114, https://doi.org/10.1016/j.ijmachtools.2023.104114.
[192] J. Xiao, W. Sheng, S. Gai, Z. Xu, R. Liu, M. Xu, S. Chen, Inter-wire current driven molten pool flow in oscillating-laser quad-wire deposition process, J. Manuf. Process. 148 (2025) 317–329, https://doi.org/10.1016/j.jmapro.2025.05.031.
[193] Z. Chen, K. Wang, W. Qu, M. Chen, S. Li, T. Dong, S. Gong, F. Wang, Hot corrosion behavior analysis and diffusion equation construction based on laser wire additive manufacturing GH3039, J. Mater. Res. Technol. 30 (2024) 1620–1630, https://doi.org/10.1016/j.jmrt.2024.03.204.
[194] A. Baghdadchi, M. Thuvander, S. Wessman, B.T. Alexandrov, J. Andersson, Effect of Ni content on 475°C embrittlement of directed energy deposited duplex stainless steel using a laser beam and wire feedstock, Materialia 36 (2024), https://doi.org/10.1016/j.mtla.2024.102155.
[195] F. Chainiau, F. Sikan, Y. Ding, M. Brochu, Microstructure and fracture toughness of laser wire deposited Ti-6Al-4V, J. Alloy. Metall. Syst. 7 (2024), https://doi.org/10.1016/j.jalmes.2024.100090.
[196] W. Liu, K. Jiang, B. Yan, J. Liu, X. Lu, Z. Cai, Y. Chen, H. Mou, Cable-stranded wire-fed laser cladding of high-aluminum lightweight high-entropy alloys, Mater. Today Commun. 39 (2024), https://doi.org/10.1016/j.mtcomm.2024.108835.
[197] R. Xiao, S. Guo, M. Zheng, B. Zhu, Q. Wu, J. Xu, T. Huang, New method for high-efficiency keyhole-based wire direct energy deposition: Process innovation and characterization, J. Laser Appl. 36 (2024), https://doi.org/10.2351/7.0001388.
[198] A. Kushwaha, A. Basak, Evaluating deposits of SS316L powder and wire consolidated using co-axial laser directed energy deposition, Int. J. Adv. Manuf. Technol. 132 (2024) 1627–1647, https://doi.org/10.1007/s00170-024-13243-1.
[199] K. Biester, L. Budde, N. Schwarz, J. Hermsdorf, L. Overmeyer, Laser hot-wire cladded gear preforms for the tailored forming process chain, Procedia CIRP 124 (2024) 673–677, https://doi.org/10.1016/j.procir.2024.08.199.
[200] O. DeNonno, A. Saville, J. Benzing, J. Klemm-Toole, Z. Yu, Solidification behavior and texture of 316L austenitic stainless steel by laser wire directed energy deposition, Mater. Charact. 211 (2024), https://doi.org/10.1016/j.matchar.2024.113916.
[201] X. Xiao, C. Zhang, D. Wu, H. Komen, J. Gou, Y. Zhang, K. Zhang, S. Uchida, M. Tanaka, Stabilising mechanism of cathode jet and droplet transfer in hybrid-laser–GMAW-based directed energy deposition of titanium alloy, Virtual Phys. Prototyp. 19 (2024), https://doi.org/10.1080/17452759.2024.2384659.
[202] T.A. Hassel, L.A. Marken, S.M. Arbo, G. Rørvik, Q. Du, V. Brøtan, K. Sørby, Microstructure development in duplex stainless steels from additive manufacturing with coaxial directed energy deposition and heat treatment, Metall. Mater. Trans. A Phys. Metall. Mater. Sci. 56 (2024) 474–505, https://doi.org/10.1007/s11661-024-07560-z.
[203] E. Fulco, D. Sorgente, Wire laser additively reinforced blanks: effect of the laser power on the bending strength of a single layer reinforcement, J. Mater. Res. Technol. (2024), https://doi.org/10.1016/j.jmrt.2024.09.036.
[204] Y. Ai, Y. Yan, P. Yuan, Y. Wang, The numerical investigation of cladding layer forming process in laser additive manufacturing with wire feeding, Int. J. Therm. Sci. 196 (2024) 108669, https://doi.org/10.1016/j.ijthermalsci.2023.108669.
[205] J. Pei, H. Yang, Y. He, K. Chen, H. Wang, X. Liu, S. Liu, Microstructure evolution and property of high manganese steel coatings by laser shock assisted laser wire cladding, J. Mater. Process. Technol. 328 (2024), https://doi.org/10.1016/j.jmatprotec.2024.118413.
[206] Webpage, 2025, Dir. Energy Depos. Pathw. Large Format Print. DM3Dhttps://3dprint.com/297077/directed-energy-deposition-the-pathway-to-large-format-metal-3d-printing/.
[207] Y. Mi, F. Sikström, L. Angelastri, P. Guglielmi, G. Palumbo, A. Ancona, Improving laser directed energy deposition with wire feed-stock through beam shaping with a deformable mirror, Opt. Lasers Eng. 185 (2025), https://doi.org/10.1016/j.optlaseng.2024.108716.
[208] J.A.D.De la Peña, P.A. Limon-Leyva, P. Cortes, K. Choo, Modeling of direct energy deposition for wire laser additive manufacturing, J. Mater. Eng. Perform. (2025), https://doi.org/10.1007/s11665-025-10665-0.
[209] J.Q. Yao, Y.S. Wang, X.W. Liu, X.F. Chen, S.M. Chen, L. Hu, H.T. Liu, Y.H. Qian, Y. Cheng, B. Song, C.Z. Yan, Y.S. Shi, Multi laser beams directed energy deposition of a high-strength and high-toughness TC11 titanium alloy with coaxial wire feeding, Mater 8 (2025), https://doi.org/10.1016/j.nxmate.2025.100576.
[210] T. Waqar, E. Pugsley, H. Jin, A. Horr, M.A. Easton, M.J. Benoit, Aging response of AA7075 + TiC fabricated by wire + laser directed energy deposition, Manuf. Lett. 44 (2025) 12–17, https://doi.org/10.1016/j.mfglet.2025.03.001.
[211] J.Q. Yao, T. Liang, Y.T. Lei, G.N. He, Y. Wu, Y.S. Wang, X.W. Liu, Microstructure and mechanical property of TC11 titanium alloy-steel bimetallic structure fabricated by coaxial-wire-feeding laser melting deposition, Vacuum 238 (2025), https://doi.org/10.1016/j.vacuum.2025.114220.
[212] S.B. Lawson, D. Yan, A. Tabei, B.K. Paul, S. Pasebani, Numerical modeling of coaxial wire-powder laser directed energy deposition process in dissimilar metal additive manufacturing, Results Mater. 26 (2025) 100701, https://doi.org/10.1016/j.rinma.2025.100701.
[213] Y. Chen, Y. Mao, M. Jiang, X. Chen, H. Wei, T. Han, Z. Wang, Z. Lei, P. He, Y. Chen, Achieving columnar to equiaxed transition in the as-deposited condition via coaxial wire feeding during laser directed energy deposition of Ti-6Al-4V, Addit. Manuf. 102 (2025) 104732, https://doi.org/10.1016/j.addma.2025.104732.
[214] Q. Wang, Y. Shi, K. Fan, S. Wang, Y. Li, Flow characteristic and solidification behavior in laser wire deposition with assistance of ultra-high frequency induction (UHF), Int. J. Therm. Sci. 214 (2025) 109834, https://doi.org/10.1016/j.ijthermalsci.2025.109834.
[215] K.M. Nagaraja, L. Budde, N. Schwarz, J. Hermsdorf, D. Qian, W. Li, Multiphysics modelling of wire-based directed energy deposition process with experimental validation, Int. J. Adv. Manuf. Technol. 136 (2025) 925–935, https://doi.org/10.1007/s00170-024-14905-w.
[216] Y. Hu, Z. Hua, G. Mi, M. Zhang, Z. Liu, X. Zhang, X. Yan, C. Wang, Investigation on the evolution of deposition layer grain structure and its effect on mechanical properties in aluminum alloy fabricated by laser directed energy deposition, Mater. Sci. Eng. A 892 (2024), https://doi.org/10.1016/j.msea.2023.145866.
[217] T.A. Hassel, I.M. Kulbotten, S.M. Arbo, G. Rørvik, V. Brøtan, K. Sørby, Corrosion, impact toughness and tensile properties of duplex stainless steels manufactured by directed energy deposition, Metall. Mater. Trans. A Phys. Metall. Mater. Sci. (2024), https://doi.org/10.1007/s11661-024-07586-3.
[218] Q. Zhang, N. Chekir, M. Brochu, Thermo-microstructural-mechanical modeling of the effect of wire diameters on single-bead Ti-6Al-4V wall deposits by laser wire deposition, J. Alloy. Metall. Syst. 8 (2024) 100134, https://doi.org/10.1016/j.jalmes.2024.100134.
[219] C. Li, J. Zhu, C. Wang, C. Deng, L. Cui, X. Zhang, C. Zhao, X. Jiao, Microstructure and properties of underwater in-situ wire-based laser additive manufactured duplex stainless steel, Virtual Phys. Prototyp. 19 (2024), https://doi.org/10.1080/17452759.2024.2401925.
[220] Y. He, H. Lu, X. Zhang, S. Xu, H. Li, Y. Hu, Study on in situ laser shock modulation of molten pool and defects in wire-feed laser additive manufacturing of steel to aluminum alloy, Thin-Walled Struct. 204 (2024), https://doi.org/10.1016/j.tws.2024.112326.
[221] J. Tweer, R. Day, T. Derra, D. Dorow-Gerspach, T. Loewenhoff, M. Wirtz, C. Linsmeier, T. Bergs, G. Natour, Initial experiments to regenerate the surface of plasma-facing components by wire-based laser metal deposition, Nucl. Mater. Energy 38 (2024), https://doi.org/10.1016/j.nme.2023.101577.
[222] Y. Cai, Y. Wang, H. Chen, J. Xiong, Searching optimal process parameters for desired layer geometry in wire-laser directed energy deposition based on machine learning, Virtual Phys. Prototyp. 19 (2024), https://doi.org/10.1080/17452759.2024.2352066.
[223] Z.H. Cai, K. Wang, J.L. Zhu, X.D. Jiao, X. Du, H.D. Wang, Characterization of microstructure and texture of lean duplex stainless steel 2101 produced by underwater laser wire direct energy deposition, J. Cent. South. Univ. 31 (2024) 72–83, https://doi.org/10.1007/s11771-023-5477-3.
[224] J. Xu, X. Wang, C. Yao, D. Zou, R. Xiong, R. Xiao, T. Huang, B. Zhang, A dual in-situ monitoring of multiphase dynamics during laser wire fusion process with

synchrotron radiation and visible light, J. Manuf. Process. 131 (2024) 2528–2534, https://doi.org/10.1016/j.jmapro.2024.10.025.
[225] Y. Cai, S. Zhang, Y. Wang, H. Chen, J. Xiong, Monitoring process stability in robotic wire-laser directed energy deposition based on multi-modal deep learning, J. Manuf. Process. 128 (2024) 111–124, https://doi.org/10.1016/j.jmapro.2024.08.033.
[226] Y. Ai, Y. Wang, S. Han, C. Ye, Investigation of cladding layer formation in uphill wire laser additive manufacturing on inclined substrate, Appl. Therm. Eng. 247 (2024), https://doi.org/10.1016/j.applthermaleng.2024.122919.
[227] T.A. Hassel, K. Sørby, V. Brøtan, Effect of preheat in DED-LB/wire of Ni-base, Cu-base and Fe-base alloys. in: Procedia CIRP, Elsevier B.V, 2024, pp. 674–679, https://doi.org/10.1016/j.procir.2024.08.286.
[228] S.N. Singh, A.B. Deoghare, Microstructure, microhardness, tensile and fatigue investigation on laser shock peened Ti6Al4V manufactured by high layer thickness directed energy deposition additive manufacturing, Opt. Laser Technol. 177 (2024), https://doi.org/10.1016/j.optlastec.2024.111132.
[229] Q. Wang, Y. Shi, K. Fan, S. Wang, Y. Li, Analysis of thermal behavior and mass transport for manufacturing deep-small hole by ultra-high frequency induction-assisted laser wire deposition, Int. J. Heat. Mass. Transf. 235 (2024), https://doi.org/10.1016/j.ijheatmasstransfer.2024.126219.
[230] L. Gao, Y. Chen, X. Zhang, A.C. Chuang, T. Sun, S.R. Agnew, Evolution of dislocations during the rapid solidi fication in additive manufacturing, Nat. Commun. 16 (2025) 4696, https://doi.org/10.1038/s41467-025-59988-5.
[231] P. Kyvelou, W. Hong, R. Zhang, L. Gardner, Mechanical properties and microstructure of wire laser metal deposited austenitic stainless steel, Mater. Des. 250 (2025), https://doi.org/10.1016/j.matdes.2024.113558.
[232] W. Huang, M. Fang, H. Zhong, Y. Jia, S. Sun, Z. Jiang, Heat transfer and flow of molten pool in single track multi-layer aluminum alloy laser wire additive manufacturing, Opt. Laser Technol. 181 (2025), https://doi.org/10.1016/j.optlastec.2024.111858.
[233] Y. Sun, X. Chen, Testing and design of wire-laser additively manufactured (WLAM) stainless steel angle section stub columns, Thin-Walled Struct. 214 (2025) 113351, https://doi.org/10.1016/j.tws.2025.113351.
[234] M. Wang, N. Al-Hamdany, Y. Deng, E. Maawad, S. Luo, N. Kashaev, Unravelling the cracking mechanism in wire-based laser-directed energy deposition processing high-strength aluminum alloy, J. Manuf. Process. 137 (2025) 437–456, https://doi.org/10.1016/j.jmapro.2025.01.046.
[235] R. Pal, N. Dreyer, A. Kushwaha, N. Menon, B.A. Sawyer, A. Basak, Anisotropic tensile properties and microstructure of SS316LSi fabricated using wire-based laser directed energy deposition, Mech. Mater. 206 (2025) 105338, https://doi.org/10.1016/j.mechmat.2025.105338.
[236] R. Pal, A. Kushwaha, K.H. Huang, A. Basak, High-temperature fatigue investigation of SS316L fabricated via laser wire-directed energy deposition, Mater. Charact. 222 (2025), https://doi.org/10.1016/j.matchar.2025.114799.
[237] A. Shakibi, M. Engquist, M. Eshraghi, Examining hatch spacing variations: Impacts on SS316L microstructure and mechanical performance in laser-wire directed energy deposition, J. Mater. Res. Technol. 39 (2025) 3794–3804, https://doi.org/10.1016/j.jmrt.2025.10.083.
[238] M. Wang, N. Kashaev, On the maintenance of processing stability and consistency in laser-directed energy deposition via machine learning, J. Manuf. Syst. 73 (2024) 126–142, https://doi.org/10.1016/j.jmsy.2024.01.005.
[239] J. Tweer, T. Derra, D. Dorow-Gerspach, M. Gago, S. Gierlings, S. Gräfe, G. Pintsuk, M. Wirtz, C. Linsmeier, T. Bergs, G. Natour, High heat flux testing of wire-based laser metal deposition coated plasma-facing components, Nucl. Mater. Energy 45 (2025), https://doi.org/10.1016/j.nme.2025.101983.
[240] Y. Feng, Q. Jiang, D. Fan, Effect of auxiliary wire feeding on cold metal transfer directed energy deposition of stainless steel: a study on droplet transfer, formation characteristics, and microstructure, J. Mater. Res. Technol. 33 (2024) 9313–9324, https://doi.org/10.1016/j.jmrt.2024.11.251.
[241] R. Melentiev, N. Yu, G. Lubineau, Polymer metallization via cold spray additive manufacturing: a review of process control, coating qualities, and prospective applications, Addit. Manuf. 48 (2021) 102459, https://doi.org/10.1016/j.addma.2021.102459.
[242] R. Melentiev, Physical theories of solid particle erosion and abrasive jet wear, J. Manuf. Process. 106 (2023) 422–452, https://doi.org/10.1016/j.jmapro.2023.10.014.
[243] Z. Lv, X. Zhang, J. Chen, M. Lang, H. Liu, Y. Cheng, Additive manufacturing of quartz glass using coaxial wire feeding technology, Opt. Laser Technol. 181 (2025) 111671, https://doi.org/10.1016/j.optlastec.2024.111671.
[244] B.T. Gibson, Y.K. Bandari, B.S. Richardson, W.C. Henry, E.J. Vetland, T. W. Sundermann, L.J. Love, Melt pool size control through multiple closed-loop modalities in laser-wire directed energy deposition of Ti-6Al-4V, Addit. Manuf. 32 (2020) 100993, https://doi.org/10.1016/j.addma.2019.100993.
[245] P. Gradl, A. Cervone, P. Colonna, Enhancement of friction factors for microchannels fabricated using laser powder directed energy deposition, Mater. Des. 251 (2025) 113673, https://doi.org/10.1016/j.matdes.2025.113673.
[246] C. Hagenlocher, P. O'Toole, W. Xu, M. Brandt, M. Easton, A. Molotnikov, The effect of heat accumulation on the local grain structure in laser-directed energy deposition of aluminium, Met. (Basel) 12 (2022), https://doi.org/10.3390/met12101601.
[247] Y. Chen, X. Chen, M. Jiang, Z. Lei, Z. Wang, J. Liang, S. Wu, S. Ma, N. Jiang, Y. Chen, Coaxial laser metal wire deposition of Ti6Al4V alloy: process, microstructure and mechanical properties, J. Mater. Res. Technol. 20 (2022) 2578–2590, https://doi.org/10.1016/j.jmrt.2022.08.068.
[248] Z. Nie, G. Wang, J.D. McGuffin-Cawley, B. Narayanan, S. Zhang, D. Schwam, M. Kottman, Y. Rong, Experimental study and modeling of H13 steel deposition using laser hot-wire additive manufacturing, J. Mater. Process. Technol. 235 (2016) 171–186, https://doi.org/10.1016/j.jmatprotec.2016.04.006.
[249] G.L. Knapp, M. Gussev, A. Shyam, T. Feldhausen, A. Plotkowski, Microstructure, deformation and fracture mechanisms in Al-4043 alloy produced by laser hot-wire additive manufacturing, Addit. Manuf. 59 (2022) 103150, https://doi.org/10.1016/j.addma.2022.103150.
[250] W. Huang, J. Xiao, S. Chen, X. Jiang, Control of wire melting behavior during laser hot wire deposition of aluminum alloy, Opt. Laser Technol. 150 (2022) 107978, https://doi.org/10.1016/j.optlastec.2022.107978.
[251] W. Jeong, S. Cho, H.J. Ryu, Optimization and characterization of C103 Nb alloy fabricated by laser wire directed energy deposition, Int. J. Refract. Met. Hard Mater. 133 (2025) 107318, https://doi.org/10.1016/j.ijrmhm.2025.107318.
[252] F. Pixner, F. Warchomicka, M. Lipińska, S. Elmiger, C. Jechtl, P. Auer, F. Riedlsperger, R. Buzolin, J. Domitner, M. Lewandowska, N. Enzinger, Thermal cycling effects on the local microstructure and mechanical properties in wire-based directed energy deposition of nickel-based superalloy, Addit. Manuf. 83 (2024), https://doi.org/10.1016/j.addma.2024.104066.
[253] V. Luna, L. Trujillo, A. Gamon, E. Arrieta, L.E. Murr, R.B. Wicker, C. Katsarelis, P. R. Gradl, F. Medina, Comprehensive and comparative heat treatment of additively manufactured inconel 625 alloy and corresponding microstructures and mechanical properties, J. Manuf. Mater. Process. 6 (2022), https://doi.org/10.3390/jmmp6050107.
[254] B. Bhatt, A. Martucci, S. Biamino, D. Ugues, F. Bondioli, L. Montanaro, M. Lombardi, P. Fino, Current trends in electron beam and laser powder bed fusion additive manufacturing of copper alloys: Composition, defects, properties, and challenges, Mater. Des. 253 (2025) 113742, https://doi.org/10.1016/j.matdes.2025.113742.
[255] J. Lee, A. Hussain, R. Eon, X. Li, Y. Sam, D. Liu, H. Seop, D. Kim, Optimization of laser powder bed fusion process to enhance mechanical properties of as-built Ti – 6Al – 4V samples, J. Mater. Res. Technol. 39 (2025) 3901–3914, https://doi.org/10.1016/j.jmrt.2025.10.018.
[256] P.D. Enrique, T. Minasyan, E. Toyserkani, Laser powder bed fusion of difficult-to-print γ' Ni-based superalloys: a review of processing approaches, properties, and remaining challenges, Addit. Manuf. 106 (2025) 104811, https://doi.org/10.1016/j.addma.2025.104811.
[257] M. Chen, Y. Ning, X. Sun, T. Liu, H. Wei, K. Zhang, W. Zhou, Z. Zhu, W. Zhai, W. Liao, Manipulating microstructure and mechanical property during laser powder bed fusion: multi-material, in-situ alloying, and processing, J. Alloy. Compd. 1007 (2024) 176438, https://doi.org/10.1016/j.jallcom.2024.176438.
[258] S. You, D. Jiang, F. Wang, F. Ning, Anisotropic sintering shrinkage behavior of stainless steel fabricated by extrusion-based metal additive manufacturing, J. Manuf. Process. 101 (2023) 1508–1520, https://doi.org/10.1016/j.jmapro.2023.07.026.
[259] T. Kurose, Y. Abe, M.V.A. Santos, Y. Kanaya, A. Ishigami, S. Tanaka, H. Ito, Influence of the layer directions on the properties of 316l stainless steel parts fabricated through fused deposition of metals, Mater. (Basel) 13 (2020), https://doi.org/10.3390/ma13112493.
[260] T. Rosnitschek, S. Tremmel, A. Seefeldt, B. Alber-Laukant, T. Neumeyer, V. Altstädt, Correlations of geometry and infill degree of extrusion additively manufactured 316l stainless steel components, Mater. (Basel) 14 (2021), https://doi.org/10.3390/ma14185173.
[261] H. Ramazani, A. Kami, Metal FDM, a new extrusion-based additive manufacturing technology for manufacturing of metallic parts: a review, Prog. Addit. Manuf. 7 (2022) 609–626, https://doi.org/10.1007/s40964-021-00250-x.
[262] J. Damon, S. Dietrich, S. Gorantla, U. Popp, B. Okolo, V. Schulze, Process porosity and mechanical performance of fused filament fabricated 316L stainless steel, Rapid Prototyp. J. 25 (2019) 1319–1327, https://doi.org/10.1108/RPJ-01-2019-0002.
[263] E. Maleki, B. Salehnasab, M. Paul, S. Shao, N. Shamsaei, Dimensional accuracy of fabricated geometries through powder bed fusion: an overview and a new benchmark artifact proposal, Mater. Des. 257 (2025) 114361, https://doi.org/10.1016/j.matdes.2025.114361.
[264] Z. Kong, G. Guillemot, M. Bellet, C. Gandin, Multiphysics simulation and microstructure prediction of coaxial wire-laser additive manufacturing process, Materialia 42 (2025) 102461, https://doi.org/10.1016/j.mtla.2025.102461.
[265] S. Wei, G. Wang, Y.C. Shin, Y. Rong, Comprehensive modeling of transport phenomena in laser hot-wire deposition process, Int. J. Heat. Mass. Transf. 125 (2018) 1356–1368, https://doi.org/10.1016/j.ijheatmasstransfer.2018.04.164.
[266] C. Tseng, C. Teng, T. Wang, Z. Xie, Numerical modelling and parametric investigation for the laser wire-feeding direct energy deposition, Int. J. Heat. Mass. Transf. 252 (2025) 127448, https://doi.org/10.1016/j.ijheatmasstransfer.2025.127448.
[267] R. Hu, M. Luo, T. Liu, L. Liang, A. Huang, D. Trushnikov, K.P. Karunakaran, S. Pang, Thermal fluid dynamics of liquid bridge transfer in laser wire deposition 3D printing, Sci. Technol. Weld. Join. 24 (2019) 401–411, https://doi.org/10.1080/13621718.2019.1591039.
[268] M.J. Torkamany, A.F.H. Kaplan, F.M. Ghaini, M. Vänskä, A. Salminen, K. Fahlström, J. Hedegård, Wire deposition by a laser-induced boiling front, Opt. Laser Technol. 69 (2015) 104–112, https://doi.org/10.1016/j.optlastec.2014.12.013.
[269] H. Gu, L. Li, Computational fluid dynamic simulation of gravity and pressure effects in laser metal deposition for potential additive manufacturing in space, Int. J. Heat. Mass. Transf. 140 (2019) 51–65, https://doi.org/10.1016/j.ijheatmasstransfer.2019.05.081.
[270] W.N. Su, P. Erasenthiran, P.M. Dickens, Investigation of fully dense laser sintering of tool steel powder using a pulsed Nd: YAG (neodymium-doped yttrium

aluminium garnet) laser, Proc. Inst. Mech. Eng. Part. C. J. Mech. Eng. Sci. 217 (2003) 127–138, https://doi.org/10.1243/095440603762554677.
[271] Y.S. Lee, D.F. Farson, Surface tension-powered build dimension control in laser additive manufacturing process, Int. J. Adv. Manuf. Technol. 85 (2016) 1035–1044, https://doi.org/10.1007/s00170-015-7974-5.
[272] J. Li, H.N. Li, Z. Liao, D. Axinte, Analytical modelling of full single-track profile in wire-fed laser cladding, J. Mater. Process. Technol. 290 (2021) 116978, https://doi.org/10.1016/j.jmatprotec.2020.116978.
[273] J. Li, H.N. Li, Z. Liao, D. Axinte, Overlapped wire-fed laser cladding on inclined surfaces: an analytical model considering gravity and a model application, J. Mater. Process. Technol. 304 (2022) 117559, https://doi.org/10.1016/j.jmatprotec.2022.117559.
[274] R. Sun, Y. Shi, X. Wang, Y. Guo, X. Zhou, Understanding the thermal process during laser assisted ultra-high frequency induction deposition with wire feeding, Int. J. Heat. Mass. Transf. 153 (2020) 119536, https://doi.org/10.1016/j.ijheatmasstransfer.2020.119536.
[275] Q. Chen, Y. Zhao, S. Strayer, Y. Zhao, K. Aoyagi, Y. Koizumi, A. Chiba, W. Xiong, A.C. To, Elucidating the effect of preheating temperature on melt pool morphology variation in Inconel 718 laser powder bed fusion via simulation and experiment, Addit. Manuf. 37 (2021) 101642, https://doi.org/10.1016/j.addma.2020.101642.
[276] L. Gao, J. Bhattacharyya, W. Lin, Z. Ren, A.C. Chuang, P.D. Shevchenko, V. Nikitin, J. Ma, S.R. Agnew, T. Sun, Tailoring material microstructure and property in wire-laser directed energy deposition through a wiggle deposition strategy, Addit. Manuf. 77 (2023), https://doi.org/10.1016/j.addma.2023.103801.
[277] J.P. Kruth, L. Froyen, J. Van Vaerenbergh, P. Mercelis, M. Rombouts, B. Lauwers, Selective laser melting of iron-based powder, J. Mater. Process. Technol. 149 (2004) 616–622, https://doi.org/10.1016/j.jmatprotec.2003.11.051.
[278] L. Liang, R. Hu, J. Wang, A. Huang, S. Pang, A thermal fluid mechanical model of stress evolution for wire feeding-based laser additive manufacturing, J. Manuf. Process. 69 (2021) 602–612, https://doi.org/10.1016/j.jmapro.2021.08.008.
[279] F.E. Bock, J. Herrnring, M. Froend, J. Enz, N. Kashaev, B. Klusemann, Experimental and numerical thermo-mechanical analysis of wire-based laser metal deposition of Al-Mg alloys, J. Manuf. Process. 64 (2021) 982–995, https://doi.org/10.1016/j.jmapro.2021.02.016.
[280] S.B. Lawson, D. Tavakoli, A. Tabei, S. Pasebani, Process-induced residual stress analysis of Inconel 625 and GRCop-42 dissimilar metal fabricated via coaxial wire-powder laser directed energy deposition, Manuf. Lett. 44 (2025) 1171–1176, https://doi.org/10.1016/j.mfglet.2025.06.136.
[281] F. Benmessaoud, M. Cheikh, V. Vidal, H. Matsumoto, V. Velay, Experimental study and modeling of the microstructural effects on the mechanical behavior of Ti-6Al-4V titanium alloy, Mech. Res. Commun. 148 (2025) 104473, https://doi.org/10.1016/j.mechrescom.2025.104473.
[282] W. Sun, F. Shan, N. Zong, H. Dong, T. Jing, A simulation and experiment study on phase transformations of Ti-6Al-4V in wire laser additive manufacturing, Mater. Des. 207 (2021) 109843, https://doi.org/10.1016/j.matdes.2021.109843.
[283] Y. Song, H. Xu, Q. Bai, Y. Zhang, X. Ding, M. Yin, G. Yin, Numerical modeling of thermally driven phase transformation and α lath width evolution during laser directed energy deposition of Ti6Al4V alloy, Int. J. Adv. Manuf. Technol. 137 (2025) 1523–1549, https://doi.org/10.1007/s00170-025-15194-7.
[284] A.D. Boccardo, Z. Zou, M. Simonelli, M. Tong, J. Segurado, S.B. Leen, D. Tourret, Martensite decomposition kinetics in additively manufactured Ti-6Al-4V alloy: In-situ characterisation and phase-field modelling, Mater. Des. 241 (2024) 112949, https://doi.org/10.1016/j.matdes.2024.112949.
[285] A. Hamed, M. Zarghami, H. Doumanidis, B. Golman, K.V. Kostas, C. Spitas, Microstructural evolution and crystalline behavior in silicon carbide nano-powder during selective laser melting: a molecular dynamics simulation, J. Cryst. Growth 650 (2025) 127985, https://doi.org/10.1016/j.jcrysgro.2024.127985.
[286] X. Liu, Y. Di, G. Wang, L. Ji, Y. Yuan, Y. Rong, Prediction of spatial yield strength distribution in Al–Mg–Sc alloy fabricated by coaxial laser wire directed energy deposition, Virtual Phys. Prototyp. 20 (2025), https://doi.org/10.1080/17452759.2025.2544757.
[287] Y. Tang, A. Zhang, H. Liu, G. Zhang, C. Li, Y. Li, Z. Dong, G. Huang, B. Jiang, Insight into scale selection of dimensionless phase-field model of alloy solidification, Mater. Des. 254 (2025), https://doi.org/10.1016/j.matdes.2025.114028.
[288] E. Roque, J. Segurado, F. Montero-Chacón, Phase-field modeling and computational design of structurally stable NMC materials, Mater. Des. 248 (2024) 113464, https://doi.org/10.1016/j.matdes.2024.113464.
[289] S. Liu, C. Brice, X. Zhang, Hierarchical bead materials multi-property design for wire-feed laser additive manufacturing, J. Manuf. Process. 80 (2022) 546–557, https://doi.org/10.1016/j.jmapro.2022.05.028.
[290] S. Liu, C. Brice, X. Zhang, Interrelated process-geometry-microstructure relationships for wire-feed laser additive manufacturing, Mater. Today Commun. 31 (2022) 103794, https://doi.org/10.1016/j.mtcomm.2022.103794.
[291] N.G. Mbodj, M. Abuabiah, P. Plapper, M. El Kandaoui, S. Yaacoubi, Bead geometry prediction in laser-wire additive manufacturing process using machine learning: Case of study, Appl. Sci. 11 (2021), https://doi.org/10.3390/app112411949.
[292] Z. Yang, A.K. Verma, L. Smith, A. Guzel, H. Chen, P.C. Pistorius, A.D. Rollett, Predicting melt pool dimensions for wire-feed directed energy deposition process, Integr. Mater. Manuf. Innov. 11 (2022) 532–544, https://doi.org/10.1007/s40192-022-00278-z.
[293] W. Huang, S. Chen, J. Xiao, X. Jiang, Y. Jia, Laser wire-feed metal additive manufacturing of the Al alloy, Opt. Laser Technol. 134 (2021) 106627, https://doi.org/10.1016/j.optlastec.2020.106627.
[294] D.J. Corbin, A.R. Nassar, E.W. Reutzel, A.M. Beese, N.A. Kistler, Effect of directed energy deposition processing parameters on laser deposited Inconel® 718: external morphology, J. Laser Appl. 29 (2017), https://doi.org/10.2351/1.4977476.
[295] M. Zhu, Y. Chen, Y. Chen, K. Hu, Application of Taguchi-grey relational analysis for optimizing process parameters of laser cladding for 316L stainless steel, Int. J. Interact. Des. Manuf. (2025) 6417–6428, https://doi.org/10.1007/s12008-024-02218-x.
[296] L. Ye, H. Xue, Z. Li, Y. Zhou, G. Chen, F. Xu, R. Melentiev, S. Newman, N. Yu, Review of online quality control for laser directed energy deposition (LDED) additive manufacturing, Int. J. Extrem. Manuf. 7 (2025), https://doi.org/10.1088/2631-7990/aded4f.
[297] J. Flores, I. Cabanes, A. Gutierrez, K.L. de Calle, O. Gonzalo, E. Portillo, An innovative smart monitoring system for DED-LB/MW process stability based on machine learning techniques, Int. J. Adv. Manuf. Technol. 137 (2025) 1759–1773, https://doi.org/10.1007/s00170-025-15134-5.
[298] M. Froend, V. Ventzke, N. Kashaev, B. Klusemann, J. Enz, Thermal analysis of wire-based direct energy deposition of Al-Mg using different laser irradiances, Addit. Manuf. 29 (2019) 100800, https://doi.org/10.1016/j.addma.2019.100800.
[299] S. Takushima, D. Morita, N. Shinohara, H. Kawano, Y. Mizutani, Y. Takaya, Optical in-process height measurement system for process control of laser metal-wire deposition, Precis. Eng. 62 (2020) 23–29, https://doi.org/10.1016/j.precisioneng.2019.11.007.
[300] R. Asadi, A. Queguineur, O. Wiikinkoski, H. Mokhtarian, T. Aihkisalo, A. Revuelta, I.F. Ituarte, Process monitoring by deep neural networks in directed energy deposition: CNN-based detection, segmentation, and statistical analysis of melt pools, Robot. Comput. Integr. Manuf. 87 (2024), https://doi.org/10.1016/j.rcim.2023.102710.
[301] L. Chen, G. Bi, X. Yao, C. Tan, J. Su, N.P.H. Ng, Y. Chew, K. Liu, S.K. Moon, Multisensor fusion-based digital twin for localized quality prediction in robotic laser-directed energy deposition, Robot. Comput. Integr. Manuf. 84 (2023) 102581, https://doi.org/10.1016/j.rcim.2023.102581.
[302] K. Wasmer, M. Wüst, D. Cui, G. Masinelli, V. Pandiyan, S. Shevchik, Monitoring of functionally graded material during laser directed energy deposition by acoustic emission and optical emission spectroscopy using artificial intelligence, Virtual Phys. Prototyp. 18 (2023), https://doi.org/10.1080/17452759.2023.2189599.
[303] Y. Li, Z. Wang, C. Liu, F. Chen, G. Bi, From geometric precision to performance: improved online monitoring system for thin-walled parts by fine wire laser directed energy deposition 4 (2025), https://doi.org/10.1016/j.amf.2025.200201.
[304] N.D. Jamnikar, S. Liu, C. Brice, X. Zhang, In-process comprehensive prediction of bead geometry for laser wire-feed DED system using molten pool sensing data and multi-modality CNN, Int. J. Adv. Manuf. Technol. 121 (2022) 903–917, https://doi.org/10.1007/s00170-022-09248-3.
[305] G. Chen, D. Zhou, Y. Gao, F. Xu, B. Wu, L. Ye, Vision-based wire stick-out measurement method in wire-fed laser additive manufacturing, Int. J. Adv. Manuf. Technol. (2026).
[306] K. Tzimanis, M.S. Koutsokeras, N. Bourlesas, N. Porevopoulos, G. Pastras, Digital transformation of wire DED - LB: enabling industrial scalability through monitoring and control systems, Springe Lond. (2025), https://doi.org/10.1007/s00170-025-16654-w.
[307] L. Chen, G. Bi, X. Yao, J. Su, C. Tan, W. Feng, M. Benakis, Y. Chew, S. Ki, In-situ process monitoring and adaptive quality enhancement in laser additive manufacturing: a critical review, J. Manuf. Syst. 74 (2024) 527–574, https://doi.org/10.1016/j.jmsy.2024.04.013.
[308] A. Heralić, A.K. Christiansson, B. Lennartson, Height control of laser metal-wire deposition based on iterative learning control and 3D scanning, Opt. Lasers Eng. 50 (2012) 1230–1241, https://doi.org/10.1016/j.optlaseng.2012.03.016.
[309] I. Garmendia, J. Pujana, A. Lamikiz, J. Flores, M. Madarieta, Development of an intra-layer adaptive toolpath generation control procedure in the laser metal wire deposition process, Mater. (Basel) 12 (2019), https://doi.org/10.3390/ma12030352.
[310] B.T. Gibson, P. Mhatre, M.C. Borish, C.E. Atkins, J.T. Potter, J.E. Vaughan, L. J. Love, Controls and process planning strategies for 5-axis laser directed energy deposition of Ti-6Al-4V using an 8-axis industrial robot and rotary motion, Addit. Manuf. 58 (2022) 103048, https://doi.org/10.1016/j.addma.2022.103048.
[311] H. Ritchie, Sector by sector: where do global greenhouse gas emissions come from?" Published online at OurWorldinData.org, OurWorldInData. Org. 2020 (2024). https://ourworldindata.org/ghg-emissions-by-sector.
[312] I.S. Jawahir, R. Bradley, Technological Elements of circular economy and the principles of 6R-based closed-loop material flow in sustainable manufacturing, Procedia CIRP 40 (2016) 103–108, https://doi.org/10.1016/j.procir.2016.01.067.
[313] M.Z. Hauschild, S. Kara, I. Røpke, Absolute sustainability: challenges to life cycle engineering, CIRP Ann. 69 (2020) 533–553, https://doi.org/10.1016/j.cirp.2020.05.004.
[314] V. Pusateri, M.Z. Hauschild, S. Kara, C. Goulas, S.I. Olsen, Quantitative sustainability assessment of metal additive manufacturing: a systematic review, CIRP J. Manuf. Sci. Technol. 49 (2024) 95–110, https://doi.org/10.1016/j.cirpj.2023.12.005.
[315] N. Goffin, J.R. Tyrer, L.C.R. Jones, R.L. Higginson, Simulated and experimental analysis of laser beam energy profiles to improve efficiency in wire-fed laser

deposition, Int. J. Adv. Manuf. Technol. 114 (2021) 3021–3036, https://doi.org/10.1007/s00170-021-07029-y.
[316] K. Biester, L. Budde, A. Barroi, M. Lammers, J. Hermsdorf, L. Overmeyer, Investigation of deposition welding in vertical and horizontal position with a coaxial laser wire welding head, Int. J. Adv. Manuf. Technol. 120 (2022) 5399–5410, https://doi.org/10.1007/s00170-022-09013-6.
[317] S.C. Bozeman, O.B. Isgor, J.D. Tucker, Effects of processing conditions on the solidification and heat-affected zone of 309L stainless steel claddings on carbon steel using wire-directed energy deposition, Surf. Coat. Technol. 444 (2022) 128698, https://doi.org/10.1016/j.surfcoat.2022.128698.
[318] G. Sun, Z. Wang, Y. Lu, M. Chen, K. Yang, Z. Ni, Underwater laser welding/cladding for high-performance repair of marine metal materials: a review (English Ed. Chin. J. Mech. Eng. 35 (2022) https://doi.org/10.1186/s10033-021-00674-0.
[319] S.W. Williams, F. Martina, A.C. Addison, J. Ding, G. Pardal, P. Colegrove, Wire + Arc additive manufacturing, Mater. Sci. Technol. (U. Kingd.) 32 (2016) 641–647, https://doi.org/10.1179/1743284715Y.0000000073.
[320] M.L. Montero Sistiaga, R. Mertens, B. Vrancken, X. Wang, B. Van Hooreweder, J. P. Kruth, J. Van Humbeeck, Changing the alloy composition of Al7075 for better processability by selective laser melting, J. Mater. Process. Technol. 238 (2016) 437–445, https://doi.org/10.1016/j.jmatprotec.2016.08.003.
[321] N.P. Barnes, Solid-state lasers from an efficiency perspective, IEEE J. Sel. Top. Quantum Electron. 13 (2007) 435–447, https://doi.org/10.1109/JSTQE.2007.895280.
[322] A. Urresti, J.I. Arrizubieta, A. Loroño, O. Ukar, Energy consumption monitoring in DED-LB for enhancing the process sustainability, Procedia CIRP 124 (2024) 210–213, https://doi.org/10.1016/j.procir.2024.08.101.
[323] A.R. Catalano, V. Lunetto, P.C. Priarone, L. Settineri, A survey on energy efficiency in metal wire deposition processes, Smart Innov. Syst. Technol. 155 (2019) 311–322, https://doi.org/10.1007/978-981-13-9271-9_26.
[324] T. Gutowski, J. Dahmus, A. Thiriez, Electrical energy requirements for manufacturing processes, Proc. 13th CIRP Int. Conf. Life Cycle Eng. LCE 2006 (2006) 623–628.
[325] I.H. Shah, N. Hadjipantelis, L. Walter, R.J. Myers, L. Gardner, Environmental life cycle assessment of wire arc additively manufactured steel structural components, J. Clean. Prod. 389 (2023) 136071, https://doi.org/10.1016/j.jclepro.2023.136071.
[326] W. Liu, H. Wei, M. Zhang, Y. Luo, Y. Zhang, Energy consumption modeling of additive-subtractive hybrid manufacturing based on cladding head moving state and deposition efficiency, Int. J. Adv. Manuf. Technol. 120 (2022) 7755–7770, https://doi.org/10.1007/s00170-022-09265-2.
[327] A.R. Catalano, P.C. Priarone, L. Settineri, An economic evaluation of hybrid WAAM-subtractive manufacturing in relation to deposition process parameters, Procedia CIRP 122 (2024) 49–54, https://doi.org/10.1016/j.procir.2024.02.003.
[328] F. Montevecchi, G. Venturini, N. Grossi, A. Scippa, G. Campatelli, Idle time selection for wire-arc additive manufacturing: a finite element-based technique, Addit. Manuf. 21 (2018) 479–486, https://doi.org/10.1016/j.addma.2018.01.007.
[329] Y. Zhao, Y. Jia, S. Chen, J. Shi, F. Li, Process planning strategy for wire-arc additive manufacturing: thermal behavior considerations, Addit. Manuf. 32 (2020), https://doi.org/10.1016/j.addma.2019.100935.
[330] European Environment Agency (EEA) (2025) Total GHG Emissions and Removals in the EU, Sustain. 11 (2025) 1–14. https://www.eea.europa.eu/en/analysis/indicators/greenhouse-gas-emission-intensi ty-of-1-1751032678/greenhouse-gas-emission-intensity-of-electricity-generation-c ountry-level.
[331] Electricity p rice statistics, (2025) 2025. https://ec.europa.eu/eurostat/statistics-explained/index.php?title=Electricity_p rice_statistics#Electricity_prices_for_non-household_consumers.
[332] S. Kokare, J.P. Oliveira, T.G. Santos, R. Godina, Environmental and economic assessment of a steel wall fabricated by wire-based directed energy deposition, Addit. Manuf. 61 (2023) 103316, https://doi.org/10.1016/j.addma.2022.103316.
[333] J.R. Gouveia, S.M. Pinto, S. Campos, J.R. Matos, J. Sobral, S. Esteves, L. Oliveira, Life cycle assessment and cost analysis of additive manufacturing repair processes in the mold industry, Sustain 14 (2022), https://doi.org/10.3390/su14042105.
[334] A.C.M. Bekker, J.C. Verlinden, Life cycle assessment of wire + arc additive manufacturing compared to green sand casting and CNC milling in stainless steel, J. Clean. Prod. 177 (2018) 438–447, https://doi.org/10.1016/j.jclepro.2017.12.148.
[335] T. Kamps, M. Lutter-Guenther, C. Seidel, T. Gutowski, G. Reinhart, Cost- and energy-efficient manufacture of gears by laser beam melting, CIRP J. Manuf. Sci. Technol. 21 (2018) 47–60, https://doi.org/10.1016/j.cirpj.2018.01.002.
[336] H.H. Shah, C. Tregambi, P. Bareschino, F. Pepe, Environmental and economic sustainability of additive manufacturing: a systematic literature review, Sustain. Prod. Consum. 51 (2024) 628–643, https://doi.org/10.1016/j.spc.2024.10.012.
[337] F.S. Gobber, P.C. Priarone, A. Pennacchio, M. Actis Grande, Effect of inert gas pressure on the properties and carbon footprint of UNS S32760 powders made from waste materials by gas atomization, J. Mater. Res. Technol. 33 (2024) 8814–8828, https://doi.org/10.1016/j.jmrt.2024.11.195.
[338] N.P. Lavery, D.J. Jarvis, S.G.R. Brown, N.J. Adkins, B.P. Wilson, Life cycle assessment of sponge nickel produced by gas atomisation for use in industrial hydrogenation catalysis applications, Int. J. Life Cycle Assess. 18 (2013) 362–376, https://doi.org/10.1007/s11367-012-0478-8.
[339] A.G. Demir, Micro laser metal wire deposition for additive manufacturing of thin-walled structures, Opt. Lasers Eng. 100 (2018) 9–17, https://doi.org/10.1016/j.optlaseng.2017.07.003.
[340] P.H. Gruber, J. Frostevarg, F. Akhtar, Laser micro-wire cladding: process insights and novel wire-bending technique, J. Manuf. Process. 155 (2025) 214–230, https://doi.org/10.1016/j.jmapro.2025.09.064.
[341] J.L. Dávila, P.I. Neto, P.Y. Noritomi, R.T. Coelho, J.V.L. da Silva, Hybrid manufacturing: a review of the synergy between directed energy deposition and subtractive processes, Int. J. Adv. Manuf. Technol. 110 (2020) 3377–3390, https://doi.org/10.1007/s00170-020-06062-7.
[342] C. Favi, L. Murgese, N. Villazzi, S. Gallozzi, M. Mandolini, M. Marconi, Integrating life cycle engineering into design for additive manufacturing: a review, J. Manuf. Syst. 82 (2025) 599–631, https://doi.org/10.1016/j.jmsy.2025.07.010.
[343] V. Lunetto, M. Galati, L. Settineri, L. Iuliano, Unit process energy consumption analysis and models for Electron Beam Melting (EBM): effects of process and part designs, Addit. Manuf. 33 (2020) 101115, https://doi.org/10.1016/j.addma.2020.101115.
[344] P.C. Priarone, G. Campatelli, F. Montevecchi, G. Venturini, L. Settineri, A modelling framework for comparing the environmental and economic performance of WAAM-based integrated manufacturing and machining, CIRP Ann. 68 (2019) 37–40, https://doi.org/10.1016/j.cirp.2019.04.005.
[345] Ansys Granta Selector: Smarter Materials Choices, Https://Www.Ansys.Com/It-It/Products/Materials/Granta-Selector (2025) R1. https://www.ansys.com/it-it/products/materials/granta-selector.
[346] P.C. Priarone, G. Campatelli, A.R. Catalano, F. Baffa, Life-cycle energy and carbon saving potential of wire arc additive manufacturing for the repair of mold inserts, CIRP J. Manuf. Sci. Technol. 35 (2021) 943–958, https://doi.org/10.1016/j.cirpj.2021.10.007.
[347] J.M. Wilson, C. Piya, Y.C. Shin, F. Zhao, K. Ramani, Remanufacturing of turbine blades by laser direct deposition with its energy and environmental impact analysis, J. Clean. Prod. 80 (2014) 170–178, https://doi.org/10.1016/j.jclepro.2014.05.084.
[348] N. Khanna, H. Salvi, B. Karaş, I. Fairoz, A. Shokrani, Cost modelling for powder bed fusion and directed energy deposition additive manufacturing, J. Manuf. Mater. Process. 8 (2024), https://doi.org/10.3390/jmmp8040142.
[349] N. Tepylo, X. Huang, P.C. Patnaik, Laser-based additive manufacturing technologies for aerospace applications, Adv. Eng. Mater. 21 (2019) 1–35, https://doi.org/10.1002/adem.201900617.
[350] Y. Chu, X. Zhao, W. Sun, S. Holdsworth, D. Guan, Y. Huang, Laser directed energy deposition additive manufacturing using friction stir channelling extruded wire, J. Manuf. Process. 154 (2025) 122–133, https://doi.org/10.1016/j.jmapro.2025.09.060.
[351] S. Kokare, J.P. Oliveira, R. Godina, A LCA and LCC analysis of pure subtractive manufacturing, wire arc additive manufacturing, and selective laser melting approaches, J. Manuf. Process. 101 (2023) 67–85, https://doi.org/10.1016/j.jmapro.2023.05.102.
[352] M. Froend, S. Riekehr, N. Kashaev, B. Klusemann, J. Enz, Process development for wire-based laser metal deposition of 5087 aluminium alloy by using fibre laser, J. Manuf. Process. 34 (2018) 721–732, https://doi.org/10.1016/j.jmapro.2018.06.033.
[353] S. Kokare, J.P. Oliveira, R. Godina, Social organizational life cycle assessment of wire arc additive manufacturing: a case study of a Belgian company, Int. J. Life Cycle Assess. (2025), https://doi.org/10.1007/s11367-025-02491-2.
[354] B. Zheng, V. Trofimov, Y. Yang, C. Han, Z. Zheng, S.F. Abbas, S. Li, L. Lei, J. Sang, J. Zhang, D. Wang, Enhancing the dimensional accuracy and manufacturing limits of laser powder bed fusion through dual-laser hybrid additive-subtractive manufacturing, Opt. Laser Technol. 188 (2025) 112947, https://doi.org/10.1016/j.optlastec.2025.112947.
[355] E. Maleki, B. Salehnasab, M. Paul, S. Shao, N. Shamsaei, Dimensional accuracy of fabricated geometries through powder bed fusion: an overview and a new benchmark artifact proposal, Mater. Des. 257 (2025), https://doi.org/10.1016/j.matdes.2025.114361.
[356] Y. Wei, G. Chen, H. Wang, N. Tao, High-precision laser powder bed fusion of 316L stainless steel and its SiC reinforcement composite materials, Opt. Laser Technol. 190 (2025) 113267, https://doi.org/10.1016/j.optlastec.2025.113267.
[357] B. Zhu, R. Li, T. Yuan, W. Li, D. Cai, N. Kang, Metal binder jetting additive manufacturing: an overview of the process, materials and reinforcement methods, J. Alloy. Compd. 1037 (2025) 182196, https://doi.org/10.1016/j.jallcom.2025.182196.
[358] A. Burr, C.A. Lopez, J.A. Becerra, J. Zeng, D. Vincent, V. Bonnefoy, A calibration method to predict shape change during sintering: application to 316L parts made by metal binder jetting, Addit. Manuf. 110 (2025) 104938, https://doi.org/10.1016/j.addma.2025.104938.
[359] K. Yu, Y. Zhang, J. Cai, B. Zhang, X. Qu, Research progress on densification behavior of component fabricated by Binder Jetting additive manufacturing, Rev. Mater. Res. 1 (2025) 100073, https://doi.org/10.1016/j.revmat.2025.100073.
[360] R. Melentiev, A. Wagih, G. Lubineau, C.A. Grande, 3D printing, debinding and sintering of stainless steel metamaterials via lithography metal manufacturing: processing, microstructure and properties relationships, Mater. Des. 256 (2025) 114352, https://doi.org/10.1016/j.matdes.2025.114352.
[361] R. Melentiev, A. Wagih, B. Van Der Heijden, G. Lubineau, C.A. Grande, Sintering-based lithography metal additive manufacturing of chiral mechanical metamaterials with a twist, Procedia CIRP 132 (2025) 104–109, https://doi.org/10.1016/j.procir.2025.01.018.
[362] R. Melentiev, G. Harakály, J. Stögerer, G. Mitteramskogler, A. Wagih, G. Lubineau, C.A. Grande, High-resolution metal 3D printing via digital light processing, Addit. Manuf. 85 (2024), https://doi.org/10.1016/j.addma.2024.104156.

[363] R. Melentiev, A. Wagih, A. Lagerweij, G. Mitteramskogler, G. Lubineau, C. A. Grande, Unlocking multiscale metallic metamaterials via lithography additive manufacturing, Virtual Phys. Prototyp. 19 (2024) 1–20, https://doi.org/10.1080/17452759.2024.2339368.
[364] R. Melentiev, A. Wagih, G. Lubineau, C.A. Grande, Lithography metal additive manufacturing of 316L steel metamaterials: effect of sintering temperature on shape distortion, microstructure and mechanical properties, Procedia CIRP 00 6 (2025), https://doi.org/10.1016/j.procir.2025.01.014.
[365] N.K. Bankapalli, V. Gupta, P. Saxena, A. Bajpai, C. Lahoda, J. Polte, Filament fabrication and subsequent additive manufacturing, debinding, and sintering for extrusion-based metal additive manufacturing and their applications: a review, Compos. Part. B Eng. 264 (2023) 110915, https://doi.org/10.1016/j.compositesb.2023.110915.
[366] F. Wang, S. You, D. Jiang, X. Yuan, R. Fu, F. Ning, Microstructure evolution, phase formation, corrosion, and mechanical properties of stainless steel fabricated by extrusion-based sintering-assisted additive manufacturing, Addit. Manuf. 75 (2023) 103746, https://doi.org/10.1016/j.addma.2023.103746.
[367] A. Bose, J.P. Reidy, J. Pötschke, Sinter-based additive manufacturing of hardmetals: Review, Int. J. Refract. Met. Hard Mater. 119 (2024) 106493, https://doi.org/10.1016/j.ijrmhm.2023.106493.
[368] I. Nandi, Q. Charron, B. Verquin, P.R. Gradl, S. Shao, N. Shamsaei, Dimensional Accuracy of 17-4 PH SS Geometric Features Fabricated Using L-PBF and MBJ Technologies, in, 2025, Solid Free. Fabr, Austin, 2025.
[369] L. C. B. Carolo, R.E. Cooper, O., A review on the influence of process variables on the surface roughness of Ti-6Al-4V by electron beam powder bed fusion, Addit. Manuf. 59 (2022) 103103, https://doi.org/10.1016/j.addma.2022.103103.
[370] L.N. Carter, V.M. Villapún, L. Grover, S.C. Cox, Exploring the duality of powder adhesion and underlying surface roughness in laser powder bed fusion processed Ti-6Al-4V, J. Manuf. Process. 81 (2022) 14–26, https://doi.org/10.1016/j.jmapro.2022.06.057.
[371] S. Rathor, D. Kumar, R. Kant, E. Singla, Influence of non-planar orientations on solidification microstructure during robot-assisted laser-wire directed energy deposition, CIRP J. Manuf. Sci. Technol. 63 (2025) 43–57, https://doi.org/10.1016/j.cirpj.2025.09.002.
[372] Y. Fu, N. Guo, L. Zhou, Q. Cheng, J. Feng, Underwater wire-feed laser deposition of the Ti–6Al–4V titanium alloy, Mater. Des. 186 (2020) 108284, https://doi.org/10.1016/j.matdes.2019.108284.
[373] Y. Fu, N. Guo, G. Wang, M. Yu, Q. Cheng, D. Zhang, Underwater additive manufacturing of Ti-6Al-4V alloy by laser metal deposition: formability, gran growth and microstructure evolution, Mater. Des. 197 (2021) 109196, https://doi.org/10.1016/j.matdes.2020.109196.
[374] P.R. Gradl, Component applications using metal additive manufacturing techniques and materials for rocket propulsion, NASA Marshal Sp. Flight Cent. (2020) 1–22. www.amcoe.org.
[375] T.S. Singhal, J.K. Jain, M. Kumar, V. Bhojak, K.K. Saxena, D. Buddhi, C. Prakash, A comprehensive comparative review: welding and additive manufacturing, Int. J. Interact. Des. Manuf. 18 (2024) 1829–1843, https://doi.org/10.1007/s12008-022-01152-0.
[376] M. Lalegani Dezaki, A. Serjouei, A. Zolfagharian, M. Fotouhi, M. Moradi, M.K. A. Ariffin, M. Bodaghi, A review on additive/subtractive hybrid manufacturing of directed energy deposition (DED) process, Adv. Powder Mater. 1 (2022), https://doi.org/10.1016/j.apmate.2022.100054.
[377] H.Z. Fan, W. Wang, G. Xi, A novel five-axis rough machining method for efficient manufacturing of centrifugal impeller with free-form blades, Int. J. Adv. Manuf. Technol. 68 (2013) 1219–1229, https://doi.org/10.1007/s00170-013-4913-1.
[378] Y. Zhou, Y. Jiang, C. Lu, J. Huang, J. Pei, T. Xing, S. Zhao, K. Zhu, H. Yan, Z. Xu, S. Ding, A review of 5-axis milling techniques for centrifugal impellers: Tool-path generation and deformation control, J. Manuf. Process. 131 (2024) 160–186, https://doi.org/10.1016/j.jmapro.2024.08.049.
[379] C.M. Choe, W.C. Yang, U.H. Kim, B.G. Ri, M.S. Om, Manufacture of centrifugal compressor impeller using FDM and investment casting, Int. J. Adv. Manuf. Technol. 118 (2022) 173–181, https://doi.org/10.1007/s00170-021-07894-7.
[380] A. Adiaconitei, I.S. Vintila, R. Mihalache, A. Paraschiv, T. Frigioescu, M. Vladut, L. Pambaguian, A study on using the additive manufacturing process for the development of a closed pump impeller for mechanically pumped fluid loop systems, Mater. (Basel) 14 (2021) 1–17, https://doi.org/10.3390/ma14040967.
[381] T.R. Barrett, G. Ellwood, G. Pérez, M. Kovari, M. Fursdon, F. Domptail, S. Kirk, S. C. McIntosh, S. Roberts, S. Zheng, L.V. Boccaccini, J.H. You, C. Bachmann, J. Reiser, M. Rieth, E. Visca, G. Mazzone, F. Arbeiter, P.K. Domalapally, Progress in the engineering design and assessment of the European DEMO first wall and divertor plasma facing components, 109–111, Fusion. Eng. Des. (2016) 917–924, https://doi.org/10.1016/j.fusengdes.2016.01.052.
[382] J. Linke, J. Du, T. Loewenhoff, G. Pintsuk, B. Spilker, I. Steudel, M. Wirtz, Challenges for plasma-facing components in nuclear fusion, Matter Radiat. Extrem. 4 (2019), https://doi.org/10.1063/1.5090100.
[383] M.Z. Tokar, An assessment for the erosion rate of DEMO first wall, Nucl. Fusion. 58 (2018), https://doi.org/10.1088/1741-4326/aa92dd.
[384] A.V. Müller, G. Schlick, R. Neu, C. Anstätt, T. Klimkait, J. Lee, B. Pascher, M. Schmitt, C. Seidel, Additive manufacturing of pure tungsten by means of selective laser beam melting with substrate preheating temperatures up to 1000 ∘ C, Nucl. Mater. Energy 19 (2019) 184–188, https://doi.org/10.1016/j.nme.2019.02.034.
[385] A.V. Müller, D. Dorow-Gerspach, M. Balden, M. Binder, B. Buschmann, B. Curzadd, T. Loewenhoff, R. Neu, G. Schlick, J.H. You, Progress in additive manufacturing of pure tungsten for plasma-facing component applications, J. Nucl. Mater. 566 (2022), https://doi.org/10.1016/j.jnucmat.2022.153760.
[386] S.H. Pan, G.C. Yao, Y.N. Cui, F.S. Meng, C. Luo, T.Q. Zheng, G. Singh, Additive manufacturing of tungsten, tungsten-based alloys, and tungsten matrix composites, Springe Nat. Singap. (2023), https://doi.org/10.1007/s42864-022-00153-6.
[387] V. Philipps, R. Neu, J. Rapp, U. Samm, M. Tokar, T. Tanabe, M. Rubel, Comparison of tokamak behaviour with tungsten and low-Z plasma facing materials, Plasma Phys. Control. Fusion. 42 (2000), https://doi.org/10.1088/0741-3335/42/12B/322.
[388] R. Melentiev, A. Yudhanto, R. Tao, T. Vuchkov, G. Lubineau, Metallization of polymers and composites: state-of-the-art approaches, Mater. Des. 221 (2022) 110958, https://doi.org/10.1016/j.matdes.2022.110958.
[389] J. Xie, H. Lu, J. Lu, X. Song, S. Wu, J. Lei, Additive manufacturing of tungsten using directed energy deposition for potential nuclear fusion application, Surf. Coat. Technol. 409 (2021) 126884, https://doi.org/10.1016/j.surfcoat.2021.126884.
[390] W. Jeong, Y.S. Kwon, D. Kim, Three-dimensional printing of tungsten structures by directed energy deposition, Mater. Manuf. Process. 34 (2019) 986–992, https://doi.org/10.1080/10426914.2019.1594253.
[391] G. Marinelli, F. Martina, S. Ganguly, S. Williams, Development of Wire + Arc additive manufacture for the production of large-scale unalloyed tungsten components, Int. J. Refract. Met. Hard Mater. 82 (2019) 329–335, https://doi.org/10.1016/j.ijrmhm.2019.05.009.
[392] G. Marinelli, F. Martina, S. Ganguly, S. Williams, H. Lewtas, D. Hancock, S. Mehraban, N. Lavery, Microstructure and thermal properties of unalloyed tungsten deposited by Wire + Arc Additive Manufacture, J. Nucl. Mater. 522 (2019) 45–53, https://doi.org/10.1016/j.jnucmat.2019.04.049.
[393] N. Group, 2023, Nav. Group. Has. 3D pritned a One-tonne ship Propeller Fr. navy 3D Pritning Ind.10https://3dprintingindustry.com/news/naval-group-has-3d-printed-a-one-tonne-ship-propeller-for-the-french-navy-182400/.
[394] B. Wu, Z. Pan, D. Ding, D. Cuiuri, H. Li, J. Xu, J. Norrish, A review of the wire arc additive manufacturing of metals: properties, defects and quality improvement, J. Manuf. Process. 35 (2018) 127–139, https://doi.org/10.1016/j.jmapro.2018.08.001.
[395] J. Liu, Y. Miao, C. Wei, Z. Wang, Y. Zhao, Y. Wu, Enhanced mechanical properties in nickel-aluminium bronze alloy via wire arc additive manufacturing with follow-weld forced cooling, Mater. Charact. 208 (2024) 113653, https://doi.org/10.1016/j.matchar.2024.113653.
[396] RAMLAB, RAMLAB unveils world's first class approved 3D printed ship's propeller, Rotterdam Addit. Manuf. (2017). https://www.ramlab.com/updates/ramlab-unveils-worlds-first-class-approved-3d-printed-ships-propeller/.
[397] B. Li, C. Han, Y. Xie, P.J.D.S. Bartolo, K. Zhou, Microstructural heterogeneity induced by thermal accumulation in a nickel–aluminum–bronze alloy additively manufactured via directed energy deposition, CIRP Ann. 72 (2023) 133–136, https://doi.org/10.1016/j.cirp.2023.04.008.
[398] G. Casalino, M. Karamimoghadam, N. Contuzzi, Metal wire additive manufacturing: a comparison between arc laser and laser/arc heat sources, Inventions 8 (2023), https://doi.org/10.3390/inventions8020052.
[399] S.J. Zinkle, G.S. Was, Materials challenges in nuclear energy, Acta Mater. 61 (2013) 735–758, https://doi.org/10.1016/j.actamat.2012.11.004.
[400] S. Wang, S. Chen, T. Yuan, X. Jiang, P. Zhao, H. Shan, H. Zhang, W. Ding, Inhomogeneity and anisotropy of Al-Zn-Mg-Cu alloy manufactured by wire arc additive manufacturing: microstructure, mechanical properties, stress corrosion cracking susceptibility, Virtual Phys. Prototyp. 19 (2024) 1–24, https://doi.org/10.1080/17452759.2024.2348038.
[401] E.A. Kenik, J.T. Busby, Radiation-induced degradation of stainless steel light water reactor internals, Mater. Sci. Eng. R. Rep. 73 (2012) 67–83, https://doi.org/10.1016/j.mser.2012.05.002.
[402] M. Azami, Z. Kazemi, S. Moazen, M. Dubé, M. Potvin, Progress in aerospace sciences a comprehensive review of lunar-based manufacturing and construction, Prog. Aerosp. Sci. 150 (2024) 101045, https://doi.org/10.1016/j.paerosci.2024.101045.
[403] M.G. Shaw, M.S. Humbert, G.A. Brooks, A. Rhamdhani, R. Alan, M.I. Pownceby, Mineral Processing and Metal Extraction on the Lunar Surface - Challenges and Opportunities, 2021.
[404] O.D. D'Angelo, F. Kuthe, S. Liu, R. Wiedey, J.M. Bennett, M. Meisnar, A. Barnes, W.T. Kranz, T. Voigtmann, A. Meyer, A gravity-independent powder-based additive manufacturing process tailored for space applications, Addit. Manuf. 47 (2021) 102349, https://doi.org/10.1016/j.addma.2021.102349.
[405] K.M.B. Taminger, R.A. Hafley, Electron beam freeform fabrication: a rapid metal deposition process, NASA Tech. Rep. Serv. (2003).
[406] S.M.A. Noori Rahim Abadi, P. Hagqvist, F. Sikström, I. Choquet, CFD-based feasibility study of laser-directed energy deposition with a metal wire for on-orbit manufacturing, Front. Sp. Technol. 3 (2022) 1–13, https://doi.org/10.3389/frspt.2022.880012.
[407] L. Castillo, Study about the rapid manufacturing of complex parts of stainless steel and titanium, TNO AIMME Rep. (2005) 1–31. http://www.lasercusing.nl/files/bestanden/binding_mechanisms_SLM_SLS.pdf.
[408] P.R. Gradl, D.C. Tinker, J. Ivester, S.W. Skinner, T. Teasley, J.L. Bili, Geometric feature reproducibility for laser powder bed fusion (L-PBF) additive manufacturing with Inconel 718, Addit. Manuf. 47 (2021) 102305, https://doi.org/10.1016/j.addma.2021.102305.
[409] M. Moshiri, G. Tosello, S. Mohanty, A new design for an extensive benchmarking of additive manufacturing machines, Eur. Soc. Precis. Eng. Nanotechnology, Conf. Proc. - 18th Int. Conf. Exhib. EUSPEN 2018 (2018) 261–262.

[410] S. Moylan, J. Slotwinski, A. Cooke, K. Jurrens, M.A. Donme, Proposal for a standardized test artifact for additive, Solid. Free. Fabr. Symp. (2012) 902–920. https://ws680.nist.gov/publication/get_pdf.cfm?pub_id=911953.
[411] S. Martínez, N. Ortega, D. Celentano, A.J. Sánchez Egea, E. Ukar, A. Lamikiz, Analysis of the part distortions for inconel 718 SLM: a case study on the NIST test artifact, Mater. (Basel) 13 (2020) 1–9, https://doi.org/10.3390/ma13225087.
[412] S. Gruber, C. Grunert, M. Riede, E. López, A. Marquardt, F. Brueckner, C. Leyens, Comparison of dimensional accuracy and tolerances of powder bed based and nozzle based additive manufacturing processes, J. Laser Appl. 32 (2020), https://doi.org/10.2351/7.0000115.
[413] M. Krasniqi, F. Löffler, 2023, Dimens. Accuracy Addit. Manuf. AlSi10Mg Part. Study Influ. Build. Platf. Position. Process. Parameters repeatability2-5.
[414] B.S. Rupal, T. Singh, T. Wolfe, M. Secanell, A.J. Qureshi, Tri-planar geometric dimensioning and tolerancing characteristics of ss 316l laser powder bed fusion process test artifacts and effect of base plate removal, Mater. (Basel) 14 (2021), https://doi.org/10.3390/ma14133575.
[415] Z. Chen, C. Han, M. Gao, S.Y. Kandukuri, K. Zhou, A review on qualification and certification for metal additive manufacturing, Virtual Phys. Prototyp. 2759 (2022), https://doi.org/10.1080/17452759.2021.2018938.
[416] J. Ralph, R. Roe, 2021, NASA Tech. Stand. Addit. Manuf. Requir. Spacefl. Syst..



Ruslan Melentiev is an Assistant Professor in Intelligent Manufacturing at the University of Nottingham and a member of The Welding Institute (TWI). He received his MSc in Metallurgy from Odesa Polytechnic and PhD in Mechanical Engineering from University College Dublin in 2020, followed by postdoctoral training at King Abdullah University of Science and Technology (2021–2024) and the University of Cambridge (2024–2025). He is listed by Stanford's rank of Top 2% scientists with just under 30 papers. His research bridges fundamental understanding of materials behavior with industrial manufacturing technologies.



Long Ye is a Research Fellow in advanced manufacturing and digital engineering at the University of Edinburgh. He received his PhD in Mechanical Engineering from KU Leuven in 2024, where his research focused on physics-informed monitoring and closed-loop control of precision machining. Dr. Ye has established an international research profile through over 30 high-impact publications in journals such as CIRP Annals and Journal of Manufacturing Systems, alongside research funding from the British Academy, Royal Society of Edinburgh, and EPSRC-related schemes. His current research focuses on AI-driven additive manufacturing.



Ahmed Wagih is a research scientist in the Mechanics of Composites for Energy and Mobility (MCEM) lab at KAUST and serves as the composite performance track leader in ENERCOMP, a Technology Consortium for Composites in Energy. Dr. Wagih earned his MS and PhD degrees from Girona University, Spain. He previously held a faculty position at Zagazig University, Egypt, and worked as a postdoctoral researcher at Chalmers University, Sweden. His research focuses on the deployment of additive-manufactured composite parts in engineering applications, alongside the toughening of composite structures, integrity assessment of composite materials and structures, and testing under harsh environmental conditions.



Guoda Chen is an Associate Professor in Mechanical Engineering at Zhejiang University of Technology (China), where he joined the faculty in 2015. He received his Ph.D. degree from Harbin Institute of Technology (China) in 2015 and was ever a Visiting Ph.D. Student with the Department of Mechanical Engineering, Northwestern University (USA), and a Visiting Scholar with the Department of Mechanical Engineering, National University of Singapore. His research interests include ultra-precision machining process and machine tool, laser metal additive manufacturing, and intelligent manufacturing equipment. He has published over 80 technical articles.



Chengzhe Zhang is currently a Master Student in Mechanical Engineering at Zhejiang University of Technology (China). His research interest focuses on laser metal additive manufacturing.



Angioletta Rita Catalano is an Assistant Professor of Manufacturing Technologies in the Department of Management and Production Engineering at Politecnico di Torino (Italy). Her research addresses the sustainability assessment and optimization of additive and hybrid manufacturing technologies. She earned a PhD in Management, Production and Design from the same institution, following her MSc in Mechanical Engineering. She is also a Research Affiliate of the International Academy for Production Engineering (CIRP).



Paolo C. Priarone is an Associate Professor of Manufacturing at the Department of Management and Production Engineering of Politecnico di Torino, as well as an Associate Member of the International Academy for Production Engineering (CIRP). He received his MSc degree cum laude in Mechanical Engineering and a PhD in Production Systems and Industrial Design from the same university. His scientific activity focuses on sustainable manufacturing and development, advanced production technologies, and the optimization and decarbonization of manufacturing systems.



Fangda Xu is the CEO of Rongsu Technology. He received his PhD from the University of Bath in 2020. Under his leadership, Rongsu Technology has expanded rapidly, earning a strong reputation in large-scale metal additive manufacturing and directed energy deposition (DED). Bridging the gap between research and industrial application, Dr. Xu has overseen the successful delivery of over 600 wire-feed DED components. His research focuses heavily on wire-based directed energy deposition, driving the continuous development of proprietary AM equipment and core devices for the industry.



Samanta Piano is a Full Professor at the University of Nottingham (UK). She received her PhD from the University of Salerno (Italy) in 2003. She is an experienced leader in Optical Metrology with a strong national and international reputation for delivering high-impact research, innovation, and academic leadership. Her research interests concern the development of innovative and unconventional optical techniques and three-dimensional probing systems for high-precision coordinate metrology to be used in industrial applications. She is currently investigating how AI approaches can be used for improving optical measurement systems and new directions in quantum super-resolution metrology for the manufacturing sector.



Christos Spitas is Manager R&D at Psyche Engineering Systems and Technologies BV, The Hague. Previously he has served as Professor of Aerospace Engineering, Machine Design and Embodiment Design respectively at the University of Nottingham Ningbo China, Nazarbayev University and Delft University of Technology, with corresponding simultaneous appointments as Head of Department, Research Group Leader and Head of Section, and prior to that in various capacities up to Manager R&D in the European high tech industry. His research spans the broad field of Machine and Systems Design with applications to Mechanical and Aerospace Engineering, from materials science and metamaterials, structures and fluid-structure interaction, to mechanisms, powertrains and vehicles, and multiphysical systems.



Nan Yu is a Full Professor of Optical Engineering at Harbin Institute of Technology (HIT), Shenzhen. He received his PhD from Cranfield University in 2017 and previously held research and academic positions at University College Dublin (2017–2018), CERN (2018–2020), and the University of Edinburgh (2020–2024). Dr. Yu has established an international reputation in digital manufacturing and precision engineering, with over 70 journal and conference publications and research funding from major agencies including Horizon-MSCA, EPSRC, the Royal Society, and NSFC. His research focuses on opto-mechanical design, energy beam processing technologies, and additive manufacturing.